

**UNIVERSITY OF SÃO PAULO
SÃO CARLOS INSTITUTE OF CHEMISTRY**

Jéssica Freire Feitor

Microfluidic Intestine-on-a-Chip as a Model for Nutrient Absorption

São Carlos, 2022

UNIVERSITY OF SÃO PAULO
SÃO CARLOS INSTITUTE OF CHEMISTRY

Jéssica Freire Feitor

Microfluidic Intestine-on-a-Chip as a Model for Nutrient Absorption

Dissertation presented at the São Carlos Institute of Chemistry, University of São Paulo, to obtain the title of Doctor of Philosophy in Chemistry.

Area: Biological and Organic Chemistry


Advisor: Daniel Rodrigues Cardoso

Exemplar revisado

O exemplar original encontra-se em
acervo reservado na Biblioteca do IQSC-USP

São Carlos, 2022

Autorizo a reprodução e divulgação total ou parcial deste trabalho, por qualquer meio convencional ou eletrônico para fins de estudo e pesquisa, desde que citada a fonte.

Assinatura: 
Data: 24/08/2022

Ficha Catalográfica elaborada pela Seção de Referência e Atendimento ao Usuário do SBI/IQSC

Feitor, Jéssica Freire
Microfluidic Intestine-on-a-Chip as a model for nutrient absorption / Jéssica Freire Feitor. — São Carlos, 2022.
125 f.

Tese (Doutorado em Química Orgânica e Biológica) — Instituto de Química de São Carlos / Universidade de São Paulo, 2022.
Edição revisada

Orientador: Prof. Dr. Daniel Rodrigues Cardoso

1. Intestine-on-a-Chip. 2. Calcium absorption. 3. Peptidomic analysis. 4. Bioavailability. I. Título.

Solange Puccinelli - CRB: 1500/8



*To my family, Mom, Dad, siblings and
husband, who always support me, no matter
how big my dreams are.*

ACKNOWLEDGMENTS

To my mother and father, Eliete and Mario, who gave me love, education, and the support to achieve my dreams. Raising five people is not easy these days, but you have made it epically. To my siblings, Vinícius, Vitor, Alice, and Lucas, who always protected and inspired me to be better. To my beloved husband, Gabriel, words will never be enough to thank you for all you have done for me. Your confidence, patience, love and humbleness inspire me every day. To all my relatives, who cheer with me for each accomplishment, especially my in-laws, Daniela, Diego, Ester, Jú, Neto, Sueli, Thay and Victor.

To Prof. Daniel Cardoso, who shows me every day that he is right. Thank you for your guidance, expertise, patience, and friendship. You are an inspiration for me with your wisdom and perception, always putting my feet on the ground. To Prof. Emanuel Carrilho, who co-advised me so many times, providing me great discussions, the lab facilities, and good bar talks. Thank you for your friendship and for always being able to help me and guide me when I needed.

To all my co-workers and friends, Aline, Carol, Dani, Felipe, Jennifer, Juliana F, Juliana B, Keila, Marcella, Nana, Priscila, Rodrigo, Silmara, Silvinha, Sinara, and Willy. Thank you for all the productive discussions and for the friendship, the lab is lighter with you all by my side.

To the BioMicS group members, especially to those I was more in touch, Amanda Hikari, Amanda Maciel, Carlos, Cleyton, Cláudia, Desiree, Eduardo, Fillipe, Jéssica, Jonathan, Laís, Larissa, Lê Marques, Lê Jordão, Lucas, Ma, Mariana, Manoel, Tati and Vini. Special thanks to Dr. Laís, who helped me with my project when I was struggling the most, Dr. Ma for teaching me everything about cells, and Dr. Vini for helping me a lot on the MS.

To all my friends, who are inspiring good souls, especially Aline, Amanda, Caju, Dani, Desi, Ederruã, Eti, Fer, Fê, Felype, Jé, Laís, Lesa, Pedro, Pri, Rafa, Sinara, Silvinha, Tati and Willian. You were always by my side and I thank you for my mental health.

To the colleagues with collaborations, Giulia, Lucas and Prof. Vanderlei Bagnato, for the Lung-on-chip collaboration. Prof. Francisco, special thank you to all the kindness and patience to make my images the best. Luís and Prof. Rosângela for kindly providing me

the Caco-2 cells, and for the beetroot collaboration. Prof. Leif and Prof. Lilia for the foreign collaboration and contributions to my work.

To IQSC/USP, for the 11 years of support. I evolved so much during this time as a person and a professional, and I need to recognize the state and federal endorsement. Without the funding and providing home and food, I could never have got this far. Special thanks to all professors who helped and taught me during this journey, and to the secretaries who were always prompt to advice and support me.

To FAPESP, for the 4 years of financial support under the grant number 2018/11657-4 linked to the thematic project 2017/01189-0. Also, to CAPES and CNPq, for providing lab resources, and helping me to develop my research.

ABSTRACT

Bioavailability and absorption of calcium are increasingly becoming a trending topic of study due to its correlation with a series of diseases such as osteosarcopenia. Those diseases are mostly related to the elderly population and are showing increasing numbers, affecting over 100 million people worldwide. Calcium malabsorption is the main cause of the low levels of this mineral into the body, and is related to the low solubility of calcium in most food types under neutral and alkaline conditions. Aside from physiological age-related problems, the poor solubility of calcium in food and the lack of calcium transporters may worsen its absorption into the intestine. The knowledge of the absorption of calcium ions by combining them with milk-derived peptides and hydroxy carboxylates is of nutritional relevance. The *in vitro* study of nutrients absorption is traditionally carried out by using pharmaceutical-derived approaches, such as the transwell® assay with the Caco-2 cells as a model for intestinal absorption. Although largely accepted, this model was proved obsolete and inconsistent if compared to the human system. The past few decades were marked by the advent of Organs-on-a-chip (OoaCs), which are now object of intense investigation for the most different approaches. Today, OoaCs are becoming an attractive substitute for the traditional methods of drug and nutrient uptake evaluation due to their dynamic character. Therefore, this work displays the study of calcium and peptide absorption by the use of two methods, the traditional static model (transwell®), and the dynamic two developed devices of intestine-on-a-chip (IoAC). By using the ESI-MS technique, the transwell® indicates an improvement of calcium absorption by the simple addition of CaCl₂ to Peptigen® commercial whey hydrolysate. The IoAC, otherwise, indicates no significant change in calcium absorption. Moreover, this work gives insights on the development of possible calcium ion carriers and the permeability of important peptides through a peptidome analysis of Peptigen® using MALDI-TOF-MS/MS. Finally, the IoAC platforms show the permeation of fast absorption peptides in high levels, in contrast with a large number of peptides found in lower levels for the transwell® platform, indicating different mechanisms for those platforms.

Keywords: Intestine-on-a-Chip, Calcium Absorption, Peptidomic analysis, Bioavailability

RESUMO

A biodisponibilidade e a absorção de cálcio se tornaram uma tendência de estudo dada à sua correlação com uma série de doenças como a osteosarcopenia. Essas doenças estão relacionadas à população idosa e apresentam números crescentes, afetando mais de 100 milhões de pessoas no mundo. A má absorção de cálcio é a principal causa dos baixos níveis desse mineral no organismo e se relaciona à baixa solubilidade do cálcio na maioria dos alimentos em condições neutras e alcalinas. O conhecimento da absorção de íons cálcio combinando-os com peptídeos derivados do leite é de relevância nutricional. O estudo *in vitro* da absorção de nutrientes é tradicionalmente realizado por meio de abordagens derivadas da indústria farmacêutica, como o ensaio de transwell® que utiliza células Caco-2 como modelo para absorção intestinal. Embora amplamente aceito, esse modelo se mostra obsoleto e inconsistente se comparado ao sistema humano. As últimas décadas foram marcadas pelo advento dos *Organs-on-a-chip* (OoaCs), que hoje são objeto de investigação para as mais diferentes abordagens. Hoje, OoaCs estão se tornando um substituto atraente para os métodos tradicionais de avaliação de absorção de drogas e nutrientes devido ao seu caráter dinâmico. Portanto, este trabalho apresenta o estudo da absorção de cálcio e peptídeos através do uso de dois métodos, o modelo estático tradicional (transwell®), e os dois dispositivos dinâmicos desenvolvidos de *intestine-on-a-chip* (Ioac). Através da técnica ESI-MS, o transwell® indica uma melhora na absorção de cálcio pela simples adição de CaCl_2 ao hidrolisado de soro comercial Peptigen®, diferentemente dos dispositivos Ioac, que não indicam alteração significativa na absorção de cálcio. Além disso, este trabalho fornece informações sobre o desenvolvimento de possíveis transportadores de íons cálcio e a permeabilidade de peptídeos importantes através de uma análise peptidômica de Peptigen® usando MALDI-TOF-MS/MS. Por fim, as plataformas Ioac mostram a permeação de peptídeos de rápida absorção em altos níveis, em contraste com um grande número de peptídeos encontrados em menores níveis para a plataforma transwell®, indicando mecanismos diferentes para essas plataformas.

Palavras-chave: *Intestine-on-a-Chip*, Absorção de cálcio, Análise peptidômica, Biodisponibilidade.

LIST OF FIGURES

Figure 1.1-1. Schematic illustration of an loaC device using laser cutting as a fabrication method. a) 3D view of the device layers, b) Vertical view of the device illustrating the apical and basal channels.....	32
Figure 1.1-2. Lithography fabrication. a–b) Spin-coated photoresist c) Mask deposited into the photoresist d) UV irradiation into photoresist followed by mask removal e) Soft lithography cure of PDMS f) Final PDMS piece embossed g) Replica molding process.....	35
Figure 1.3-1. Pictures of the fabrication process: A) laser cutting of PDMS sheet covered with Arcare® tape, B) Device #4 with the clippers to ensure adherence.....	38
Figure 1.3-2. Schematics of sterilization methodology. The image shows all the steps used for decontaminating the microchips.....	40
Figure 1.4-1. Design, dimensions and 3D view of the device #1 a) Pieces of the chip with their dimensions b) Top view of the device with the indication of the main components and c) 3D view indicating the assembly of the device.	42
Figure 1.4-2. Design, dimensions and 3D view of the loaC #2 a) Pieces of the chip with its dimensions b) Top view with key components of the chip and c) Assembly of the chip under a 3D view.....	43
Figure 1.4-3. Design, dimensions and 3D view of the loaC #3 a) Pieces of the chip with dimensions b) Top view with key components of the chip and c) 3D view with chip assembly.	44
Figure 1.4-4. Design, dimensions, and assembly of the loaC models #4 and #5 a) Pieces of chip #4 (Acrylic) with their dimensions (mm) and top view b) Pieces of chip #5 (PDMS) with dimensions and top view, and c) 3D view of chip #5 showing its assembly.	45
Figure 1.4-5. Flow testing with different colored dyes: A) chip #1 flow test approved, B) chip #2 flow test failed, C) chip #3 flow test approved, D) chip #4 flow test approved and E) chip #5 flow test approved.	47
Figure 1.4-6. Process of device sterilization including a few steps used for this matter. From left to right, top to bottom, this image shows the washing, UV irradiation, assembly, and culture medium infusion of chip #5.	48

Figure 1.4-7. Comparison between white (up) and transparent (down) PE membranes showing fluorescence and optical microscopy images (10x magnification). From left to right, an image of the membrane, the membrane with cells, and the membrane with stained cells.	49
Figure 1.4-8. Comparative cell growth and differentiation in different platforms. Optical microscopy of the loaC channels and transwell® before seed, 4 and 8 days of differentiation.	51
Figure 2.1-1. Reaction mechanism of the reduction of MTT to formazan.	56
Figure 2.1-2. Schematics of a hemacytometer or Neubauer chamber counting showing a zoom in one of the chambers and a close look to the number of live and dead cells.	57
Figure 2.1-3 Chemical mechanisms for live-dead counterstaining. A) Calcein-AM entering the cell membrane and hydrolyzing into green fluorescent calcein, B) EthD-1 crossing the damaged membrane and reaching the genetic material, intercalating the DNA strain and generating a red fluorescence.	59
Figure 2.4-1. Cytotoxicity of supersaturated solutions with Peptigen®, showing the survival index (SI) bar chart for the different solutions.	65
Figure 2.4-2. Cytotoxicity of a range of CaCl ₂ solutions showed in a bar chart of SI <i>versus</i> CaCl ₂ concentrations.	66
Figure 2.4-3. Bar chart of SI <i>versus</i> the solutions of Pep and Pep combined with CaCl ₂ (PepCa), showing their cytotoxicity.	67
Figure 2.4-4 Comparative micrographs for Caco-2 cell growth in static and dynamic systems. Transwell® shows the 8 th and 21 st days of differentiation, while acrylic and PDMS chips were evaluated for 8 days of culture to show the differences in the differentiation time.	68
Figure 2.4-5 Confocal micrographs of live/dead stained cells. A) Counterstained monolayer of cells in each platform with 21 days for well and transwell® and 8 days for the chips, B) 3D view of transwell® monolayer, C) 3D view for the PDMS chip monolayer.	69
Figure 2.4-6 Optical microscopy images of the triplicate monolayer of Caco-2 cells in three different platforms: transwell®, Acrylic chip, and PDMS chip.	70

Figure 2.4-7 Confocal micrographs of Caco-2 cell monolayers counterstained with DAPI and ZO-1. The images exhibit intact monolayers ready for the transport experiment. 71

Figure 2.4-8. PR diffusion percentages and apparent permeability. A) calibration curve with PR concentration versus absorbance B) PR diffusion bar chart per triplicate sample C) Table with Papp calculations, and D) Papp chart per triplicate sample. 73

Figure 3.1-1. Pathways for calcium balance in the human body, including the intake, passing through absorption and ending in the excretion with a final negative balance of 10 mg/day..... 79

Figure 3.1-2. Schematics showing the mechanisms of nutrient absorption across epithelial cells..... 80

Figure 3.4-1. Mass spectrometry data A) SIM mode spectrum of a 1 mM Ca/EDTA sample, B) Example of a collected area of the EIC analysis, C) Broad concentration range calibration curve, showing the linear range limit, and D) Final calibration curve with equation and R^2 89

Figure 3.4-2. Transwell® transport experiment of calcium ions: A) Cell monolayer viability, B) Cell monolayer assessment, with nuclei and TJ, C) Papp (cm/s) for PR in red as an average for the 3 wells used to each sample, and for the solutions (color bar) for the triplicate well of each investigated solution D) Comparative apical 0 min and basal 60 min calcium ion concentrations of the transport experiment. 90

Figure 3.4-3. Acrylic loaC transport experiment of calcium ions. A) Cell monolayer viability, B) Cell monolayer assessment, with nuclei and TJ, C) Papp for PR in red, and for the solutions in the triplicate devices in colors, D) Comparative apical 60 min and basal 60 min calcium ion concentrations of the transport experiment, the small graphs are the triplicate. 92

Figure 3.4-4. PDMS loaC transport experiment of calcium ions. A) Cell monolayer viability, B) Cell monolayer assessment, with nuclei and TJ, C) Papp for PR in red and for the solutions in the triplicate chips (colors), D) Comparative apical 60 min and basal 60 min calcium ion concentrations of the transport experiment, the small graphs are the triplicate. 93

Figure 3.4-5. Chemical structures of peptides m/z 1100.49 and 1679.78, indicating the possible binding sites for calcium into the side chain of the amino acids.	100
Figure A-1. Mass spectrum of 0 mM Calcium/ 30 mM EDTA	120
Figure A-2. Mass spectrum of 0.3 mM Calcium/ 30 mM EDTA	120
Figure B-1. RAMAN spectroscopy for identifying PDMS adsorption	122
Figure C-1. MALDI spectra for the transwell® samples	124
Figure C-2. MALDI spectra for the Acrylic loaC.....	124
Figure C-3. MALDI spectra for the PDMS loaC.....	125

LIST OF TABLES

Table 1.4-1. Estimating costs for the developed devices according to the materials used.....	46
Table 1.4-2. Comparative cell growth for devices #4 and #5 under different flow rates and consequently, distinct shear stresses.....	50
Table 2.4-1. Calculated values for the total percentage of live and dead cells by using the ImageJ plugin for color segmentation	69
Table 3.4-1. Transport of peptides and Papp for the Peptigen® solution with the protonated masses, AA sequence attributed to the mass, possible protein origin, and the Papp. Uncalculated Papp is due to the absence of the ion on the apical compartment in time 0.....	95
Table 3.4-2. Transport of peptides and Papp for the Peptigen® + Ca solution (PepCa), with the protonated masses, AA sequence attributed to the mass, possible protein origin, and the Papp. Uncalculated Papp is due to the absence of the ion on the apical compartment.....	97
Table 3.4-3. Analysis of possible calcium transporters from transwell® with the masses from basal and apical compartments, and their subtractions. The designations were based on the literature.	98
Table 3.4-4. Transport of peptides for the acrylic loaC, with the protonated masses, AA sequence attributed to the mass, possible protein origin, and the Papp. Uncalculated Papp is due to the absence of the ion on the apical compartment.....	100
Table 3.4-5. Analysis of possible calcium transporters from the acrylic loaC with the masses from basal and apical compartments, and their subtractions. The designations were based on the literature.	101
Table 3.4-6. Transport of peptides for the PDMS loaC, with the protonated masses, AA sequence attributed to the mass, possible protein origin, and the Papp. Uncalculated Papp is due to the absence of the ion on the apical compartment.....	102
Table 3.4-7. Analysis of possible calcium transporters for the PDMS loaC with the masses from basal and apical compartments, and their subtractions.	104

LIST OF ACRONYMS AND ABBREVIATIONS

3D – Tridimensional
AA – Amino acid
ANOVA – Analysis of variance
APCI – Atmospheric pressure chemical ionization
ATP – Adenosine triphosphate
BLM – Bilayer membrane
CaBP - Calcium Binding Protein
CI – Chemical ionization
DAPI - 4',6-Diamidine-2'-phenylindole dihydrochloride
DMEM – Dulbecco's Modified Eagle Medium
ECM - Extracellular matrices
EDTA - Ethylenediaminetetraacetic acid
EI – Electron ionization
EIC – Extracted ion chromatogram
ESI - Electrospray ionization
EthD-1 - Ethidium homodimer
FBS - Fetal bovine serum
FTIR – Fourier Transform Infrared
GC – Gas chromatography
GI – Gastrointestinal
HBSS - Hanks Balanced Salt Solution
ID/ED – Internal and External diameters
IoaC - Intestine-on-a-Chip
ITMA – Ion trap mass analyzer
LAF bench – Laminar Air Flow bench/hood
LC – Liquid chromatography
LOD – Limit of detection
LOQ – Limit of quantification
LY – Lucifer yellow
MALDI - Matrix assisted laser desorption ionization

MS - Mass spectrometry
MTT - 3-(4,5-dimethylthiazol-2-yl)-2,5-diphenyltetrazolium bromide or Thiazolyl Blue
Tetrazolium Bromide
Na₃Cit.2H₂O or NaCit - Sodium Citrate dihydrated
NADPH – Nicotinamide adenine dinucleotide phosphate
NHE3 – Na⁺/H⁺ exchanger 3
OoaC - Organ-on-a-Chip
Papp – Apparent permeability
PBS - Phosphate Buffer Solution
PC - Polycarbonate
PDMS – Poly(dimethyl siloxane)
PE - Polyester
Pep – Peptigen®
PepCa - Peptigen® + CaCl₂
PEST - penicillin/ streptomycin solution
Pgp – P-glycoprotein
PK/PD - pharmacokinetics, pharmacodynamics
PMMA or acrylic - Poly(methyl methacrylate)
PR – Phenol red
PTH - Parathyroid hormone
PVC - Polyvinyl Chloride
QMA – Quadrupole mass analyzer
RDA - Recommended Dietary Allowance
SD – Standard deviation
SI – Survival Index
SIM - Selective ion monitoring
SIM – Selected ion monitoring
SMA – Sector mass analyzer
TC treated – Tissue culture
TEER - Trans-epithelial electrical resistance
TJ – Tight junction

TOF – Time of flight

UV – Ultraviolet

ZO-1 – Zonula Occludens 1

TABLE OF CONTENTS

OVERVIEW.....	26
<i>Development, Fabrication, and Evaluation of Intestine-on-a-Chip Devices</i>	28
1.1. INTRODUCTION.....	30
1.1.1. Lab-on-a-chip and the evolution of pharmaceutical testing	30
1.1.2. Materials for OoaC.....	32
1.1.3. Fabrication techniques	33
1.1.4. Flow control and shear stress	35
1.1.5. Sterilization methods.....	36
1.2. OBJECTIVES.....	36
1.3. MATERIALS & METHODS	37
1.3.1. Devices design and fabrication	37
1.3.2. Flow control test	39
1.3.3. Sterilization	39
1.3.4. Cell culture on-chip and shear stress.....	40
1.4. RESULTS & DISCUSSION.....	41
1.4.1. Devices design and fabrication	41
1.4.2. Flow control test	46
1.4.3. Device sterilization.....	47
1.4.4. Membrane choice	48
1.4.5. Cell culture on-chip and shear stress.....	50
1.5. CONCLUSION	52
<i>Caco-2 Cell Growth, Differentiation and Evaluation</i>	53
2.1. INTRODUCTION.....	55
2.1.1. Caco-2 cell and transport of nutrients	55
2.1.2. Cell cytotoxicity.....	56
2.1.3. Cell viability	57
2.1.4. Cell monolayer assessment	59

2.2. OBJECTIVES	61
2.3. MATERIALS & METHODS.....	61
2.3.1. Cell culture.....	61
2.3.2. Cytotoxicity evaluation	61
2.3.3. Cell characterization and viability	62
2.3.4. Monolayer assessment.....	63
2.4. RESULTS & DISCUSSION	64
2.4.1. Cytotoxicity evaluation	64
2.4.2. Static vs dynamic cell characterization.....	67
2.5. CONCLUSION.....	73
<i>Transport of Calcium and Peptides using ESI-MS and MALDI-TOF/TOF-MS.....</i>	75
3.1. INTRODUCTION	77
3.1.1. Calcium absorption and dietary deficiency	77
3.1.2. Intestinal absorption of nutrients	79
3.1.3. Analytical techniques.....	82
3.2. OBJECTIVES	85
3.3. MATERIALS & METHODS.....	85
3.3.1. Transport experiment.....	85
3.3.2. ESI-MS Analysis	86
3.3.3. MALDI analysis.....	87
3.4. RESULTS & DISCUSSION	87
3.4.1. ESI-MS evaluation	87
3.4.2. MALDI evaluation of peptides	95
3.5. CONCLUSION.....	105
<i>FINAL REMARKS.....</i>	108
<i>REFERENCES.....</i>	110
<i>APPENDIX A.....</i>	120
<i>APPENDIX B.....</i>	122

OVERVIEW

This thesis is divided into three chapters including all the results obtained during four years of research supported by FAPESP (Grant #2018/11657-4).

Chapter 1 will introduce concepts and techniques of microfabrication, addressing all the materials and results obtained, with the final development of two functional models. One of the developed models is also being used for pharmaceutical applications in collaboration.

Chapter 2 will show the Caco-2 cell characterization, including on- and off-chip cell evaluation, toxicity, and control assays. Moreover, it will compare all the results regarding cell growth on the designed microdevices, and the static commercial model (transwell®).

Chapter 3 will outline all the analytical results regarding the transport experiment of calcium and peptides using two different methodologies, transwell®, and the developed intestine-on-a-chip devices. These results include proteome analysis using mass spectrometry (MS) and MALDI-TOF/TOF-MS.

CHAPTER 1

Development, Fabrication, and Evaluation of Intestine-on-a-Chip Devices

1.1.INTRODUCTION

1.1.1. Lab-on-a-chip and the evolution of pharmaceutical testing

The most conventional methods for analyzing the behavior of intestinal disorders are *in-vivo* and *in-vitro* modeling. Animal testing for pathologies evaluation and drug screening is still very common, but this type of test often fails to predict the function in humans. Moreover, the search for non-animal methodologies is intensifying, given the ethical and efficacy issues related to this approach.¹ *In-vitro* intestine models are commonly used for barrier function studies, using epithelial cell lines cultured on porous membranes of transwell® inserts. Despite the practicality of these devices, they fail to reproduce the expected physiological and morphological intestinal characteristics, since it is a static system.^{1,2}

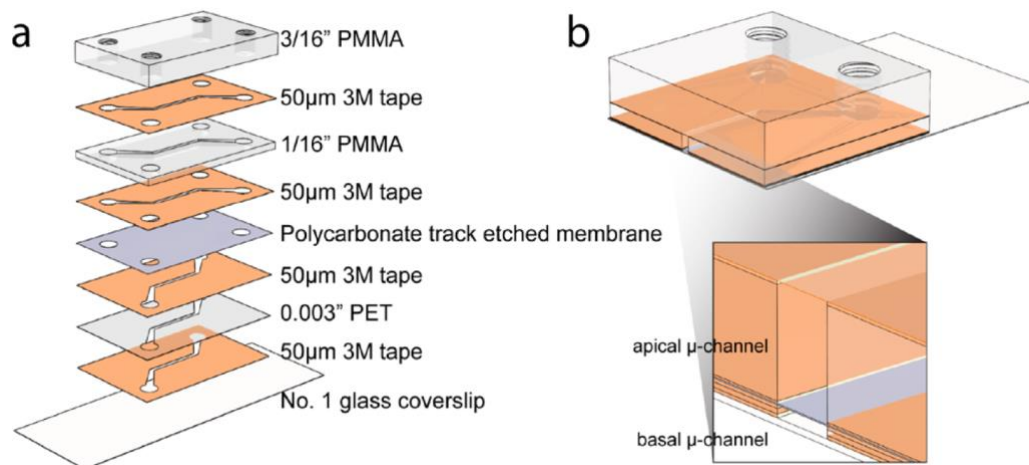
Over the past few years, scientists developed a series of new devices and methods for studying metabolism, nutrition, infection, and drug pharmacokinetics.² Included on this list are *ex-vivo* modeling with the everted gut sac³, using animal-derived tissues for evaluating drug absorption and the Ussing chamber⁴, using surgery-derived human cells and tissues for drug/nutrient transport evaluation. Although offering advances for the medical and pharmaceutical fields, those devices could not faithfully reproduce the morphological and physiological human intestinal environment, presenting a series of disadvantages for drug and nutrient delivery.^{3,4} More recently, organoids, spheroids, and 3D cell culture started to be a reality⁵⁻⁸, by using extracellular matrices (ECM) to grow biopsy-derived stem cells in three dimensions to evaluate organ behaviors. Again, this approach is a huge advance, but alone, it is an unfaithful tool regarding the dynamicity of organs. Moreover, these approaches are inadequate for *non-in-situ* experimentation, invalidating the collection of samples from the 3D gel and disabling its use for drug screening and nutrient absorption studies.²

Recently, the development of the Organ-on-a-Chip (OoaC) created the possibility to resemble specific environments more closely to the human systems bringing the possibility to simulate organ behaviors, such as intestinal absorption, more realistically.⁹ Those OoaC are generally fabricated using techniques originated from the micromachine industry and will be explained in the next topic with details. An example of OoaC - the Intestine-on-a-Chip (Ioac), is usually built of two-hollow microchannels, a porous

membrane, and inlets and outlets for continuous perfusion of culture medium.¹⁰ The most fundamental devices allow immortalized cells to grow inside the channel, bringing the possibility to study the absorption of nutrients, pharmacokinetics (PK), pharmacodynamics (PD), and other barrier function studies.^{11,12} The most advanced models of loaC are now using primary human 3D culture from biopsy to transfer the culture for on-chip differentiation. These devices allow co-culture with vascular cells under continuous flow, cyclic deformation, and exposure to a living commensal microbiome, closely resembling the intestinal environment for advanced medical research.¹³ Among the most common applications for loaCs are the ones aimed for the pharmaceutical, medical, and food industries. The drug development process involves the control of the drug absorption, transportation across the intestine, toxicity, efficacy, and pharmacokinetics. The possibility to use loaC to all these purposes is becoming a frequent reality, besides its use for the elucidation of rare diseases, studying more closely the mechanisms of those¹⁰ Similar to the pharmaceutical industry, nutrients absorption, food metabolism, inflammations, and allergies are important processes for the food industry. Although not much explored by the literature, loaC is now a tool to explore these systems in a more efficient and ethical manner.¹⁰

As the intention of this work was to develop a functional, under the possibilities, inexpensive device for evaluating calcium and peptides transport across the epithelial barrier, simpler devices were used as an initial inspiration.^{14,15} These models allow the growth and differentiation of immortalized cells under continuous fluid flow, not having other characteristics such as peristaltic-like deformation, co-culture, and exposure to the microbiome. However, they represent an advance for nutrient uptake evaluation if compared to static models, saving time with shorter differentiation periods and manufactured with inexpensive materials. A typical model of loaC must contain a membrane support for cell growth, an apical and a basal side for simulating the intestinal environment, and inlets and outlets for the continuous perfusion of culture medium.^{14,15} Figure 1.1-1 shows an illustration of a typical inexpensive loaC device fabricated by laser cutting technique.

Figure 1.1-1. Schematic illustration of an IoaC device using laser cutting as a fabrication method. a) 3D view of the device layers, b) Vertical view of the device illustrating the apical and basal channels.



Source: Reprint (adapted) with permission from Husic S. et al. Rapid Prototyping of Multilayer Microphysiological Systems. ACS Biomaterials Science & Engineering 2021 7 (7), 2949-2963. DOI: 10.1021/acsbiomaterials.0c00190

1.1.2. Materials for OoaC

For developing a new OoaC device, two main factors must be considered, the materials available for fabrication and the techniques that will be applied to the chosen materials to model them. This section will explore the main materials recently used for OoaC production, as well as the major techniques applied for fabricating them. Each organ presents specific characteristics, however, most of the devices are developed under the same fundamental idea, a double-hollow channel with support for cell growth and continuous fluid perfusion.⁹ Therefore, the materials and techniques used to create any OoaC are the same and originated from the micromachine industry.

Among the main materials used for OoaC fabrication are poly(dimethyl-siloxane) (PDMS), glass, and thermoplastics such as poly(methyl-methacrylate) (PMMA or acrylic). Moreover, among the common platforms for cell growth on-chip are PDMS, polyester and polycarbonate membranes or hydrogels, and extracellular matrices for 3D culture.^{16,17}

PDMS presents the most desired characteristics for OoaC production, since it is temperature-resistant, flexible, stretchable, transparent, biocompatible, and gas permeable. In addition, PDMS presents great sealing properties and it is relatively low cost (\$0.30/g).¹⁸ Those are key characteristics for cell characterization and a good

simulation of organ behavior. However, a few downsides of this material are the hydrophobicity, absorbability, and intrinsic fluorescence, which might cause inconveniences for experimentation.¹⁶

Glass also presents desirable features, being transparent, hydrophilic, inert, biocompatible, and low cost (\$ 0.017/g).¹⁹ In addition, this material is very resistant to high temperatures and degradation. Although it may seem like the perfect material, glass is rigid, which is a downside for the majority of organs, and demands time and expensive resources for OoC production.^{16,20}

Among the thermoplastics, PMMA or acrylic is the most widely used for OoaC manufacture. Being biocompatible, low-cost (\$0.015/g)²¹, transparent, and inert, acrylic is easily shaped and does not require exquisite and expensive molding techniques. However, it might present autofluorescence, it is rigid and sensitive to high temperatures and a range of solvents.^{16,22}

As a platform for growing cells, the desirable features of the material are transparency, biocompatibility, adhesion and permeation properties, and easy fabrication. Most of the plastic membranes (polyester (PE), polycarbonate (PC), PDMS) are either track-etched or photolithographed to create the pores. Track-etched membranes are usually expensive due to their complex manufacturing technique, and normally present light scattering under fluorescence microscopes.²³ However, it is a ready-to-use, and easy option for low-manufacturing capabilities laboratories. PDMS instead, requires sophisticated photolithography to manufacture small porous membranes, and besides being a great platform for cell growth, its fabrication is time-consuming and expensive.¹⁶ Other cell supports for OoaC are hydrogels and ECM. Those were originated from 3D organoid culture and are biocompatible, highly permeable, biodegradable, and long-lasting. Although these materials are easily adaptable for cell culture, they are not broadly used for OoaC due to their high stiffness and poor adaptability to fabrication techniques.¹⁶

1.1.3. Fabrication techniques

The fabrication technique will depend mostly on the type of material chosen for building the OoaC and the desired characteristics for this chip. The most widely used techniques for OoaC fabrication are soft and photolithography for PDMS-based chips

photolithography for glass-based, and photolithography, injection molding, and laser cutting for thermoplastics.^{16,24} 3D printing is also becoming an important technique for OoaC manufacture since it is capable of printing entire tissues, matrices, and biomaterials.¹⁶

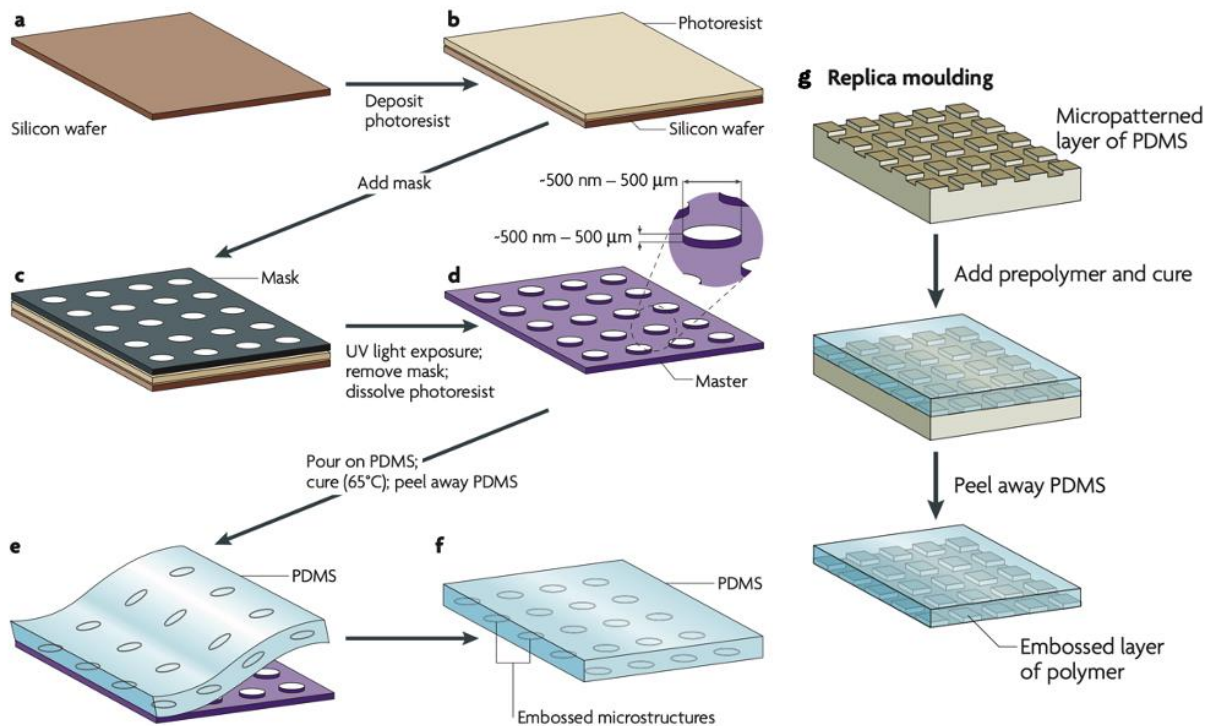
Photolithography is a traditional method developed by the microelectronics industry to develop semiconductors. This technique is destined for the development of photoresists and silicon masters, essential materials for microfluidic fabrication since it is the base for soft lithography. This is also the major approach used for making glass OoaCs, although those are not frequently reported in the literature. This technique though is expensive, limited to clean rooms, and strict substrates, which popularized the use of soft lithography for OoaC.^{16,25}

Soft Lithography is the most widely used technique for OoaC fabrication, due to the wide range of elastomers compatibility. This technique uses silicon masters or simple negative pieces to produce cured devices. There is a range of methods that can be used in this case, such as replica molding, capillary molding, and microcontact printing, among others. This technique was proven adaptable, fast, and low-cost compared to others. Figure 1.1-2 shows the fabrication process of PDMS pieces by using photo and soft lithography.^{16,25}

Injection Molding is a very complex technique with accurate control of temperature, pressure, and injection rate. It can be used for a wide range of polymers and it has advantages such as the independence of a photoresist and the relatively low cost for mass production.¹⁶

Finally, the laser cutting technique is one of the most inexpensive approaches for OoaC development. Normally a CO₂ laser is used in this technique to make precise cuts (micrometer scale) according to the sketch made on AutoCad® or similar software. Although restricted to the laser energy, and material susceptibility to cut, this approach covers a wide range of low-cost materials and is becoming an honest option for limited-budget laboratories.²⁴

Figure 1.1-2. Lithography fabrication. a–b) Spin-coated photoresist c) Mask deposited into the photoresist d) UV irradiation into photoresist followed by mask removal e) Soft lithography cure of PDMS f) Final PDMS piece embossed g) Replica molding process.



Source: Reprint (adapted) with permission from Weibel, D. *et.al*. Microfabrication meets microbiology. *Nat Rev Microbiol* **5**, 209–218 (2007). <https://doi.org/10.1038/nrmicro1616>

1.1.4. Flow control and shear stress

Flow rate is an important parameter to control in OoaC since it directly affects the shear stress, polarity, concentration gradients, and a range of other things. The fluid flow on OoaC works in a laminar regime and flow rate values will depend on the research objectives.²⁶ Mostly, the physiological flow rate is used as a parameter (60 μL/h) and the shear stresses involved will depend on the microchannel dimensions, calculated by equation 1.1.²⁷

$$\tau = \frac{6\mu Q}{wh^2} \quad (\text{Eq. 1.1})$$

Where μ is the fluid viscosity (Pa·s), Q is the flow rate (μL/s), w is the width of the channel (m), and h is the height of the microchannel (m). The shear stress is then expressed in Dyn/cm².

It is possible to control the flow in OoaC using a few techniques, such as pressure-controlled, electroosmotic, shear flow, and a range of others. Pressure and the electroosmotic flow are the most common controls and are operated by using syringe, reciprocating and peristaltic pumps. Syringe pumps are the most broadly used, due to their convenience.¹⁶

1.1.5. Sterilization methods

Sterility is an important element for cell culture and microfluidic devices require an accurate procedure to guarantee that all components are safe against microbial contamination. The sterilization process will be highly dependent on the type of material used for the device fabrication and must be carefully considered to avoid damaging the device material and components.²⁸ Autoclave sterilization is one of the most common methods used, although it is not adequate for low-thermal resistant polymers such as PMMA, PC, and PE. For temperature-resistant materials instead, such as PDMS and glass, this is a low-cost, and efficient technique.²⁸ Other common techniques, that are available in any cell culture laboratory, are UV and ethanol disinfection. Although it is an easy option for sterilization, PMMA is incompatible with ethanol, and PDMS absorbs ethanol for long periods of contact, interfering with cell growth. Moreover, UV light penetration is limited to the surface of the materials and is affected by the material's opacity. Gamma irradiation instead, penetrates the entire material, guaranteeing full sterilization. Similarly, ethylene oxide and other gas treatments provide full and clean sterilization. Even though these last methodologies are the most indicated and easily applied to most materials, they are time-consuming and costly.^{28,29}

1.2. OBJECTIVES

This part of the research aims to fully develop a functional device capable of growing intestinal-like (Caco-2) cells, also known as Intestine-on-a-chip. Also, to characterize this device and define whether it is capable of performing transport experiment of nutrients.

1.3. MATERIALS & METHODS

1.3.1. Devices design and fabrication

The process of creation included drawing, cutting, and assembling the devices. The first step of the development was drawing the pieces and figuring out their assembly. The chips design was inspired by (Ma *et al*, 2021)³⁰ and by (Kasendra *et al*, 2018)¹³. The pieces were designed by using AutoCAD® and cut into a laser cutter (Kawai 13 Combat Laser 600 x 400 High Power CO₂). For the PDMS pieces, soft lithography and laser cutting techniques were used. During the research, 5 different models were developed, they are named chips #1, #2, #3, #4, and #5.

Chip #1 materials were silica capillary (ID: 74.4µm, ED: 193.6µm) silica capillary (ID: 76.9µm, ED: 362.6µm), Cyclopore track-etched PC membrane from Whatman® (47mm, 0.4 µm), a dialysis tubing cellulose membrane from Sigma Aldrich® (14kDa) and a PE membrane (24mm, 0.4µm) from a Corning® transwell® insert, transparency sheets (Acetate) and ARcare® double-sided tape (model 90106NB, 142µm thickness). This prototype was entirely made by using the laser cutter and was assembled manually.

Chip #2 materials were silica capillary (ID: 76.9µm, ED: 362.6µm), dialysis tubing cellulose membrane from Sigma Aldrich® (10mm, 0.4in), pipette tips (200µL), transparency sheets (Acetate) – for the covers, and ARcare® double-sided tape for the channel. This prototype was entirely made by using the laser cutter and was assembled manually. The top inlets were made of pipette tip pieces, cut using scissors, and glued using Araldite® Hobby.

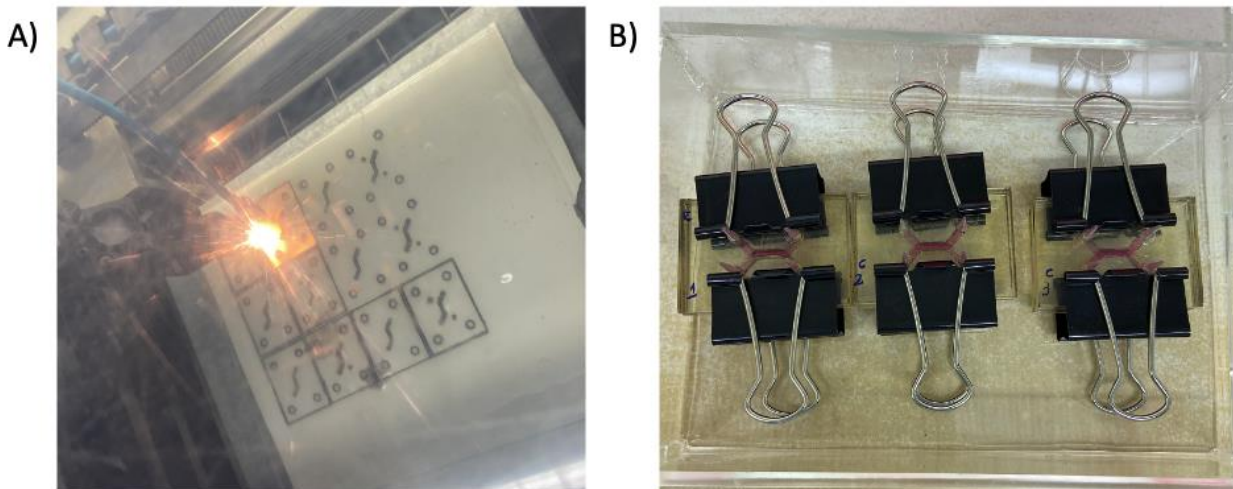
Chip #3 materials were a dialysis tubing cellulose membrane from Sigma Aldrich® (10mm, 0.4in), a Cyclopore track-etched PC membrane from Whatman® (47mm, 0.4µm), pipette tips (200µL), transparency sheets (Acetate) – for the covers, and ARcare® double-sided tape for the channel. This prototype was entirely made by using the laser cutter and was assembled manually. The inlets and outlets were made of pipette tip pieces, cut using scissors, and glued using Araldite® Hobby. Later, the whole pipette tips were glued to the chip.

Chip #4 materials were a transparent PE membrane from Corning® transwell® (24mm, 0.4µm pore), and a white track-etched PE membrane from GVS® (47mm, 0.4µm).

pipette tips (200 μ L), Acrylic sheets (2mm thick), and ARcare[®] double-sided tape. This prototype was entirely made by using the laser cutter and was assembled manually. The inlets and outlets were made of pipette tip pieces, cut using scissors, and glued using PVC glue from Tigre[®]. The final membranes used for both chips #4 and #5 were detached from transwell[®] inserts and cut into the laser cutter. Assembled chips were submitted to pressure using clippers for gluing better.

Chip #5 materials a transparent polyester membrane from Corning[®] transwell[®] (24 mm, 0.4 μ m pore), a white track-etched PE from GVS[®] (47mm, 0.4 μ m), pipette tips (200 μ L), Acrylic sheets (2mm thick), PDMS (SYLGARD[™] 184 Silicone Elastomer Kit), and ARcare[®] double-sided tape. The PDMS was cured by replica molding soft lithography into a lab-made tray, homogenized by manual adjustment, and placed into a 70[°] C incubator for 4 hours. Then, the pieces were cut into the laser cutter and assembled manually. The inlets and outlets were made of pipette tip pieces, cut using scissors, and glued using Polyvinyl Chloride (PVC) glue from Tigre[®]. Figure 1.1-1 shows pictures of the fabrication process.

Figure 1.3-1. Pictures of the fabrication process: A) laser cutting of PDMS sheet covered with Arcare[®] tape, B) Device #4 with the clippers to ensure adherence.



Source: Own authorship.

1.3.2. Flow control test

Flow control testing was performed to guarantee that the devices would not have clogs, leaks, or collapses under the required flow rates. Therefore, all models were evaluated with food coloring (green, yellow, red, and blue). For microchip #1 the assay was made by adding red color on top of the membrane and water at the bottom. In the beginning, the red color goes out on top and water at the bottom. As soon as the membrane allows permeation, the liquids mixture generates a pinkish color scaping both outlets. For chip #2 the assay was made by using a culture medium, and this chip was quickly disregarded due to intense leakages on the first attempt. For the following models #3, #4, and #5 two different colors were used, one for the top, and the other for the bottom, being possible to check the exact point of possible leaks or holes.

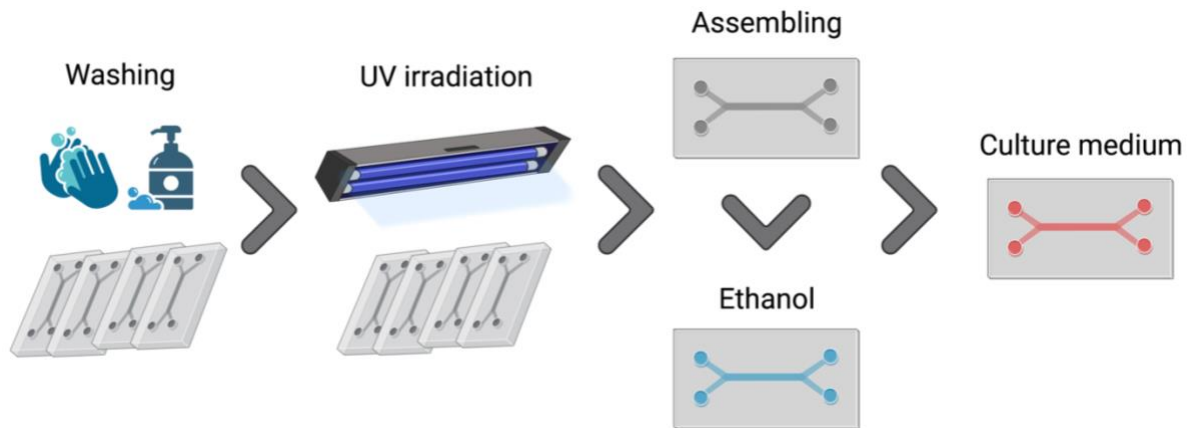
All flow tests were made by using syringe pumps (New Era pump systems NE-300 and NE-1000), by gradually increasing the flow rates of the dyes to check the point of fatigue of these chip models. Models #4 and #5 did not reach a fatigue point until 50 $\mu\text{L}/\text{min}$, then it was decided to stop the experiment by this point since higher flow rates would not be used anyway.

1.3.3. Sterilization

This chapter's introduction presented a few of the common methods of sterilization used for organ-on-chips. For the chip models developed in this research, a few methods were analyzed and a final methodology was adequate for the final microchips created #4 and #5. This method consisted in washing each piece after cutting, submitting each side of the piece to UV disinfecting irradiation for 3 hours, assembling, washing the channel with ethanol, and then washing the channel with culture medium. Figure 1.3-2 shows a schematic for the methodology used.

Materials: Laminar Flow Hood (LFH), ethanol 70%, detergent, Dulbecco's modified Eagle's medium (DMEM) high glucose (4,500 mg/L glucose) with L-glutamine (without pyruvate) (Gibco/Invitrogen, cat. no. 41965-039) supplemented with 10% fetal bovine serum (FBS), 1% 100X nonessential amino acids (Gibco/Invitrogen, cat. no. 11140-035) and 1% PEST (penicillin 10,000 U/mL – streptomycin 10,000 mg/mL solution (100X); Gibco/Invitrogen, cat. no. 15140-122).

Figure 1.3-2. Schematics of sterilization methodology. The image shows all the steps used for decontaminating the microchips.



Source: Own authorship created with Biorender.com.

1.3.4. Cell culture on-chip and shear stress

Caco-2 cell line (ATCC® HTB-37™) was cultured under culture flasks and sub-cultured at least once a week. For seeding cells on chip, they were trypsinized and resuspended in culture medium, counted, and diluted to a concentration of $3 \cdot 10^6$ cells/mL. Cells were then injected into the apical (or top) side of the chip and incubated for 5 hours under 5% CO₂ and 37° C. After this, the devices were submitted to a continuous flow rate of 1 μL/min for 8 days and routed to the transport experiment. Cell culture and all processes related to cell characterization are more detailed in Chapter 2. For the shear stress experiment, cells were submitted to the same process mentioned above and after incubation, each of the four microdevices was submitted to its respective flow rate (0.2, 0.5, 1, and 10 μL/min) for 8 days at 37° C, to verify possible changes in cell growth and differentiation according to the applied shear stress.

Materials: LFW, CO₂ incubator (Water Jacketed – Forma Scientific), Orbital Shaker (Marconi MA410), Neubauer counting chamber (Blaubrand®), inverted optical microscope (Olympus CKX41), syringe pumps (New Era pump systems NE-300 and NE-1000), sterile syringes (3mL), polystyrene cell culture flasks (Corning, US), BD Asepto Scalp, Trypsin-EDTA solution (Sigma Aldrich® MFCD00130286), PBS (Phosphate buffer solution), ethanol 70%, DMEM high glucose with L-glutamine (without pyruvate) (Gibco/Invitrogen cat. no. 41965-039) supplemented with 10% FBS (Vitrocell Embriolife),

1% 100x nonessential amino acids (Gibco/Invitrogen cat. no. 11140-035) and 1% PEST (penicillin 10,000 U/mL streptomycin 10,000 mg/mL⁻¹ solution (100X); (Gibco/Invitrogen cat. no. 15140-122), and Trypan blue solution 0.4% (CAS 72-57-1 Sigma Aldrich®).

1.4. RESULTS & DISCUSSION

The original idea for the loaC required infrared transparency since it was supposed to be a device for real-time analysis of calcium under a microscopy Fourier Transform Infrared (FTIR). This idea required using a non-interfering material for FTIR as well as being transparent under a microscope. The best choice was using CaF₂ windows as a supporting material for this chip, then the search for a fabrication method started. Since CaF₂ cannot be cut into the laser cutter, acid corrosion with chloric and nitric acids was used instead, although it did not succeed in showing imperceptible corrosion to the material and small depth numbers under the profilometer. Therefore, it was decided to pursue a different strategy, using different materials and approaches for calcium detection. It was decided to use Electrospray Ionization Mass Spectrometry (ESI-MS) as an approach for the calcium evaluation, eliminating limitations of material choice for the chip development.

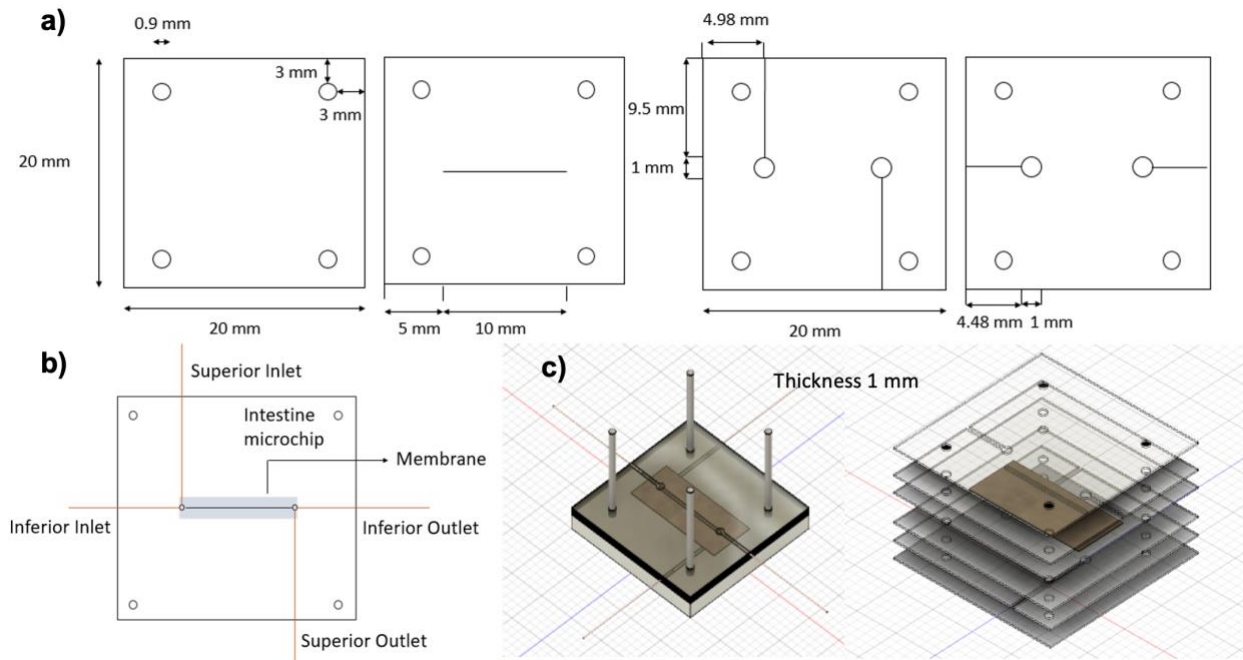
1.4.1. Devices design and fabrication

A full development of a functional OoaC is laborious and complex considering the fabrication limitations and the whole learning process. During this research, five different types of devices were developed and analyzed, as mentioned above in the materials and methods section. While issues appeared, the design and materials changed to finally obtain two functional devices.

Model #1, the first designed, was inspired by (Ma *et al*, 2021)³⁰ and used silica capillaries for the inlets and outlets. Capillaries were used in an effort to directly connect them to the ion source of the MS for real-time analyses. This microchip is composed of two inlets and two outlets, one set above and the other below the membrane, all connected to the microchannel. A few types of membranes were investigated for use in this chip to figure out the desired characteristics to attend this chip's needs, and this will be better explained in the topic "membrane choice" of this chapter. Figure 1.4-1 shows

the design, dimensions, and assembly of this chip that was later disregarded due to clogs formed during the cell injection.

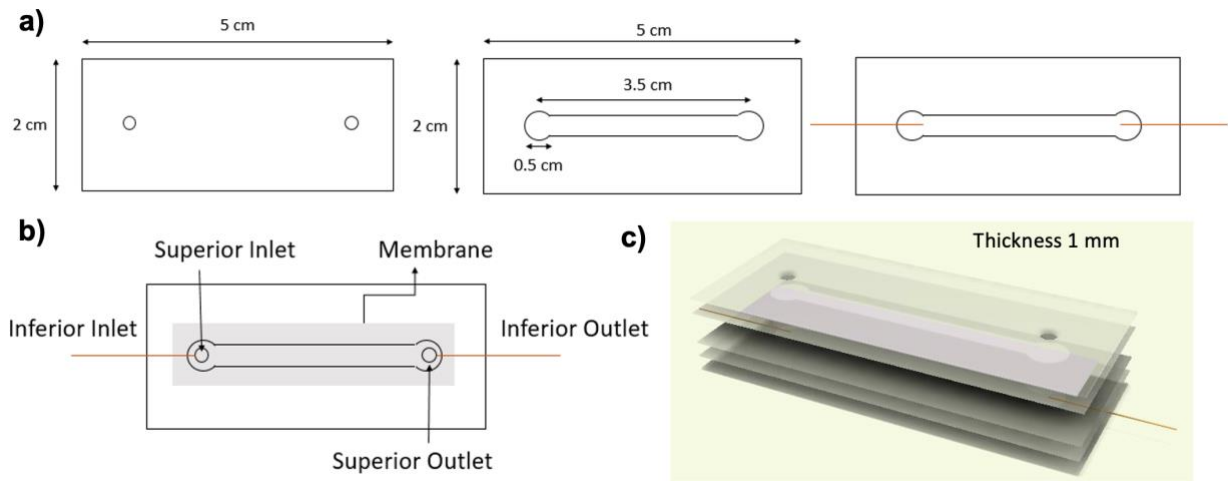
Figure 1.4-1. Design, dimensions and 3D view of the device #1 a) Pieces of the chip with their dimensions b) Top view of the device with the indication of the main components and c) 3D view indicating the assembly of the device.



Source: Own authorship.

The second device, #2, was designed inspired by the same idea as the former, but with a larger channel for better accommodating the Caco-2 cells. This microchip is as well composed of two sets of inlet and outlet connected to the channel through the membrane. The inlets in this prototype are made of pipette tips and the outlets, of silica capillary. Figure 1.4-2 shows the design, dimensions, and assembly of chip #2. This model was disregarded during flow testing, in which it collapsed due to the intense pressure caused by its mismatched proportions.

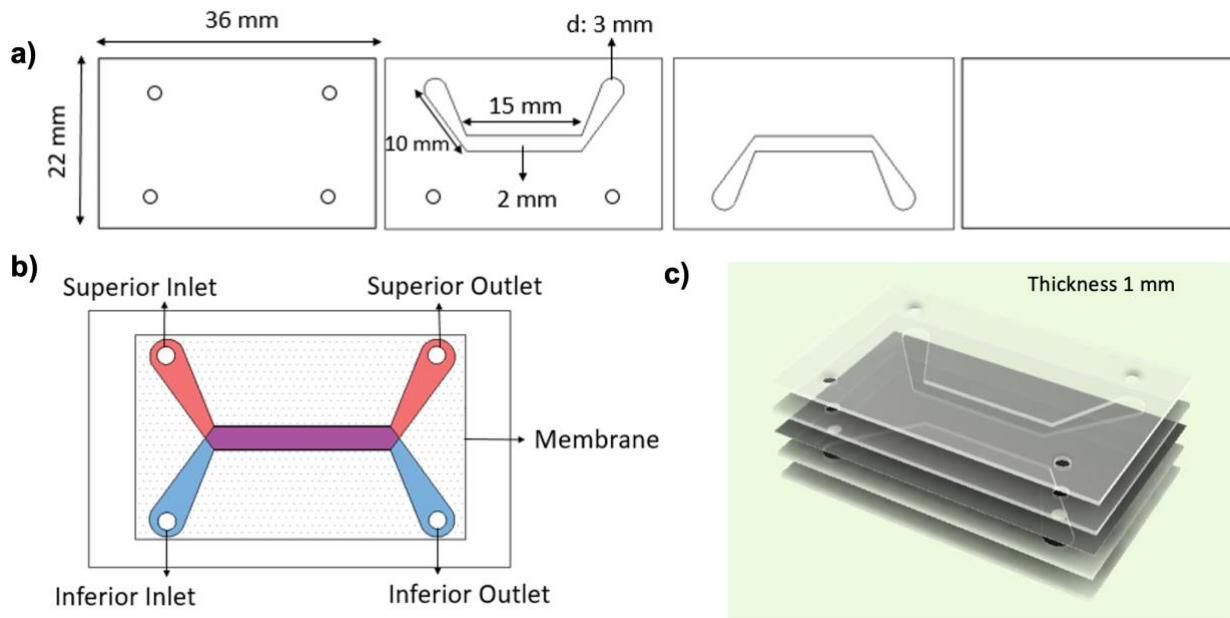
Figure 1.4-2. Design, dimensions and 3D view of the loaC #2 a) Pieces of the chip with its dimensions b) Top view with key components of the chip and c) Assembly of the chip under a 3D view.



Source: Own authorship.

The third prototype, #3, was designed inspired by (Kasendra *et al*, 2018)¹³, containing a larger channel compared to #1 and a different approach for inlets and outlets to ensure a tender flow with less pressure, making the introduction of cells easier. This microchip is composed of two sets of inlet and outlet made of pipette tips, placed above and below the membrane, all connected to the channel. The membranes used for this chip were a dialysis tubing cellulose membrane and a track-etched PC membrane. The better design guaranteed the best possibility to work with low-cost materials, although later, these materials had proven to be inadequate for a long period of cell culture. Figure 1.4-3 shows the schematics for the chip design, dimensions, and assembly.

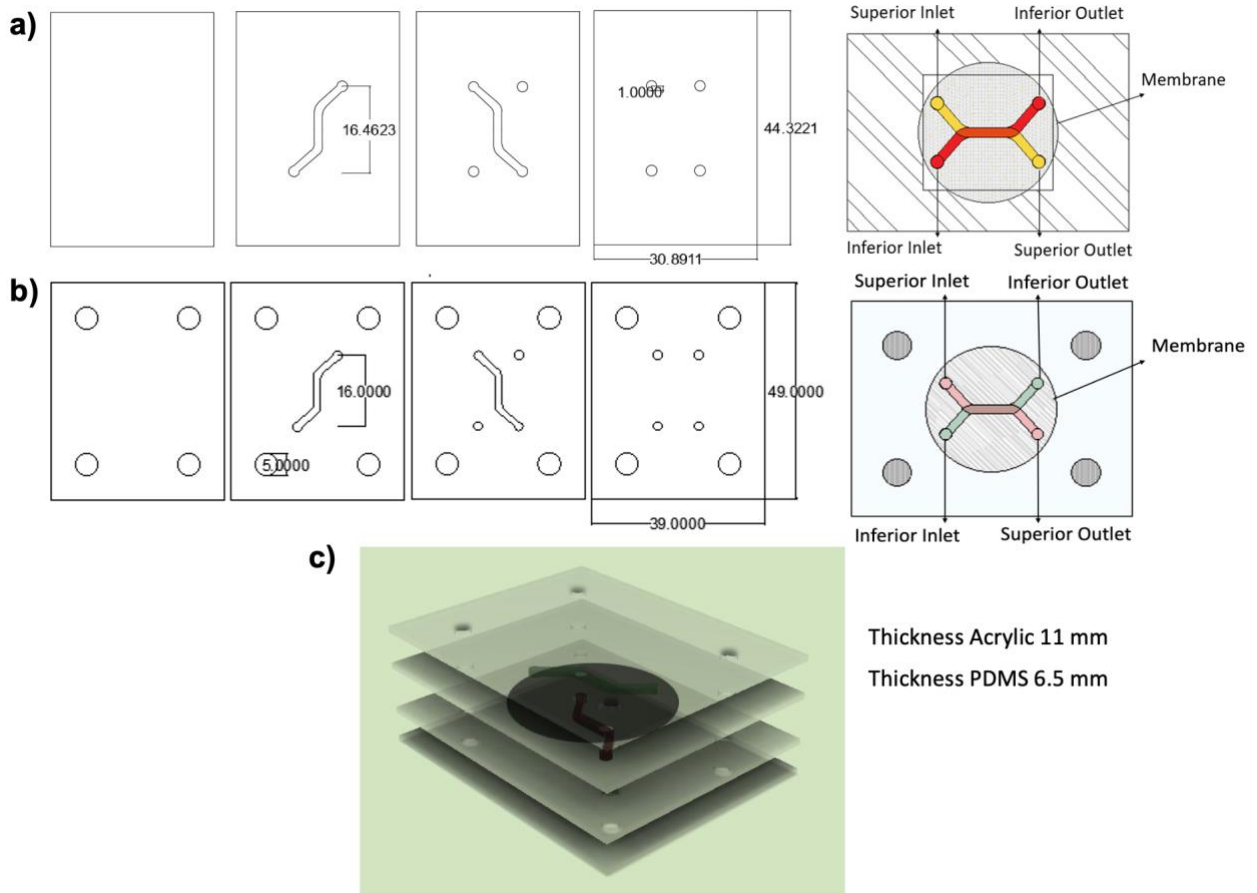
Figure 1.4-3. Design, dimensions and 3D view of the loaC #3 a) Pieces of the chip with dimensions b) Top view with key components of the chip and c) 3D view with chip assembly.



Source: Own authorship.

The last two models #4 and #5 were also inspired by (Kasendra *et al*, 2018)¹³, but used more robust materials since #3 fell apart after more than 4 days of continuous experiments. The assembly of these chips is the same as the others, having an apical and a basal side divided by a porous membrane. The inlets and outlets are made of pipette tips and the membranes used were track-etched PE and PC membranes to resemble the transwell® assay. Both models #4 and #5 present the same design, changing only the materials used for constructing these devices. For #4 all layers are made of acrylic and junctions of ARcare® double-sided tape. For #5, the layers (channel) were made of PDMS and ARcare® double-sided tape, and the covers, of acrylic. This later model also contains four sets of bolts and nuts to seal the chip. As these two models were the ones used for further experiments they will also be mentioned in this thesis as Acrylic and PDMS chips, respectively. Figure 1.4-4 shows the models' design, dimensions, and 3D view.

Figure 1.4-4. Design, dimensions, and assembly of the loaC models #4 and #5 a) Pieces of chip #4 (Acrylic) with their dimensions (mm) and top view b) Pieces of chip #5 (PDMS) with dimensions and top view, and c) 3D view of chip #5 showing its assembly.



Source: Own authorship.

Prototypes #4 and #5 presented better results regarding cell culture, draining, and robustness. These final devices are being applied not only for Intestine-on-chip purposes but for Lung-on-chip as well, in a collaboration. Model #5 or PDMS chip, also counts with the advantage of reuse, since it is a portable device with the possibility of disassembling. However, it is important to emphasize that the replica molding of the PDMS is a crucial step, in which perfectly uniform pieces must be made to pass the flow test.

Since the whole intention of this research was to find a way to create an inexpensive device, the estimated general and individual costs for the developed chips are shown in Table 1.4-1. The final estimated costs per unit of each device are US\$0.80 for #4 and US\$3.74 for #5, being the last one reusable. These final values are not considering the costs involved in the fabrication, such as the use of a laser cutter and its expenses.

Table 1.4-1. Estimating costs for the developed devices according to the materials used.

Material	General cost (US\$)	Cost per unit #4 (US\$)	Cost per unit #5 (US\$)
Acrylic	Board (2/1000/2000 mm) - 80	0.22	0.16
PDMS	0.5 kg - 125	-----	0.60
Arcare tape*	-----	-----	-----
Pipette tips	1000 pack - 90	0.36	0.36
Nut and bolt	50 pack - 15	----	2.40
Membrane**	10 sheet pack - 430	0.22	0.22
Final cost (per chip)	-----	0.80	3.74

*Arcare tape is donated by Adhesives Research® and it is not available for sale.

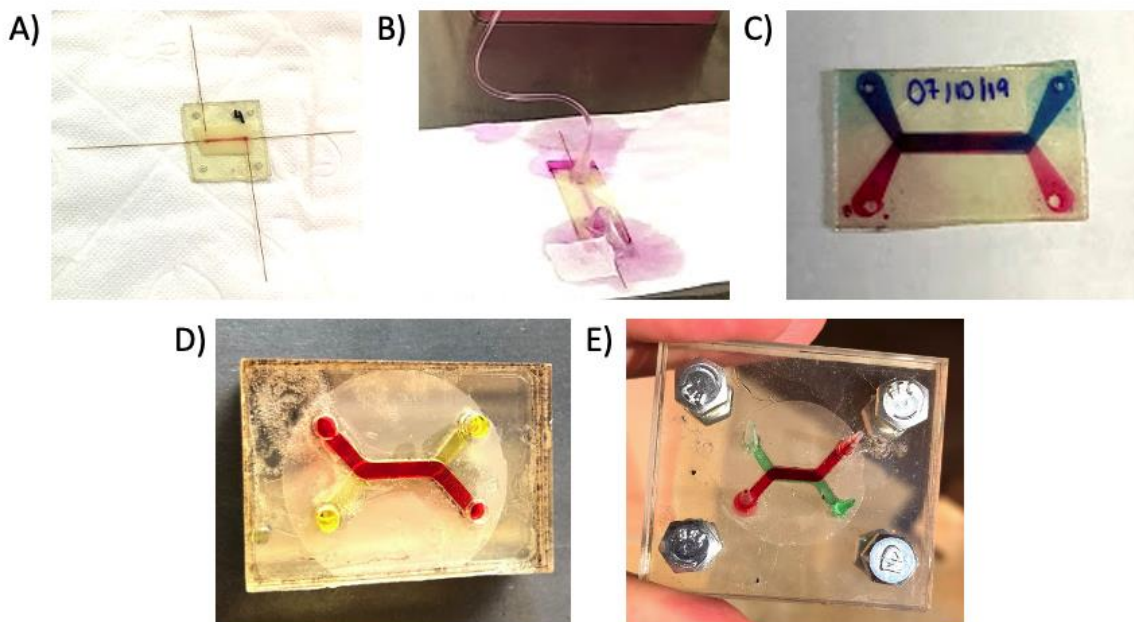
** Membrane prices will vary according to the specificities. For this estimation, a PE track-etched transparent membrane sheet from IP Cell Culture™ was used for calculations.

1.4.2. Flow control test

After designing, cutting, and assembling the desired models of devices, the next step was analyzing possible leaks and tension points. All models' designs passed through this checking point and it was possible to dismiss one of the models during this step. This test was also important to correct a few details during the fabrication, such as rounding edges and piece dimensions. For model #1, flow tests indicated tension, causing leakages, which was crucial to start making round edges on the channel. After this change, flow tests indicated that the membrane permeation occurred within less than one minute using 1 $\mu\text{L}/\text{min}$ flow). It was also observed that flow above 3 $\mu\text{L}/\text{min}$ caused the chip to collapse because of the high pressure caused inside. For chip #2, the flow test evidenced a huge pressure caused by the different proportions of the ins and outlets, causing the chip to collapse and leak, leading the fabrication to different approaches. Device #3 presented no issues during the flow test, although it presented problems during the culture of cells. Flow tests showed the possibility to use up to 5 $\mu\text{L}/\text{min}$ flow without compromising this chip. Although this chip did not present flow problems, cell culture for more than 4 days with continuous perfusion of culture medium, compromised this chip structure. Due to the

persistent stress, this chip collapsed in a few experiments for more than 4 days, presenting leakages. Devices #4 and #5 allowed flow rates up to 50 $\mu\text{L}/\text{min}$ without collapsing. Cell culture was carried out for up to 8 days for both devices and no leakages were observed for the majority of the experiments, although for cell growth, it was used flow rates below 10 $\mu\text{L}/\text{min}$. Therefore, these models were suitable for the transport experiments, the focus of this work. Figure 1.4-5 shows pictures of the flow testing for the different devices.

Figure 1.4-5. Flow testing with different colored dyes: A) chip #1 flow test approved, B) chip #2 flow test failed, C) chip #3 flow test approved, D) chip #4 flow test approved and E) chip #5 flow test approved.



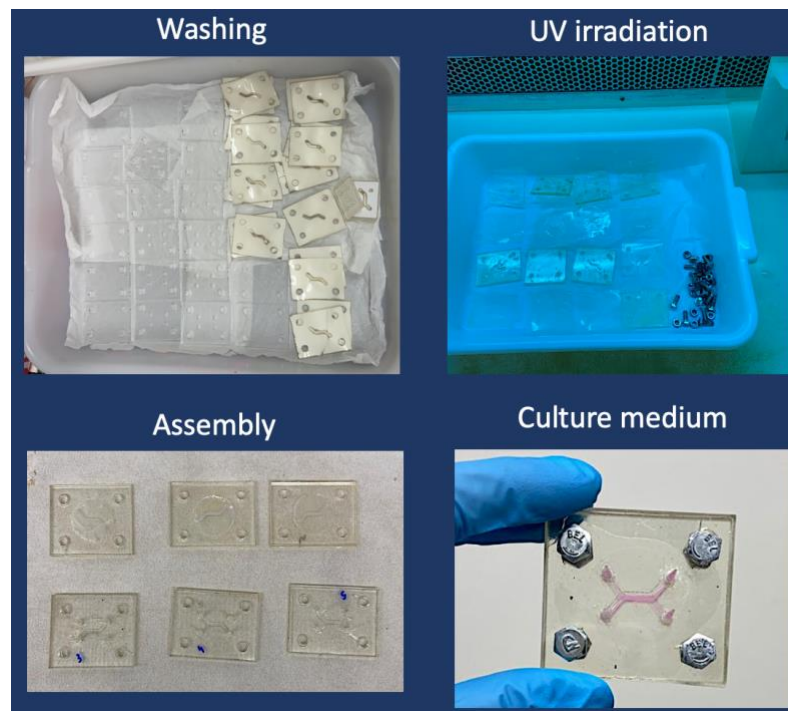
Source: Own authorship

1.4.3. Device sterilization

Considering that only chips #4 and #5 were used for further transport experiments, the sterilization methods addressed in this section are related to these devices. Both #4 and #5 were submitted to the same sterilization experimentation, which was autoclaving the pieces, washing, and UV irradiating with ethanol 70%. The autoclave approach would be a good choice, but the acrylic pieces melted at high autoclave temperatures. Therefore, the strategy used for sterilizing the pieces was soap/detergent washing, followed by ultraviolet irradiation for 3 hours on each side. Additionally, before cell seeding, ethanol 70% was infused into the channels to guarantee they were disinfected and the chip was

washed with culture media before seeding. It is important to highlight that a few devices were contaminated, not necessarily due to the sterilization process, but sometimes because of an eventual contamination opening spot. Figure 1.4-6 shows pictures of these processes.

Figure 1.4-6. Process of device sterilization including a few steps used for this matter. From left to right, top to bottom, this image shows the washing, UV irradiation, assembly, and culture medium infusion of chip #5.



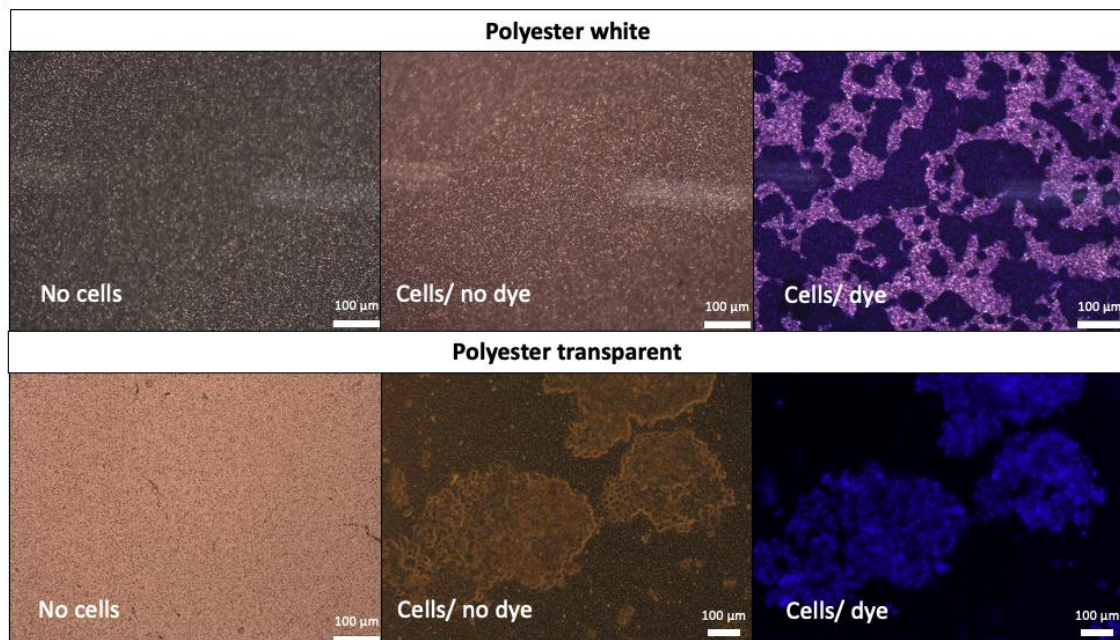
UV – Ultraviolet
Source: Own authorship

1.4.4. Membrane choice

There are a few types of platforms for growing cells on-chip as mentioned previously in the introduction section of this thesis. The best choice for this project, considering the facilities, materials, and equipment available, was to buy ready-to-use membranes. A few types of membranes were evaluated to choose the best for this application. Usually, for cell growth, PC, PE, PDMS, and cellulose membranes are the most common. For this work, a transparent membrane with an adequate pore size would be a perfect choice, since it is possible to follow cell growth along the days under the microscope, using no dye. Considering this, cellulose, PE, and PC membranes were investigated, being only

cellulose and PE (detached from transwell®) transparent. All the analyzed membranes were good surfaces for cell growth, although track-etched PC and PE membranes (white) presented opacity under the optical microscope (Olympus CKX41), resulting in no visibility of cells without a dye. PE transparent membrane (detached from transwell®) was the best choice for this application, showing good visibility under both optical (Olympus CKX41) and fluorescence microscopes (Zeiss Axio Observer Z1). The cellulose membrane was adequate for cell growth and visibility; however, it was non-viable for this project, since its pores are too tiny for transport experiments. Figure 1.4-7 shows comparative images of cell culture with a transparent and a white opaque membrane. It is possible to observe that without a dye, cells cannot be seen under an inverted microscope with a white membrane, while with a transparent membrane, cells are watched either with or without a dye. The dyes used for this purpose were crystal violet (Sigma Aldrich ® CAS 548-62-9) for the inverted microscope and DAPI (1mg/mL) (Thermo Fisher cat. no. 62248) for the fluorescence microscopy. Fluorescence microscopy was carried out by using a mercury arc lamp, with a DAPI filter for its detection at the excitation/emission wavelengths of 358/461 nm.

Figure 1.4-7. Comparison between white (up) and transparent (down) PE membranes showing fluorescence and optical microscopy images (10x magnification). From left to right, an image of the membrane, the membrane with cells, and the membrane with stained cells.

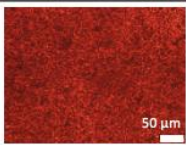
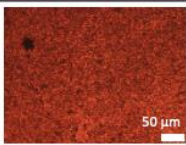




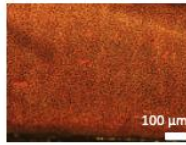
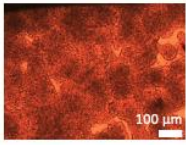


Source: Own authorship

1.4.5. Cell culture on-chip and shear stress

For Caco-2 cell seeding inside the chip, cells were trypsinized and resuspended in culture medium at a concentration of $3 \cdot 10^6$ cells/mL at passages 50-70. After 5 hours post seeding incubated under 37°C and $5\% \text{CO}_2$, cells were submitted to a continuous flow of culture medium under 37°C incubation. Microchips #4 and #5 were submitted to cell seeding and all control assays for further transport experiment of nutrients. Table 1.1. shows the flow rate of the culture medium used and their respective calculated shear stresses for each device. After an 8-day growth, it is possible to identify that the cells are all attached and differentiating, indicating that these flow rates were not harmful to the cell layer. Also, the different flow rates did not indicate any perceptible distinction for cell differentiation, meaning that the tensions used were not a threat to cells detaching from the membrane. After evaluating this, all chips used in experiments were submitted to $1 \mu\text{L}/\text{min}$ flow rate of culture medium, equivalent to the physiological fluid flow.¹³ The $10 \mu\text{L}/\text{min}$ flow rate was used for the further transport experiment of calcium and peptides, to obtain a sufficient amount of sample to analyze.

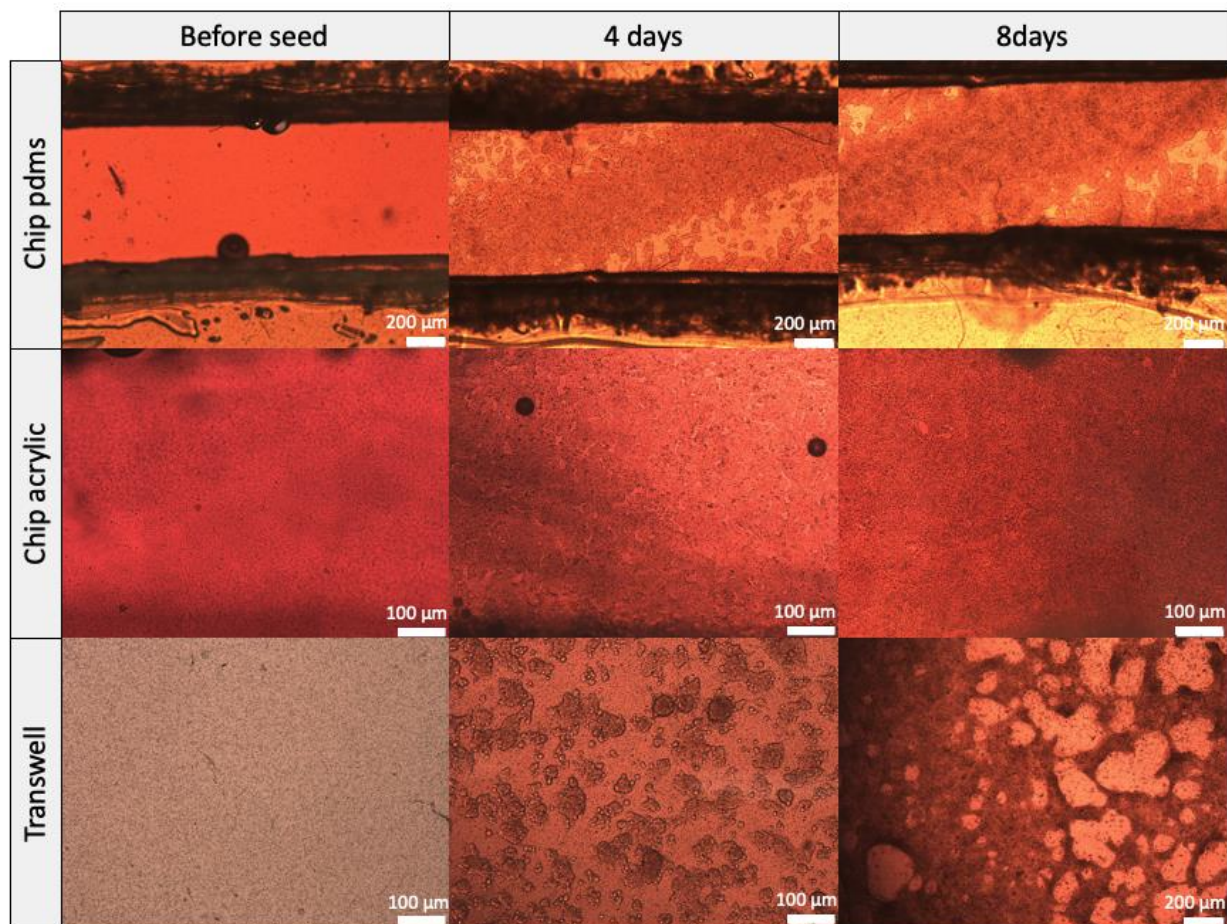
Table 1.4-2. Comparative cell growth for devices #4 and #5 under different flow rates and consequently, distinct shear stresses.

Flow rate ($\mu\text{L} \cdot \text{min}^{-1}$)	Shear stress #4 (Dyn.cm ²)	Shear stress #5 (Dyn.cm ²)	8-day #4 culture	8-day #5 culture
0.2	$2.24 \cdot 10^4$	$1.02 \cdot 10^5$		
0.5	$5.60 \cdot 10^4$	$2.55 \cdot 10^5$		
1	$1.12 \cdot 10^5$	$5.10 \cdot 10^5$		
10	$1.12 \cdot 10^6$	$5.10 \cdot 10^6$		

*All images are 20x magnified, except for the $10 \mu\text{L}/\text{min}$ line, which are 10x magnified.

As a matter of comparison, a sequence of optical microscopy images was taken for the three platforms (PDMS chip, acrylic chip, and transwell® static culture) during the cell differentiation and is shown below in Figure 1.7. It was observed that under a continuous flow of culture medium over 8 days, the cells presented a high confluence into the microchips, covering the microchannel area. While in the transwell®, the cells are far from the confluency, showing to cover the whole area satisfactorily only by the 21st day of culture as already reported and confirmed by the literature.^{9,11,15} Further cell characterization on-chip and off-chip will be presented in Chapter 2 of this thesis.

Figure 1.4-8. Comparative cell growth and differentiation in different platforms. Optical microscopy of the loaC channels and transwell® before seed, 4 and 8 days of differentiation.



*Images for PDMS chip are 4x magnified and for acrylic chip and transwell® are 10x magnified.
Source: Own authorship.

1.5. CONCLUSION

Organ-on-a-chip is becoming an important substitute for pharmaceutical and nutritional assays, showing results that more closely resemble the reality of physiological processes. In this work, two functional devices (#4 and #5, or Acrylic and PDMS loaC, respectively) were fully developed, by using simple techniques such as laser cutting and soft lithography, and inexpensive materials such as acrylic and PDMS. The costs of the developed devices were estimated based on their materials and dimensions, obtaining rough costs of US\$0.80 for #4 and US\$3.74 for #5 and highlighting the possibility of reuse for #5. Flow testing indicated that those devices allowed fluid flow up to 50 $\mu\text{L}/\text{min}$, being adequate for long experiments under intense shear stress. The device sterilization was developed according to the materials' properties and has proven to be adequate since the minority of the devices presented contamination. The membrane choice for Caco-2 cell growth on-chip was majorly based on the detection methods for ensuring cell visibility since all the evaluated membranes allowed cell growth. As a practical choice, transparent PE membranes detached from transwell® filter supports were used for the final microchips, allowing full visibility of unstained cells. The final devices were also submitted to different culture media flow rates during an 8-day cell differentiation process. The flow rates applied indicated no perceptible difference for cell growth and differentiation, and proven to be of no danger for the cell layer detaching from the membrane. Finally, it was possible to apply the physiological fluid flow (1 $\mu\text{L}/\text{min}$) for Caco-2 growth on-chip and establish a faster differentiation compared to the static model (transwell®).

CHAPTER 2

Caco-2 Cell Growth, Differentiation and Evaluation

2.1. INTRODUCTION

2.1.1. Caco-2 cell and transport of nutrients

Caco-2 cell (ATCC® HTB-37™) is a line of immortalized human epithelial colorectal adenocarcinoma recognized for its ability to spontaneously differentiate and reach confluence under normal culture conditions (glucose and serum). This cell line presents morphological polarity, total development of brush borders and microvilli, formation of intracellular junctions, and, therefore, the progression of a uniform monolayer of enterocyte-like cells, in a period of 20-30 days.³¹ An important occurrence in the differentiation process is the development of tight junctions (TJ), defined as intersections between cells made essentially of proteins found in epithelia, the occludens. These TJ form a barrier, separating two regions of the cell, the luminal (or basal) and the apical, allowing selective permeation of nutrients, consequently being the most important step to the paracellular pathway. Given these characteristics and the similar profile compared to intestinal absorptive cells, the Caco-2 line is widely used as a model for small intestine absorption studies.³¹

Caco-2 cells are usually grown in serum-containing cell culture medium (DMEM – Dulbecco's Modified Eagle Medium) in normal (non-treated) culture flasks. These cells attach strongly to the plastic of the tissue culture flasks, forming cell clusters, which are later transferred to permeable flasks for transport studies.³² Transport assays are classically performed using permeable cell culture inserts with certain specifications (0.4µm pore/ TC- treated). The seeding is made by using the same culture medium (DMEM + serum) but with a specific periodicity to ensure the formation of a perfectly functional monolayer with the expression of the right transporters. A cell passage is the number of times that these cells were subcultured, and this is an important parameter for experiments involving the transport of substances across an epithelial barrier. Although there is not much consensus, higher passages offer the expression of important proteins for transport, being recommended for this type of study, passages from 50-70.^{33,34}

A range of factors including permeability, solubility, dissolution, substance active transport, and in some cases, pre systemic metabolism, influences absorption of nutrients. In order to be absorbed by the organism, the nutrient must cross a series of barriers in the gastrointestinal (GI) tract, including the mucosa, lamina propria and most importantly, the

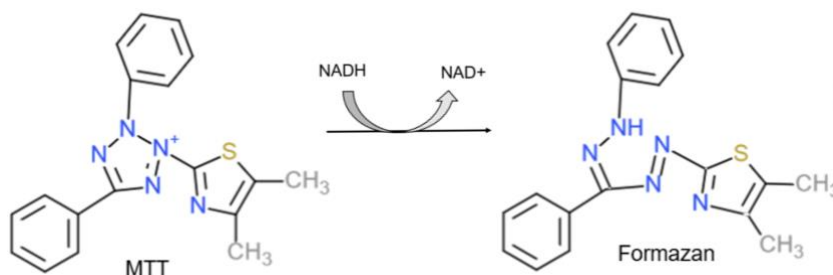
monolayer of epithelial cells (epithelia). Therefore, an *in-vitro* model of the small intestine was created to study the absorption of nutrients, the so-called transwell® assay, in which permeable flasks are used to grow and maintain a monolayer of Caco-2 cells, and to evaluate drugs and nutrients passing through it.^{35,36}

Transport experiments are carried out based on a protocol³⁷ for the correct use of the transwell®. A series of checkpoints are made in the whole process, including cell viability assays, assessment of monolayer integrity, and the detection of the transported substance. The transport of calcium and peptides across the transepithelial barrier, and their mechanism will be better explained in Chapter 3 of this thesis.

2.1.2. Cell cytotoxicity

Cytotoxicity is an important factor to consider in absorption experiments, since the target substance may be a potential danger to the cell monolayer integrity. In this work, MTT (3-(4,5-dimethylthiazol-2-yl)-2,5-diphenyltetrazolium bromide) was used as a marker to determine cell viability after treatment with a range of different solutions.³⁸ This experiment consists of the reduction of MTT to formazan through the action of oxidoreductase mitochondrial enzymes present in living cells. The mechanism consists of the reduction of MTT caused by nicotinamide adenine dinucleotide phosphate (NADPH)-dependent enzymes, only present in live cells. The reduction turns MTT into formazan, which are purple in ethanol solution. Figure 2.1-1 shows the redox reaction. It is possible to detect live cells by using the absorbance of formazan ($\lambda_{\text{abs}} = 570\text{nm}$) monitored in an UV-Vis absorption spectrophotometer. The more purple the solution, the most live cells the sample presents.³⁸

Figure 2.1-1. Reaction mechanism of the reduction of MTT to formazan.

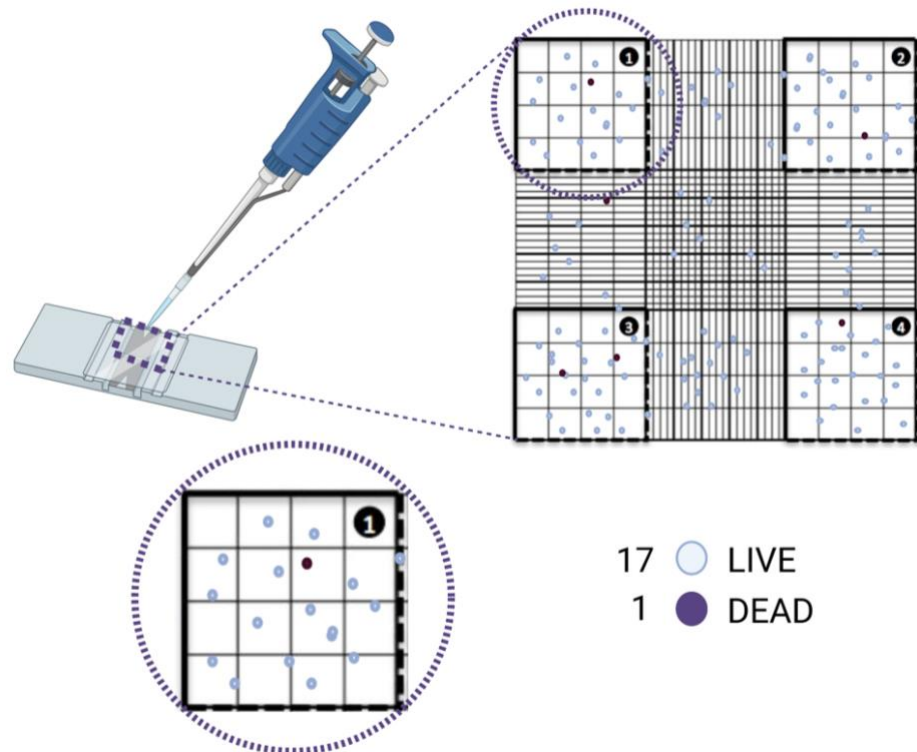


Source: Own authorship

2.1.3. Cell viability

One of the most widely used methods for cell viability counting is the Trypan Blue dye exclusion test. This test determines the number of viable cells in a suspension. Certain dyes, such as Trypan Blue, are excluded from the nucleus of cells with intact membranes. Oppositely, dead cells allow the entrance of dye, marking the whole nucleus blue. The experiment consists of suspending cells in a Trypan Blue solution and evaluating the suspension at an optical microscope. Viable cells will present a clear cytoplasm, while dead cells will be entirely blue. Viability greater than or equal to 95% is excellent.^{39,40} Cell counting is usually done by using a hemacytometer or Neubauer chamber, where the suspension of cells is placed on the chamber and cells are counted under the microscope. It is possible to observe eight square spaces filled with nonviable and viable cells. Cells are counted and their concentration calculated considering the size of the squares and dilution factor.⁴¹ Figure 2.1-2 shows the process of cell counting with the hemacytometer.

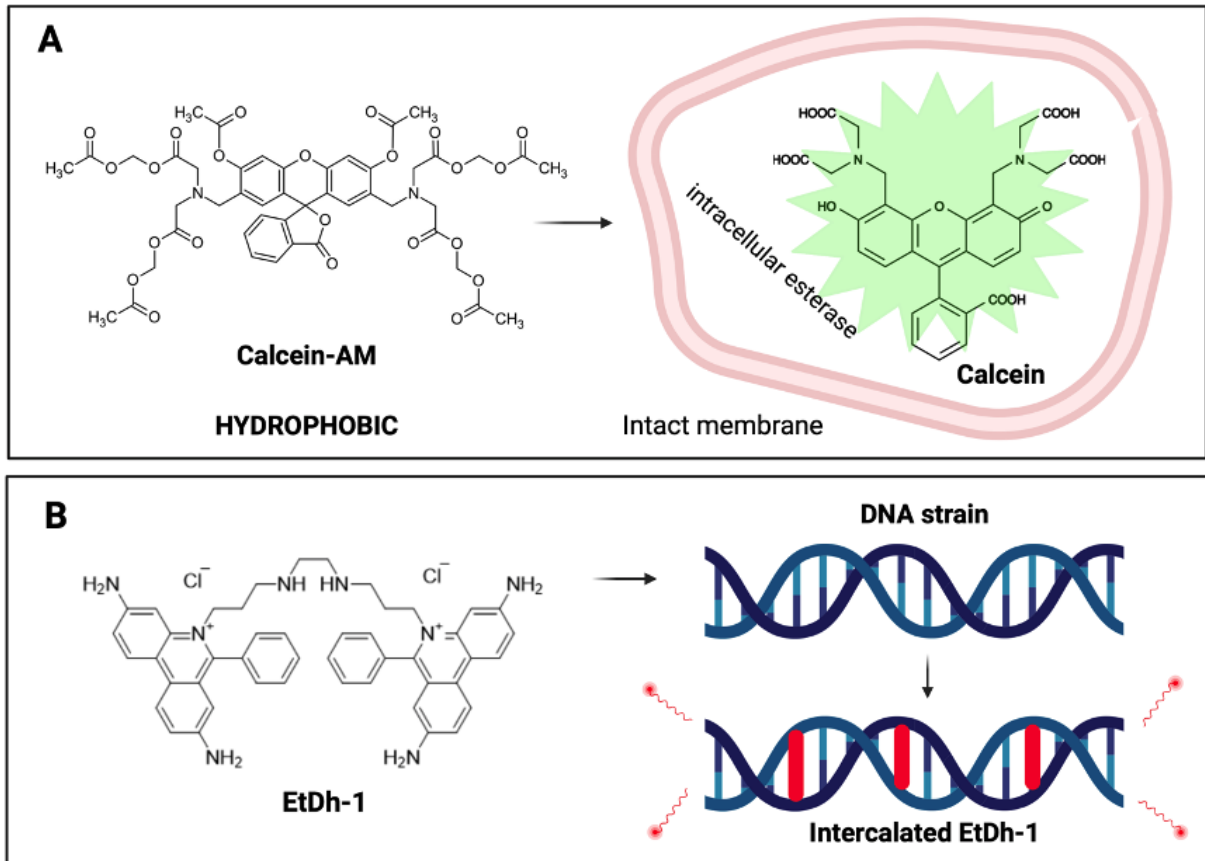
Figure 2.1-2. Schematics of a hemacytometer or Neubauer chamber counting showing a zoom in one of the chambers and a close look to the number of live and dead cells.



Source: Own authorship, created with Biorender.com

Another method for evaluating cell viability is by staining cells with fluorescent dyes. This method assesses the image with both dead and live cells and it is a possibility for measuring cell viability in more complex matrices, such as permeable supports and loaC devices. Live/Dead counterstaining is used for simultaneous detection of viable and non-viable cells in a matrix. Calcein-AM is a dye used for detecting living cells by permeating the membrane, generating calcein inside viable cells with fluorescence emission centered at 515 nm when excited with 490 nm light. For non-viable cells, a possible dye is the ethidium homodimer (EthD-1). This dye stains the nucleus of damaged cells with a strong fluorescence emission centered at 617 nm when excited at 535 nm.⁴² The principles and mechanisms of action of these dyes are complex. When crossing the cell membrane, calcein-AM is hydrolyzed by endogenous intracellular esterases (enzymes) inside the living cells. Hydrolysis cleaves the AM group, converting the non-fluorescent calcein AM to a green fluorescent calcein. As the calcein formed is more hydrophilic, it is trapped inside cells with intact membranes. On the other hand, non-viable cells, stained with EthD-1 are submitted to the exposure of this dye into the nucleus, since their membranes are damaged. Into the nucleus, EthD-1 binds to the nucleic acid chains by intercalation, more specifically through hydrogen bonds between EthD-1 amino acids and the phosphate groups within DNA/RNA strands.^{42,43} Figure 2.1-3 shows the mechanisms involved in live/dead staining.

Figure 2.1-3 Chemical mechanisms for live-dead counterstaining. A) Calcein-AM entering the cell membrane and hydrolyzing into green fluorescent calcein, B) EthD-1 crossing the damaged membrane and reaching the genetic material, intercalating the DNA strain and generating a red fluorescence.



Source: Own authorship, created with Biorender.com

2.1.4. Cell monolayer assessment

A series of different methods are reported for the assessment of the monolayer integrity. The literature recommends the use of two of them to guarantee monolayer wholeness. Therefore, the most common and simple approaches use paracellular markers such as phenol red (PR) and lucifer yellow (LY), or radioactive markers such as ^{14}C -mannitol to track their permeability and diffusion. The experiment consists of placing a certain amount of the marker on the apical chamber containing the monolayer of cells, then after a few hours (~1-2 hours), detecting the amount of marker on the basal compartment of the flask. The marker's concentration is determined and the diffusion percentage or the apparent permeability can be calculated.^{44,45} Paracellular markers are transported to the luminal parts of the cells via the paracellular route, between the cell

junctions. This via happens exclusively through passive diffusion and convection processes. The markers are transported by the claudins, transmembrane proteins that constitute the TJ. Therefore, if a monolayer of cells is not fully developed with TJ, the marker will leak, showing high concentrations in the basal compartment.⁴⁶

Another widely used method to assess cell monolayer integrity is the measurement of the trans-epithelial electrical resistance (TEER). This technique consists of placing two electrodes (Ag/AgCl) on the apical and basal compartments of the transwell®, and measuring the electrical resistance across the monolayer of cells during the whole process of differentiation. The principle of this technique is to detect the ionic conductance of the paracellular pathway in epithelial cells, controlling over the days, the formation of the TJ pores. The more resistance this system provides, the most well-developed the TJ net is. This is considered a reliable method to check monolayer integrity and permeability across the cells.^{47,48}

The same methods used to assess the monolayer integrity, are also used to evaluate the permeability of nutrients. Then, it is possible to use chemical probes such as phenol red and ¹⁴C-mannitol, as well as the TEER technique to determine the permeability of nutrients across the cells.⁴⁹ Moreover, the analytical choice for detection and quantification will depend on the analyte characteristics.

Finally, immunofluorescence staining and imaging techniques are also widely used as an approach for monolayer integrity evaluation. A series of different antibodies and dyes can be used for different approaches. For this specific application, TJ and nuclei are the targeted components of the cells to observe. For this matter, DAPI (4',6-diamidino-2-phenylindole) and Zonula Occludens 1 (ZO-1) antibody are the most common substances to stain the nucleus and the TJ, respectively. DAPI strongly binds to the adenosine-thyamine (A-T) regions of DNA through electrostatic interaction due to its strong cationic charge, generating an intense blue fluorescent emission.⁵⁰ For the TJ, a mammalian ZO-1 antibody containing a fluorophore is placed on the Caco-2 cells for binding the proteins present on the TJ, the claudins. The fluorescence will appear as long as this group of proteins is present in the cell monolayer and the fluorescence will depend on the fluorophore.⁵¹ The counterstaining gives an image with the complete structures, showing an intact monolayer of developed cells.

2.2. OBJECTIVES

The aims for this part of the work are to grow Caco-2 cells in different types of platforms, compare the differentiation processes in each, and evaluate parameters to release those cells for transport experiments.

2.3. MATERIALS & METHODS

2.3.1. Cell culture

Caco-2 cells (ATCC® HTB-37™) were kindly provided by Dra. Rosângela M. N. Bezerra from UNICAMP. For subculturing and maintaining cells over three years, cell culture flasks were used (Corning® cat. no. 430372). Cells were subcultured once a week at a $1 \cdot 10^5$ cell/mL concentration with a 0.25% Trypsin EDTA solution (Sigma Aldrich, cat. no. T4549). For all experiments, Dulbecco's modified Eagle's medium (DMEM) high glucose (4,500 mg/L glucose) with L-glutamine (without pyruvate) (Gibco/Invitrogen, cat. no. 41965-039) supplemented with 10% fetal bovine serum (FBS, Vitrocell Embriolife), 1% 100X nonessential amino acids (Gibco/Invitrogen, cat. no. 11140-035) and 1% PEST (penicillin 10,000 U/mL, streptomycin 10,000 mg/mL solution (100X); Gibco/Invitrogen, cat. no. 15140-122) was used as a culture medium.

2.3.2. Cytotoxicity evaluation

For this experiment, 96-well TC-treated microplates (Corning® cat. no. 3997) were used to grow a 3×10^5 cell/mL concentration of Caco-2 cell line. Cells were incubated at 37° C and 5% CO₂. After 24 hours, the culture medium was removed and the investigated solutions were added. The investigated solutions were at a concentration-range of hydrated Ca(II) ions (zero (negative control), 0.01, 0.02, 0.03, 0.04 and 0.05 M), a positive control (60% phenol solution), calcium hydrogen phosphate solution (CaHPO₄) (0.002 g/mL), sodium citrate solution (Na₃Cit.2H₂O or NaCit) (0.0094 g/mL), Peptigen® (0.01g/mL) and Peptigen® (0.01g/mL) + CaCl₂.2H₂O (0.03M) solutions, all solubilized in Hanks Balanced Salt Solution (HBSS). Solutions were added to wells and incubated for 2 hours at 37° C, and then cells were washed with Phosphate Buffer Solution (PBS) for Thiazolyl Blue Tetrazolium Bromide (MTT) solution addition (1mg/mL). After 3 hours of incubation at 37° C and 5% CO₂, MTT was removed and 50µL ethanol + 150µL

isopropanol/PBS (50% v/v) were added to each well. Finally, the absorbance was determined using a Multiskan GO spectrophotometer (Thermo Scientific®) at 570 nm. The survival index (%) of the cells after treatment (SI) was determined based on the survival of the negative control by the following equation:

$$SI (\%) = X_{av} \cdot 100 / C_{av} \quad (\text{Eq. 2.1.})$$

Where X_{av} is the absorbance's average (each sample), and C_{av} the absorbance's average of the negative control.

Materials: $\text{CaCl}_2 \cdot 2\text{H}_2\text{O}$ (Synth® cat no. 01C2013.01), CaHPO_4 (Sigma Aldrich CAS 7757-93-9), $\text{Na}_3\text{Cit} \cdot 2\text{H}_2\text{O}$ (Sigma Aldrich CAS 6132-04-3), Peptigen® IF3080 (Arla Foods Ingredients), MTT (Sigma Aldrich CAS 57360-69-7).

2.3.3. Cell characterization and viability

Optical microscopy was used during all the processes of cell culture under all the platforms for verifying possible problems and pursuing cell differentiation. Two different approaches were used for assessing cell viability. The trypan blue exclusion method was used for cell counting and viability before seeding cells into the experiment platforms (transwell® and loaC). The methodology used for cell counting is detailed in the introduction section of this thesis. For the cell monolayers grown for days on the platforms, the live/dead staining approach was used for assuring a major coverage of live cells. For live/dead staining, the dyes were solubilized in PBS in a 1:1000 (Calcein AM)/ 2:1000 ethidium homodimer-1 (EthD-1) proportion, then kept for 30 minutes on top of cells, and washed away with PBS for further imaging. Fluorescence confocal microscopy was carried out under a Zeiss LSM 780 confocal microscope with a 488 nm Argon-ion laser and a Coherent Chameleon laser (Ti:sapphire) as a source for two-photon excitation at the wavelength of 800 nm. In all experiments, at least three isolated areas of the samples for each treatment were studied using a $400 \times 400 \mu\text{m}^2$ field of view, optimally divided into 1024×1024 pixels, resulting in a lateral resolution of about 400 nm.

Materials: Trypan blue solution 0.4% (Sigma Aldrich® CAS 72571), Neubauer counting chamber (BLAUBRAND®), inverted microscope (Olympus CKX41), LIVE/DEAD™ Viability/Cytotoxicity Kit (Invitrogen™ cat no L3224), PBS, confocal microscope (Zeiss LSM 780).

2.3.4. Monolayer assessment

A few different methods for assessing the cell monolayer integrity are reported and displayed in the introduction section of this chapter. In this work, phenol red (PR) diffusion and immunofluorescence of DAPI/ZO-1 were used to guarantee an intact monolayer of cells.

For the PR diffusion, a 10 μ M solution of phenol red (in HBSS) is placed on the apical compartment of the transwell®, and an HBSS solution is placed on the basal side. After a 60-min incubation at 37° C and mild shaking, aliquots were collected from the basal compartment. A 96-well microplate (BRAND® 701330) was used to place the aliquots from t0 apical, t0 basal, and t60 basal. The plate was then analyzed on a Multiskan GO spectrophotometer (Thermo Scientific®) at 558 nm. The concentrations of PR were calculated through a calibration curve and the diffusion percentage was calculated by the following equation.

$$\text{Diffusion \%} = \frac{(C_b(t60) - C_b(t0))}{C_a(t0)} \times 100 \quad (\text{Eq. 2.2.})$$

Where $C_b(t60)$ is the concentration of PR in the basal chamber at 60 minutes, $C_b(t0)$ is the concentration of PR in the basal chamber at the start of the experiment, and $C_a(t0)$ is the concentration of PR in the apical chamber at the start of the experiment.

Another possible and more accurate way to determine this diffusion is through the apparent permeability, calculated by the following equation.¹³

$$P_{app} = \frac{V_b \times dC_b}{A \times dt \times C_a(t0)} \quad (\text{Eq 2.3.})$$

Where V_b is the volume of the basal chamber, C_b is the concentration of the basal chamber, A is the seeded area and, C_a is the concentration of the apical chamber.

Both calculations were carried out to compare with the literature and define the equivalent values found in this work.

Materials: DAPI solution (1mg/mL) (Thermo Fisher cat. no. 62248), Hank's balanced salt solution (HBSS), Phenol red solution 0.5% (Sigma Aldrich, CAS: 143-74-8), Phosphate buffer solution (PBS), Zonula occludens 1 (ZO-1) monoclonal antibody Alexa Fluor 488 (0.5 mg/mL, 339188, Invitrogen by Thermo Fisher).

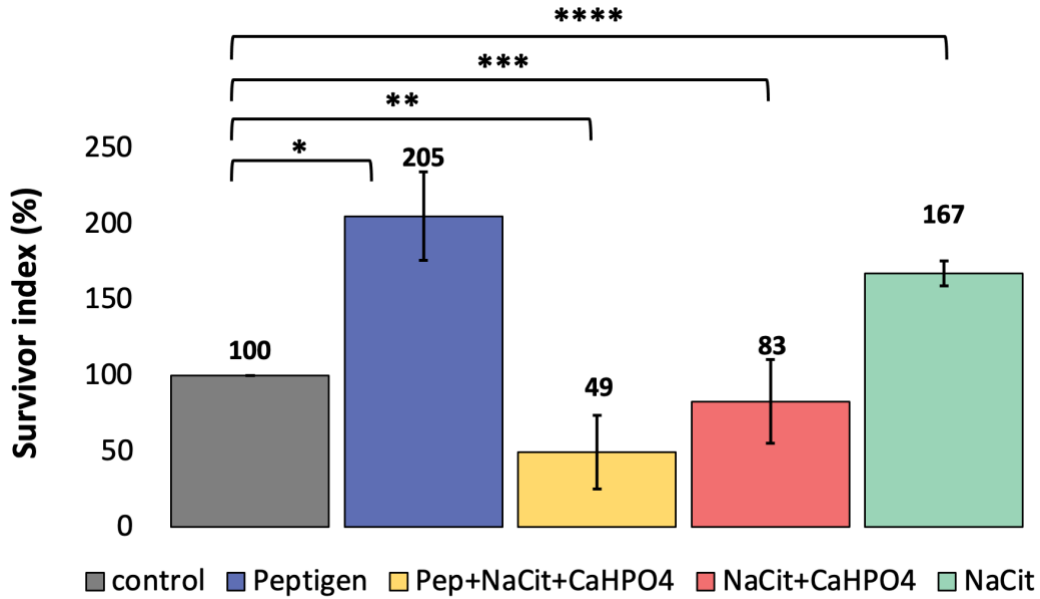
2.4.RESULTS & DISCUSSION

Caco-2 cells were cultured over almost three years, obtaining high passages for the transepithelial transport experiments. Cell passages from 50-70 were used in the assays, guaranteeing mature cells with the formation of important structures. Moreover, Caco-2 cells were counted by using the Trypan blue exclusion method before all experiments to ensure their adequate concentration.

2.4.1. Cytotoxicity evaluation

A crucial step before analyzing the absorption of substances/nutrients in a cell system is to evaluate the substance solution's toxicity. This is executed by placing cells in contact with the substance solutions for a period and evaluating their survivor index. As the final goal of this work is to analyze the transepithelial transport and absorption of calcium ions and peptides from a commercial whey hydrolysate (Peptigen®) enriched with hydrated calcium ions, a few chemicals were evaluated. Among them are Peptigen® (Pep), CaCl_2 , NaCit, and CaHPO_4 . Initially, supersaturated solutions of calcium were idealized for evaluating a possible boost in calcium bioavailability, resulting from a higher amount of free calcium ions in the solution in the supersaturated solutions. The process for supersaturating calcium is detailed in the materials & methods section of this chapter and uses Pep, NaCit, and CaHPO_4 . Therefore, the first evaluated solutions for cytotoxicity were these solutions together and individually. The bar chart in Figure 2.4-1 shows the survivor index (SI, %) results of these solutions. The student's T-test ($p < 0.05$) was carried out to evaluate the significance of these indexes. Survivor indexes are calculated according to equation 2.1 and the values are presented as the mean \pm standard deviation (SD).

Figure 2.4-1. Cytotoxicity of supersaturated solutions with Peptigen®, showing the survival index (SI) bar chart for the different solutions.

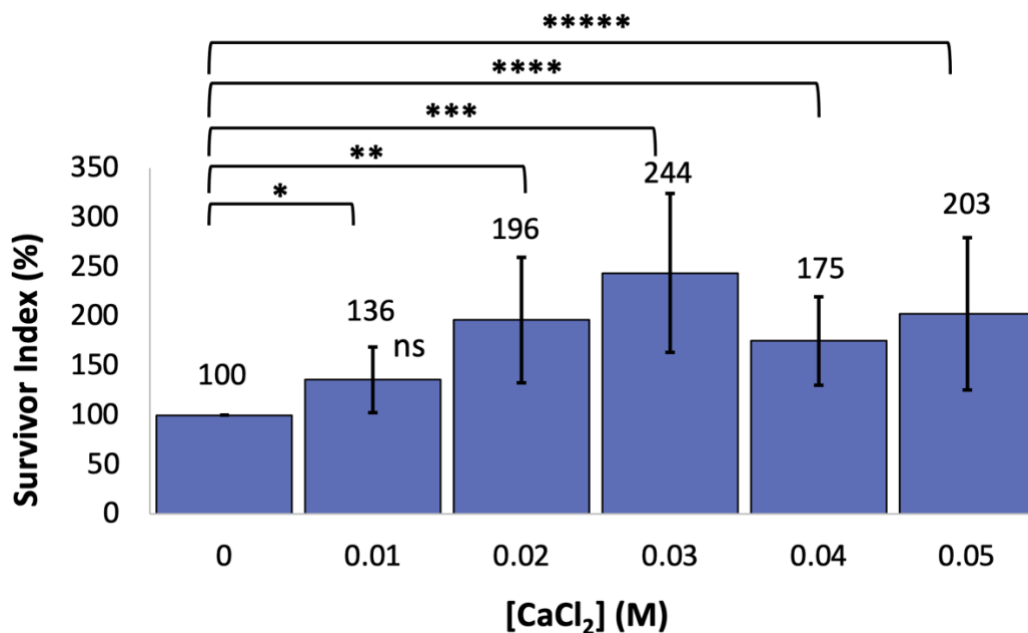


Student's t-test: * ($p < 0.000001$), ** ($p < 0.00001$), *** ($p < 0.02$), **** ($p < 0.0000001$).
 Source: Own authorship

It is possible to conclude from the results of this assay, that Pep not only presents no harm to cell growth but also assists it, increasing significantly the survival rates. The supersaturated calcium solutions instead, decreased the SI by half, indicating a threat to their survival. Analysis of both citrate and phosphate salts individually showed that the citrate in the presence of calcium phosphate, decreased SI, while citrate alone, increased. Therefore, CaHPO_4 was considered a toxic substance for cells in the given concentrations and in combination with the other chemicals. All results were considered significant by the paired t-test.

As a final goal to evaluate calcium transport across Caco-2 cell monolayer in the commercial hydrolysate, other approaches for enriching Pep with calcium were used. Therefore, the idea was to evaluate the toxicity of another calcium salt, CaCl_2 . A range of 5 different concentrations was analyzed and the results are shown in Figure 2.4-2. Besides the great SD values, all concentrations of this substance showed no harm and enhanced cell growth. The only non-significant value in comparison to the control was the 0.01M solution, which can be explained by the similarity of those samples. Although not significantly different, these SI values are always above 100%.

Figure 2.4-2. Cytotoxicity of a range of CaCl₂ solutions showed in a bar chart of SI *versus* CaCl₂ concentrations.

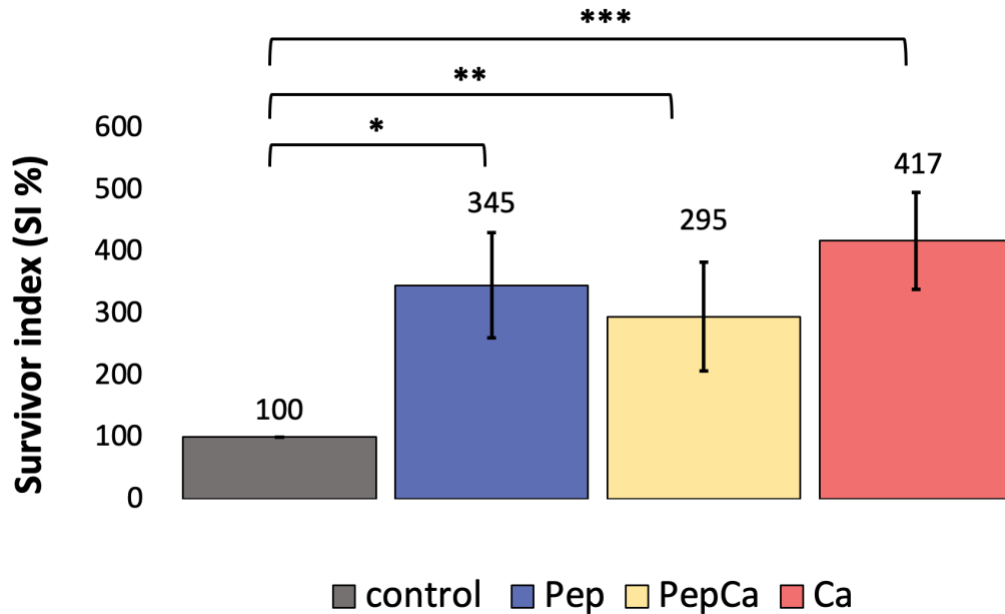


Calculated p values for each sample compared to the control: * ns, ** (p < 0.05), *** (p < 0.02), **** (p < 0.02), ***** (p < 0.05). ns: non-significant.

Source: Own authorship

According to the previous results, CaCl₂ was not a threat to the Caco-2 cells, then the strategy was to combine this salt with Pep and evaluate the effective absorption of calcium and peptides when the concentration of this salt is increased in the Pep solution. Therefore, the cytotoxicity test was performed for the final testing solutions of Pep and CaCl₂ together (PepCa), and for the individual solutions of Pep and CaCl₂ in the same concentrations used for the transport experiment. Figure 2.4-3 shows the bar chart and p values for Pep, PepCa, and Ca SI's. All solutions were considered harmless for cell and present high survival index values. Then, it was finally decided to carry out the transport across the Caco-2 monolayer experiments with those solutions.

Figure 2.4-3. Bar chart of SI versus the solutions of Pep and Pep combined with CaCl₂ (PepCa), showing their cytotoxicity.



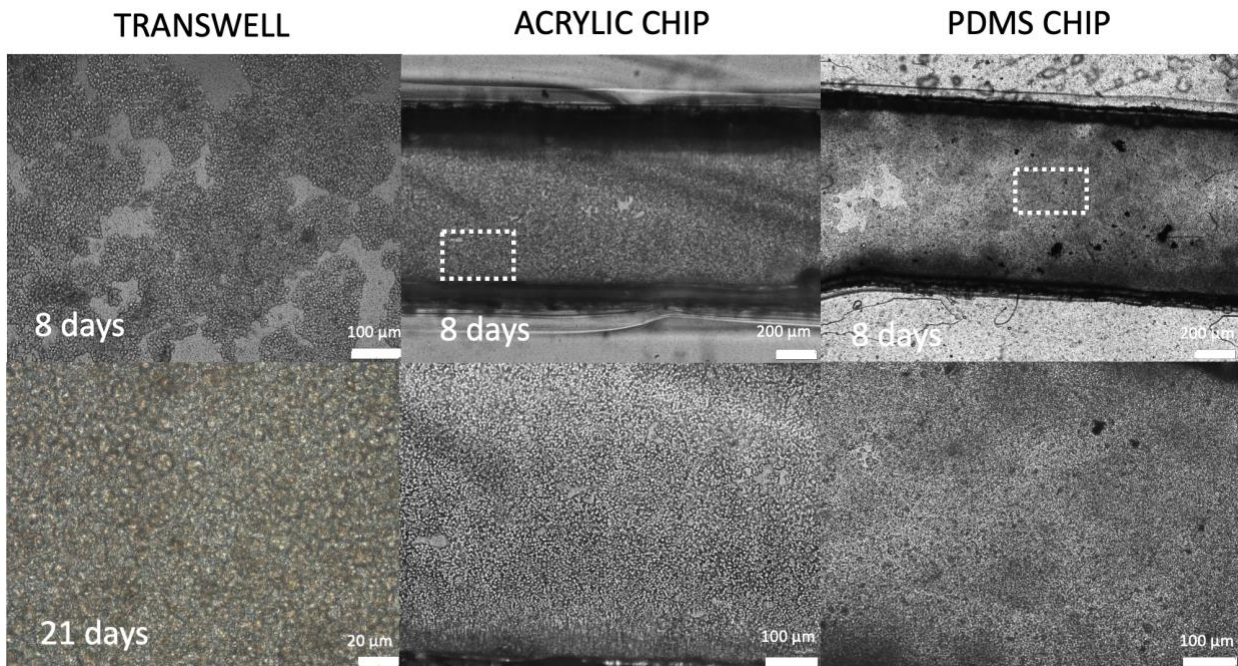
Calculated p values: * (p <0.0000000001), ** (p <0.005), *** (p <0.00001).
 Source: Own authorship

2.4.2. Static vs dynamic cell characterization

In this section, all results will be expressed comparatively. All Caco-2 cell characterization procedures were carried out for both experiment's platforms, the transwell® (static system) and the loaC devices (dynamic).

The first parameter compared for both systems was the time for Caco-2 cell growth and differentiation. For this, a series of optical microscopy images were taken along the cell culture for both approaches. By Figure 2.4-4 it is possible to infer that in 8 days the devices' membranes are mostly covered, presenting only a few small free spaces without cells. For the transwell® instead, there are mostly free spaces in the membrane in 8 days and the cells are fully differentiated and covering most of the area only by the 21st day. In conclusion, for the dynamic system, cells grow and differentiate almost 3-fold faster, showing a more efficient method for further evaluation of nutrient absorption.

Figure 2.4-4 Comparative micrographs for Caco-2 cell growth in static and dynamic systems. Transwell® shows the 8th and 21st days of differentiation, while acrylic and PDMS chips were evaluated for 8 days of culture to show the differences in the differentiation time.



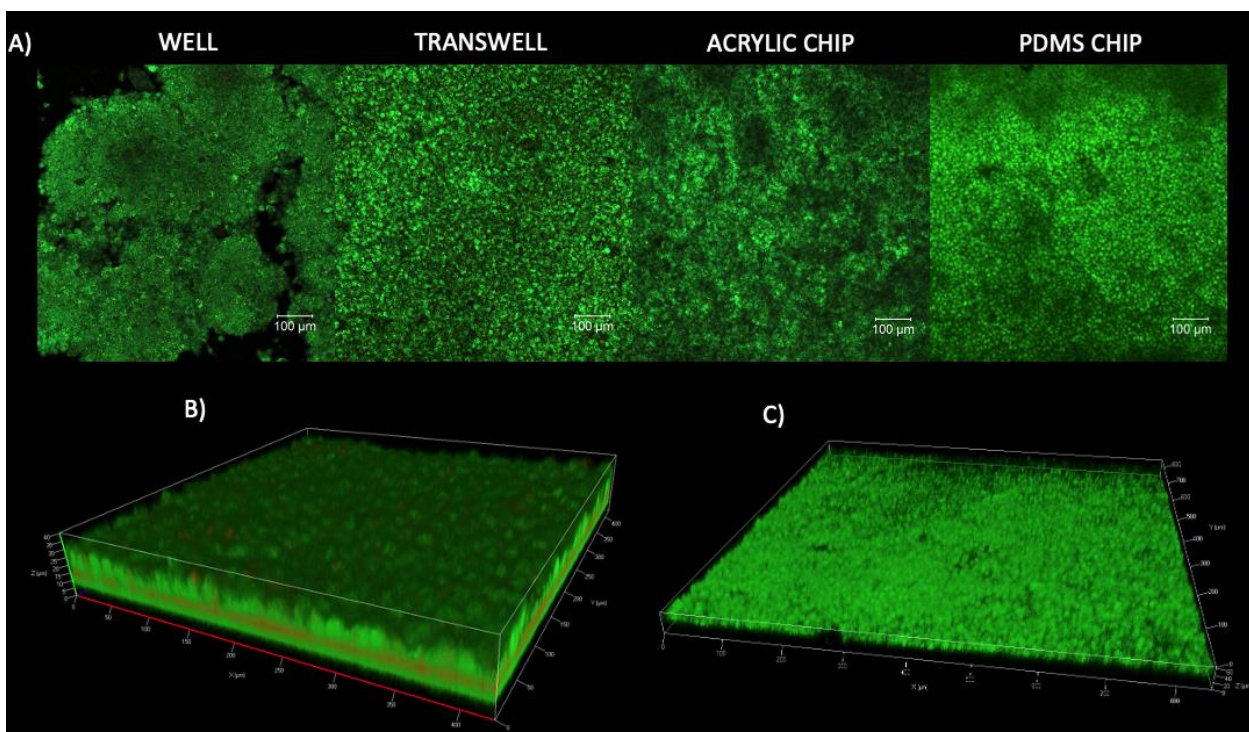
Source: Own authorship

2.4.2.1. Cell Viability

Before using the cells for experiments, it is important to make sure that the Caco-2 cells are viable. For this, live/dead assays were made in all platforms to compare and guarantee live and viable cells for the transport experiment. All images were obtained in a confocal microscope and treated by using the ImageJ software. Figure 2.4-5 shows the live/dead stained cells in four different platforms and 3D images indicating the formation of a monolayer. The evaluation of live/dead results led to the conclusion that cells are viable in all platforms and the measurement of the layer of cells on top of the platforms was 15-20 μm for the transwell® and 20-25 μm for the developed devices. These numbers are rough estimations since the light scattering in the loaC platforms unsettled the real measurements. In addition to the images, a color segmentation ImageJ plugin was run to obtain the rough percentages of live and dead cells. Table 2.4-1 shows the results for each cell platform. Most of the area in all platforms were covered by live cells, presenting percentages above 90%. From the images is easy to recognize that only a few cells are dead. The calculation by color segmentation is a rough estimation of the percentage area,

although it is a reliable method for defining if a cell monolayer is viable and ready for experimentation.

Figure 2.4-5 Confocal micrographs of live/dead stained cells. A) Counterstained monolayer of cells in each platform with 21 days for well and transwell® and 8 days for the chips, B) 3D view of transwell® monolayer, C) 3D view for the PDMS chip monolayer.



Source: Own Authorship

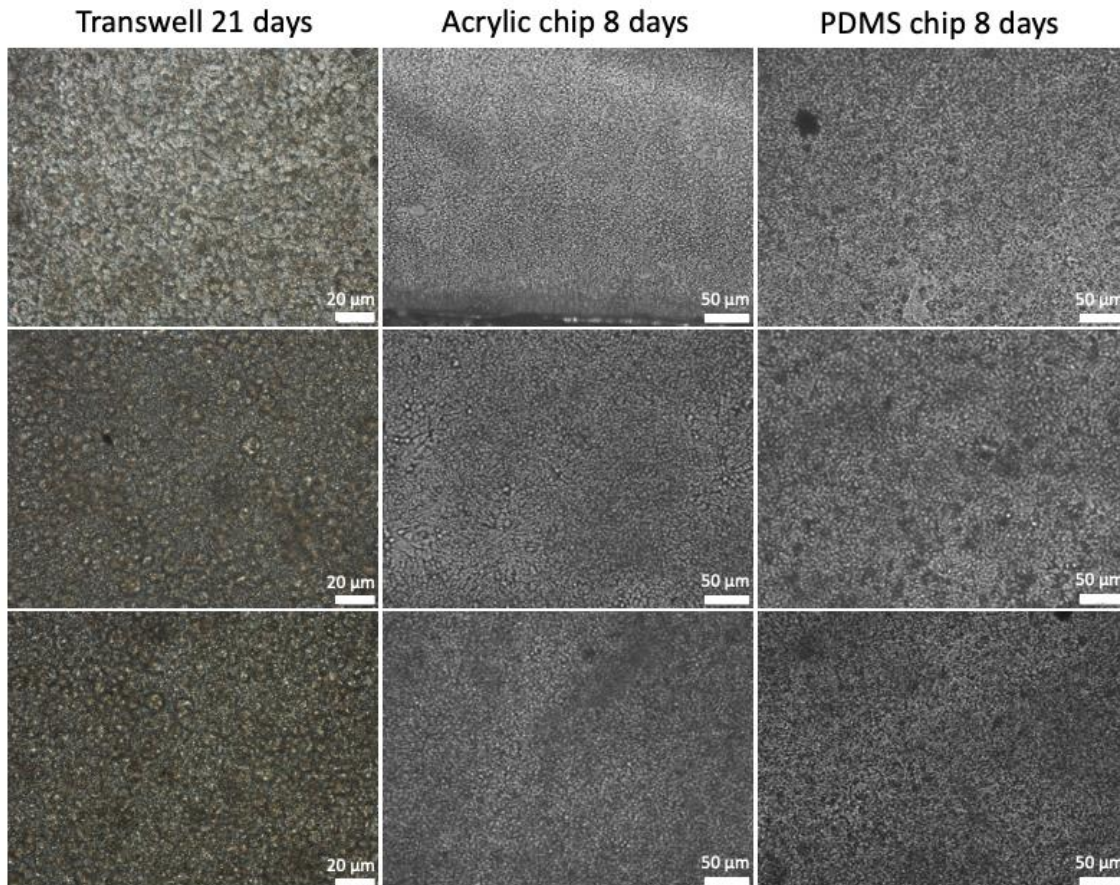
Table 2.4-1. Calculated values for the total percentage of live and dead cells by using the ImageJ plugin for color segmentation

Area %	Well	Transwell	Acrylic chip	PDMS chip
Dark live	49.7	56.9	57.8	52.8
Light live	17.9	17.4	7.9	25.4
Dead	5.2	6.5	0.3	3.3
Black	27.2	19.9	33.8	18.4
Total live (%)	92.9	91.9	99.5	95.9
Total dead (%)	7.1	8.1	0.5	4.1
Pixels	4915200	4915200	313600	313600

2.4.2.2. Monolayer assessment

An important control before submitting cells to a transport experiment is the monolayer assessment. This assay guarantees that the monolayers of cells are not leaking across their holes and are intact for the transport experiment. There are a few approaches for assessing the monolayer as mentioned in this section's introduction. For this work, the phenol red diffusion and the DAPI/ZO-1 counterstaining (immunofluorescence) were the approaches used for verifying the cell monolayer. In addition, optical microscopy was carried out during the days of culture to ensure cell differentiation over the experiment time. Figure 2.4-6 shows the before transport experiment triplicate monolayers for all the platforms used for this matter. All monolayers presented to be intact with no apparent holes before the transport experiment.

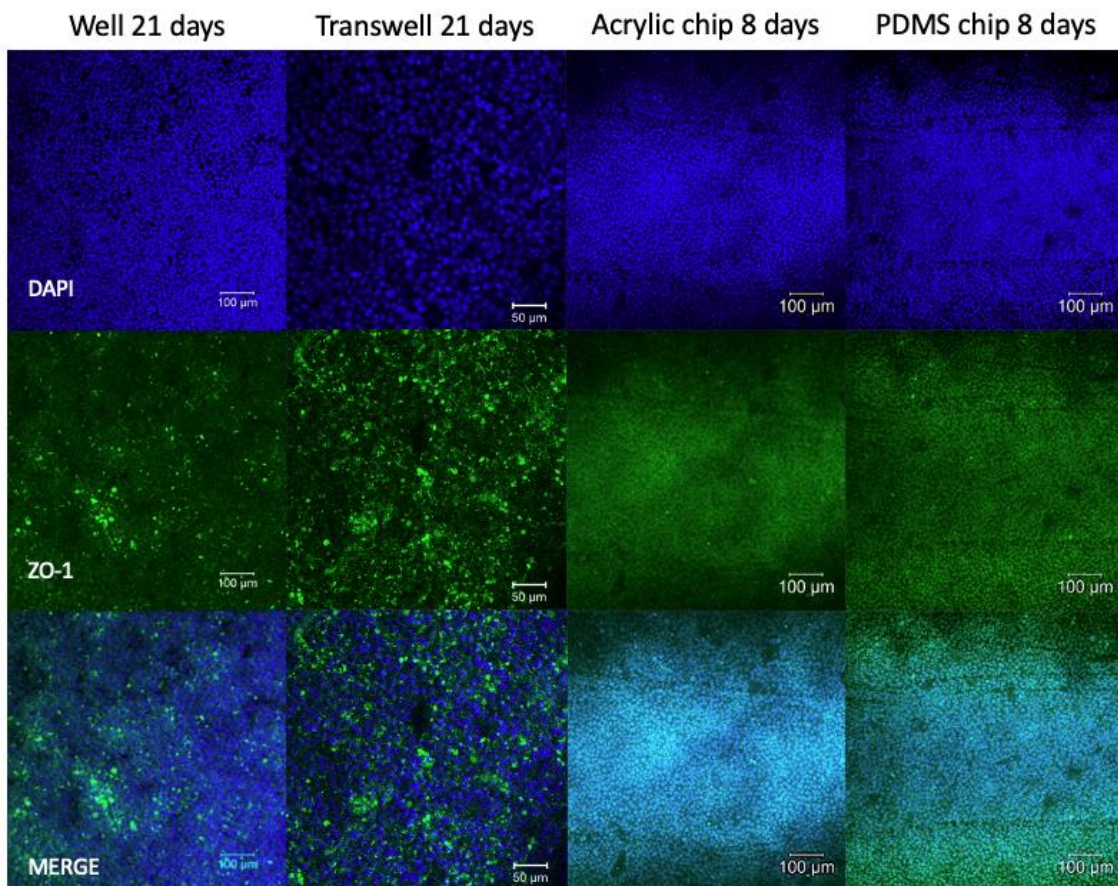
Figure 2.4-6 Optical microscopy images of the triplicate monolayer of Caco-2 cells in three different platforms: transwell®, Acrylic chip, and PDMS chip.



*These micrographs were taken right before the transport experiment.
Source: Own authorship

DAPI/ZO-1 counterstaining is a very common reported method to verify the monolayer integrity and the formation of tight junctions, important cell structures for nutrient uptake evaluation.³⁷ Figure 2.4-7 shows the comparative images for four different platforms for cell growth: well, transwell®, acrylic chip, and PDMS chip. The staining was performed on the day that the transport experiments was carried out. Caco-2 cells presented the required structures and the correct differentiation stage for the transport experiment. However, it is important to highlight the challenges encountered during the devices' imaging. The materials composing the devices are light scattering, worsening the image's resolution and impeding the use of higher magnifications, leading to a poor level of detail. Even though there were issues, it was possible to define good parameters for the cell monolayers and approve them for transport experiment in agreement with the PR diffusion and permeability (% and cm/s, respectively).

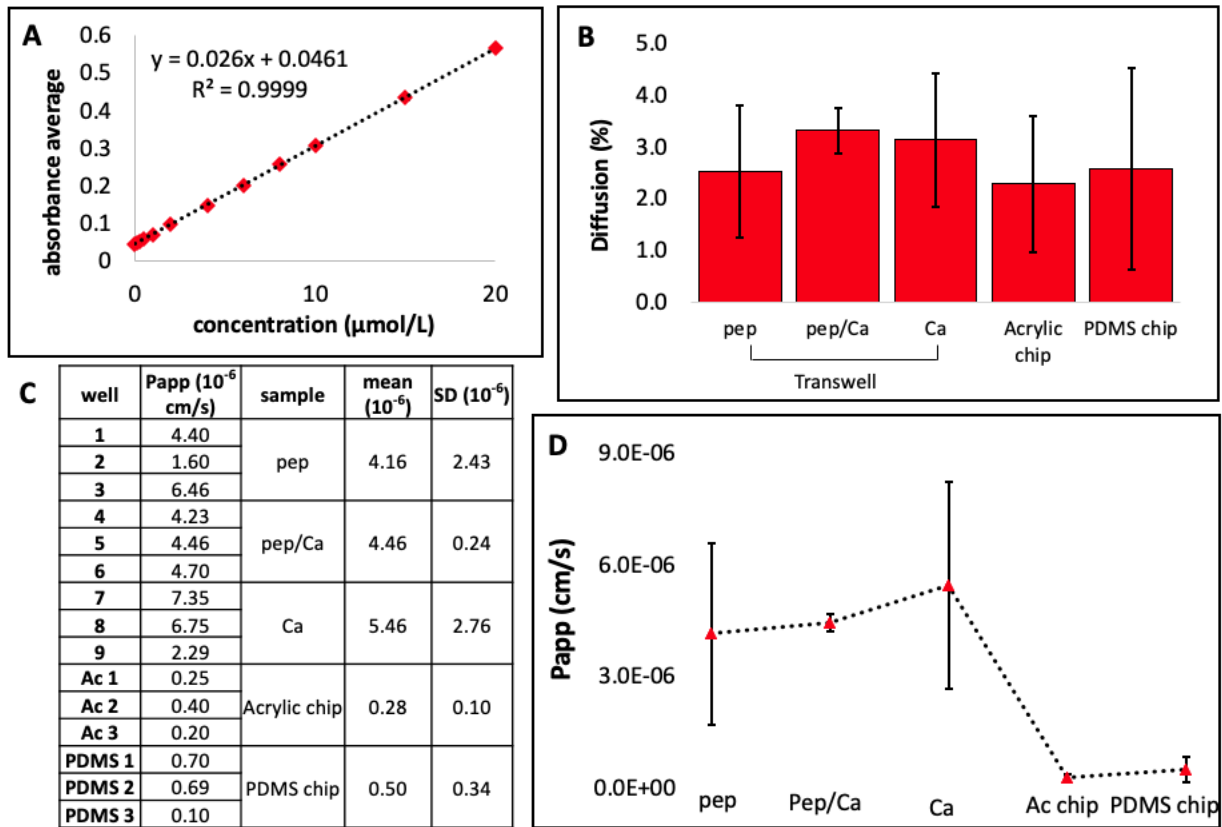
Figure 2.4-7 Confocal micrographs of Caco-2 cell monolayers counterstained with DAPI and ZO-1. The images exhibit intact monolayers ready for the transport experiment.



Source: Own authorship

In addition to cell monolayer imaging, paracellular markers are used to measure the degree of diffusion across the cells. In this work, phenol red (PR) paracellular marker was used to define its diffusion percentage and the apparent permeability. Before all transepithelial transport experiments, a 60-minute phenol red diffusion assay was performed and its absorbance was determined by using a UV plate reader. The PR concentrations and their apparent permeability were determined through an external calibration curve. Figure 2.4-8 shows the external calibration curve constructed for phenol red, a bar chart of the diffusion percentages, and the results for apparent permeability of PR for all the final transport experiments. Biological triplicates were used to obtain a broad data set. For the transwell®, three wells were used for each sample, and for the loaC devices, three different chips were used for each sample. All diffusion percentages were below 5% and it is important to emphasize that there is no consensus around these values in the literature, being indicated by some as <1% or <5%, others as $P_{app} < 10^{-5}$ cm/s. Therefore, in this work, monolayers presenting $P_{app} < 10^{-5}$ cm/s were considered intact, according to (Zhang, X. *et al*, 2019)⁵² and consequently, with diffusion percentages below 5%. Future works can be based on these numbers when performing phenol red diffusion across Caco-2 cell monolayer. P_{app} and diffusion percentage values are expressed as the mean \pm SD of the triplicate samples.

Figure 2.4-8. PR diffusion percentages and apparent permeability. A) calibration curve with PR concentration versus absorbance B) PR diffusion bar chart per triplicate sample C) Table with Papp calculations, and D) Papp chart per triplicate sample.



Source: Own authorship

2.5. CONCLUSION

The cell characterization included cytotoxicity, viability, cell imaging, and monolayer assessment assays. For the cytotoxicity, the chemicals used for preparing a calcium supersaturated hydrolysate presented certain toxicity, decreasing by half the survival index of the Caco-2 cells, particularly by the use of the CaHPO_4 salt. Therefore, it was decided to increase the calcium ion concentration of the whey hydrolysate by adding CaCl_2 at high concentrations. Toxicity tests were performed either for calcium chloride solutions alone in a range of concentrations or together with Peptigen®, and all tests indicated no harm to cells survival. On the contrary, these solutions seem to enhanced cell growth and display high values for the survival index.

Optical microscopy was used during all processes, being a practical tool for evaluating day-by-day cell growth and possible contaminations. Moreover, it indicated that the loaC devices are faster for cell differentiation and monolayer formation, being 8 days the ideal, while for transwell®, at least 21 days are required. Another important parameter is cell viability, and it was acquired through live/dead staining of all cell platforms. For the last day of differentiation on each platform, the rate of live and dead cells was calculated, presenting high viability (>90% live) in all samples. In addition, it was possible to roughly estimate the height of the cell monolayer through the fluorescence confocal image, being 15-20 μm for the transwell®, and 20-25 μm for the devices.

For the cell monolayer assessment two assays were carried out, an immunofluorescence assay with DAPI and ZO-1 counterstained, and the phenol red diffusion. The immunofluorescence showed structures such as tight junctions being formed in all platforms, which is very important for the transport experiments. It also revealed a whole, intact monolayer of Caco-2 cells. The paracellular marker, phenol red, also corroborates to the intact monolayers, presenting Papp $<10^{-5}$ cm/s and diffusion percentages below 5%. In summary, all cells in all platforms were ready for the transport experiment after the characterization.

CHAPTER 3

Transport of Calcium and Peptides using ESI-MS and MALDI-TOF/TOF-MS

3.1. INTRODUCTION

3.1.1. Calcium absorption and dietary deficiency

Numerous studies in the past decades have established the central role that dietary calcium intake plays in health. Milk and dairy products, rich sources of nutrients such as calcium, vitamins, and proteins, are listed as a fundamental group of recommended food all over the world.⁵³ The benefits that these nutrients offer to bone maintenance and the prevention of diseases are widely explored.^{54,55} Disorders such as osteoporosis, type 2 diabetes mellitus, arterial hypertension, and cancers (e.g., colorectal cancer) may all be associated with a lack of nutrients and aging effects.⁵⁶ Clearly, those diseases have a list of causes, but dietary calcium can be a potential guide to prevent them.⁵⁶ The recommended dietary allowance (RDA) of calcium ions is established at around 1000 mg/day (in general) for adults, around 1300 mg/day for adolescents, and around 1200 mg/day for the elderly.⁵⁷ These dietary calcium levels are defined as safe for not experiencing both excess, causing negative balance, and lack, causing bone loss. As most people consume less than 2/3 of RDA⁵⁸, it is important to explore novel approaches to increase the intake of dietary calcium, even more specifically for the risk groups, in which these numbers are critical.

It is established that 70% of the dietary calcium intake is obtained from milk and dairy products, 16% from green vegetables and dried fruits, and 6 to 7% from drinking water. Therefore, it is safe to imply that milk and dairy products are the most abundant calcium source in food and beverages.⁵⁶ However, the food's table of nutritional values not always reflects the actual amount of nutrients that the body will absorb. A vast number of factors may affect the absorption of different nutrients, including body type, age, conditions, disorders, and vitamin deficiencies, among others. Calcium assumes many different configurations in food types, depending on the food content. Those configurations may affect calcium solubility in water leading to poor calcium absorption in the small intestine.^{56,59} The amount of calcium effectively absorbed from food and employed in a range of physiological processes in the human body is named bioavailable calcium.

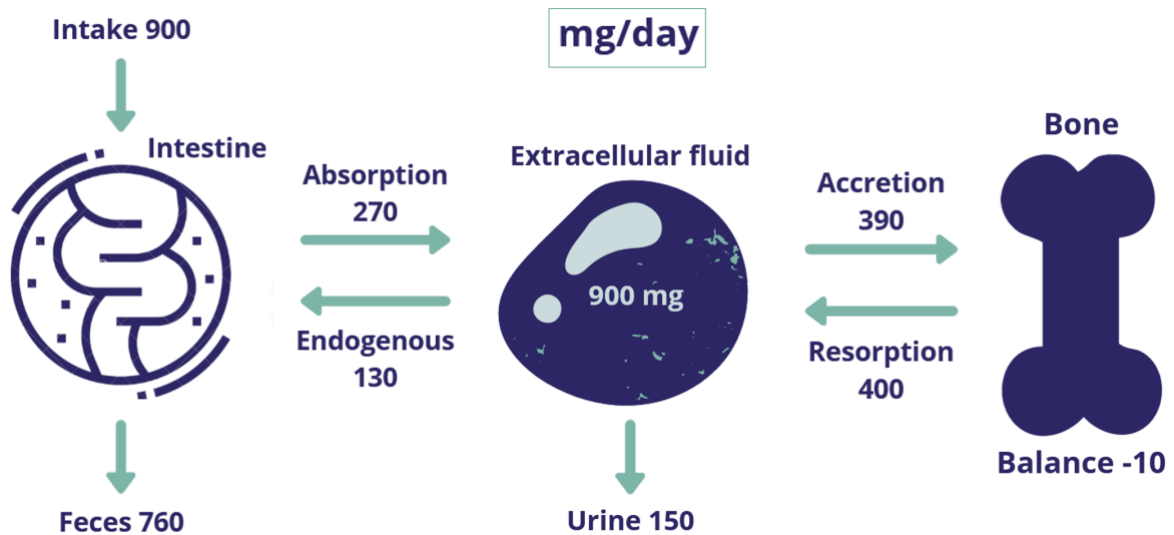
The bioavailability of nutrients is an important parameter, although it is not an easy data to collect, since it involves a deep physiological study. Three important processes

must be considered for evaluating bioavailability: the absorbability of the nutrient into the intestines, its incorporation into the bones, and the excretion including urinary, and fecal loss. However, bioavailability is dependent on a primary process, the potential absorption of the nutrient into the intestines.^{56,60} Fortunately, the potential absorbability depends only on the type of food and the absorptive capacity of the intestines, which is easier data to analyze and an important primary parameter for evaluating bioavailability. The potential absorbability is affected by physiological factors such as the presence of hormones and vitamins. To exemplify, vitamin D is a famous agent affecting the absorption of calcium in the intestines, especially important for the incorporation of calcium into the bones. Aside from these factors, calcium and small nutrients have an easy pathway, named the paracellular way to be absorbed, and this will be further explored in this work.^{56,61}

Malabsorption of calcium ions is one of the causes of osteoporosis and other disorders affecting mostly the elderly population. Even for individuals with high dietary calcium intake, malabsorption is a concern. This malfunction can be associated with a series of factors, such as hormone regulation, physiological factors, and diet. Roughly, all absorbed calcium is stored in the human skeleton (99%), and dietary intake is not the main factor affecting its storage in the bone, instead physiological factors are the most relevant in this scenario.^{62,63} However, dietary calcium is still important for calcium balance, and the guarantee of its availability in food is a means to prevent malnutrition.

Calcium balance is an object of investigation and it is an important parameter for enhancing calcium availability in food. The excess of calcium ions, that is not stored into the bone, is excreted in the urine, feces, and sweat, being the balance of calcium in adults always equal to zero. That means that all calcium absorbed is afterward, released. The fraction of urinary loss comes from glomerular filtration (10 mg/day) and tubular reabsorption (recover almost 98% of the filtered calcium).⁶³ Figure 3.1-1 illustrates the major pathways for calcium balance in the human organism. Hormones, especially parathyroid hormone (PTH), tightly regulate calcium balance, and a negative balance of 10 mg of calcium per day, which can be 10x higher in women during post-menopause, is usual. The amount of calcium in human urine is much larger than that found in other animals, and this is very important for calcium balance. Likewise, dietary intake can be useful when the goal is to increase bioavailability.^{62,64}

Figure 3.1-1. Pathways for calcium balance in the human body, including the intake, passing through absorption and ending in the excretion with a final negative balance of 10 mg/day.



Source: Own authorship

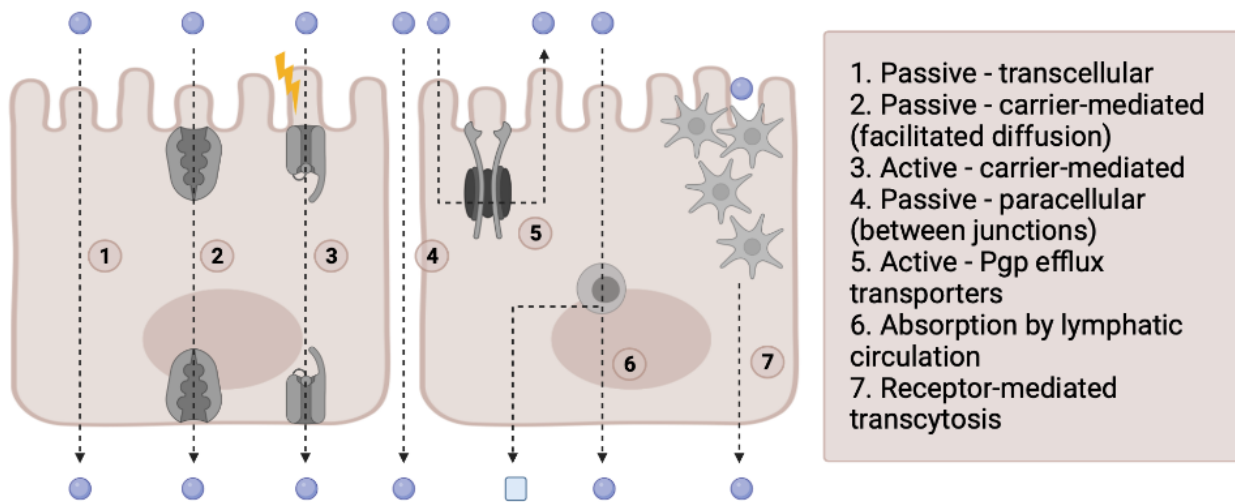
3.1.2. Intestinal absorption of nutrients

Intestinal absorption of calcium and other nutrients, such as peptides is the result of two phenomena: active transport across cells (occurs in the duodenum and upper jejunum) and passive diffusion (mainly in the small intestine – ileum).^{65,66} Among the passive transports are transcellular, operating mostly through membrane enterocytes, the carrier-mediated, mediated by transporters such as proteins, and the paracellular, occurring between the cells, across the tight junctions. Among the active transports are the carrier-mediated, operated by transporters such as proteins, the P-glycoprotein (Pgp) efflux, transporting nutrients through the membrane protein P, the lymphatic absorption, using the lymphatic system to absorb fats and vitamins, and the receptor-mediated transcytosis, transporting essential macromolecules through receptor-mediated vesicles. Figure 3.1-2 shows the types of transport from apical to basal compartments of epithelial cells.^{31,46,67}

Active transport of calcium is a saturable process regulated by dietary intake and body needs. The active transport occurs in three stages: Entry across enterocyte, diffusion across cytoplasm, and secretion into extracellular liquid.^{68,69} The entry is through a positive electrochemical gradient since the Ca^{2+} concentration in the cytoplasm is generally low. Calcium channels and membrane-binding transport proteins are the main

bridges for the active transport of calcium through the membrane. Examples are calmodulin and a few other proteins binding to calcium. CaBP (Calcium-Binding Protein) transports calcium ions across the cytoplasm through CaBP binding or vesicle forming.⁶⁸ Calcium is then extruded into the extracellular liquid against the electrochemical gradient, via an exchange of 3 Na⁺ for 2 Ca²⁺ (minor contributions) or a calcium pump (major contribution) activated by calcium, CaBP, and calmodulin.⁶⁸

Figure 3.1-2. Schematics showing the mechanisms of nutrient absorption across epithelial cells.



Source: Own authorship, created with Biorender.com
 Inspired by Smetanová L, *et. al.* Caco-2 cells, biopharmaceutics classification system (BCS) and biowaiver. *Acta Medica*, 2011;54(1):3-8. PMID: 21542416.

Vitamin D also executes an important function in the active transport of calcium ions. Vitamin D is transformed into 1,25-dihydroxy cholecalciferol (calcitriol), a metabolite derived from liver and kidney phase-1 hydroxylation of vitamin D.⁶⁸ This metabolite controls the synthesis of CaBP, thus regulating the transport of calcium across the intestine. In addition, calcitriol increases membrane permeability and activates the enzyme Ca-ATPase. Calcitriol acts like a hormone, being its production regulated by PTH and its secretion stimulated by the reduction in the plasma concentration of calcium. The PTH-calcitriol system is also very important due to its involvement in bone reabsorption of calcium and the intensification of the reabsorption of calcium by the renal tubule.^{68,69}

On the other hand, the active absorption of calcium is negatively correlated to the total intake. In the elderly, the low number of calcitriol receptors and the less active renal

hydroxylase account for the negative balance. Much of this problem can be related to the deficiency of vitamin D, something easier to diagnose and treat. Apart from vitamin D, other CaBP might be useful to improve calcium absorption in the elderly. It is worth mentioning the use of milk-derived alpha-lactalbumin for calcium binding, which may act as calmodulin and is already present in food and supplements.⁶⁸ Calcium intestinal absorption is crucial for calcium homeostasis and bone mineralization, however, to be absorbed, calcium must be in a soluble form or labile bound to an organic molecule (carry compound), for crossing the epithelium barrier of the intestine.⁶⁸

The passive absorption (or paracellular diffusion) of calcium is a non-saturable process and increases with the dietary intake of calcium in a soluble form. The paracellular diffusion occurs within intracellular junctions, by an electrochemical gradient involving water, sodium, and glucose. It is important to highlight that passive absorption is independent of vitamin D and aging factors.^{66,68,69} Calcium in its soluble form inside the ileum stimulates passive diffusion. Among the possibilities to increase calcium solubility in food are binding it to phosphopeptides, especially from casein, or to amino acids such as L-lysine and L-arginine, among other calcium-chelating agents. This approach may inhibit the formation of precipitates of calcium in neutral and alkaline pHs, enabling its absorption in the intestine.⁶⁹ Moreover, lactose in high levels is known to increase passive absorption, decreasing intestinal CaBP concentration and active transport. However, dietary intake of other food constituents may turn calcium irreversibly insoluble and hamper passive absorption.⁶⁹

Amino acids (AAs) are transported across the bilayer membrane (BLM) through a complex number of systems. Those systems are dependent on solutes, electrolytes, and transporters. Among the systems there are Na⁺, Cl⁻, and H⁺ dependent and independent transports, and this is defined by the type of amino acid. Features such as the size of the chain, the polarity, and the stereochemistry of the amino acid will influence in their transport.⁷⁰ Peptides likewise, can be efficiently absorbed in the small intestine and are majorly dependent on transporters such as the Na⁺/H⁺ exchangers 3 (NHE3). Small peptides may be transported in passive ways, but overall, peptides containing four or more AAs need a carrier protein to transport them. In a healthy system with the required

transporters, peptides present a high capacity to be absorbed, failing to transport only a very small portion.⁷⁰

3.1.3. Analytical techniques

Multiplex analytical evaluation has been extensively investigated with the advent of microdevices. The ideal loaC in this scenario would monitor calcium absorption in real-time connected to the desired equipment. However, this is a complicated task considering the materials used for chip fabrication combined with the methods used for free calcium ion detection. There are a few established methods for determining free calcium ion concentration in a solution. Reported on the literature are several colorimetric probes^{71,72} and the use of time-resolved fluorescent imaging.^{73,74} Alternatively, methods such as electrospray ionization mass spectrometry (ESI-MS)⁷⁵ and sensors⁷⁶ are also reported for the detection of free calcium ions. For this work, ESI-MS in combination with EDTA complexing agent was used as an approach for detecting free calcium in the absorbed samples. Moreover, to collect and identify the peptide profile of the Caco-2 transepithelial transport experiment samples, matrix-assisted laser desorption ionization (MALDI)-TOF/MS/MS was used.

3.1.3.1. Mass Spectrometry

Mass spectrometry (MS) is a widely used technique popularized in the last century and is now in use for a variety of applications. This technique is based on the principle of ionization and fragmentation of molecules. Therefore, it is used to determine molecular information, such as structure details, identification, and concentration of substances.⁷⁷ The operation counts with the sample ionization, ions (positive or negative) acceleration, and deflection through an electromagnetic system, eventual ion fragmentation, and the final detection with the signal processing. The whole system is maintained in vacuum, with pressures of over 10^{-7} Pa, to guarantee the sensitivity of the analysis.⁷⁷ With the passing years and the development of new sophisticated tools, the MS components evolved and it is possible to list a range of different machinery for this technique. The sample introduction can be made directly, with the direct insertion of solid, liquid, and gases using a probe with a vacuum system. Moreover, liquid chromatography (LC) and gas

chromatography (GC) – MS coupled systems are the most usual and count with the sample introduction into the chromatography system for further orientation to the mass analysis.⁷⁷ There are numerous types of different ion sources, including techniques such as electron (EI), chemical (CI), electrospray (ESI), and atmospheric pressure chemical ionization (APCI), with the ESI being the most usual for LC-MS systems. The mass analyzer, where the ions are accelerated and focused, may also count with a broad range of types. Among them are the sector mass analyzer (SMA), with electric or magnetic fields routing the ions and fragments, the time-of-flight (TOF), based on the acceleration of ions through a pathway, the quadrupole mass analyzer (QMA), containing a set of 4 rods and directing the ions through radiofrequency, and the Ion trap analyzer (ITMA), based on electrodes strategically positioned to trap the ions.⁷⁷ This technique is used to quantify known materials, identify unknown compounds within a sample, and elucidate the structure and chemical properties of different molecules.^{77,78}

Determination of free calcium ion using mass spectrometry is previously described in the literature⁷⁵ and can be carried out by mixing the solution containing calcium ion with a buffered EDTA solution. The spectrum shows a peak at mass/charge (m/z) 329 (negative mode), referring to the calcium-EDTA complex. By mixing a buffered EDTA (0.05% methanol/ ammonia solution (1:1 v/v)) with the calcium solution, it is possible to detect the metal complex, using an electrospray ionization (ESI)–MS system. For the detection of Ca^{2+} using this assay, the negative mode is required, detecting $[\text{EDTA}+\text{Ca}^{2+}-3\text{H}^+]^-$ ion at m/z 329 when this ion is present.⁷⁵

The analysis includes the preparation and determination of a calibration curve, followed by the analysis of the sample of interest, in this case, the basal side content of the microchip and the transwell®. A fitting into the calibration curve will give the concentration of calcium present in the sample.

3.1.3.2. Limit of detection and quantification

The limit of detection (LOD) is defined as the lowest concentration of a substance that can be detected and distinguished from a blank solution.⁷⁹ There are three different methods for determining the LOD, based on visual evaluation, on the signal-to-noise relationship, and on the standard deviation of the response and the slope. The best

method for determining the LOD, will depend on the type of analysis and the instrumentation.^{79,80} Since MS was used as a tool for determining the calcium concentration, the most indicated method for determining the LOD is based on the SD of the response and the slope. This methodology includes two possibilities, based on the SD of the blank, or on the SD of multiple calibration curves' intercept. Since the blank gives no responses for the m/z 329, the second SD of the intercept on the calibration curves was used for the calculations. LOD values are calculated by using equation 3.1.⁸⁰

$$LOD: (3.3 \times \sigma) / S \quad (\text{Eq. 3.1.})$$

Where σ is the SD of the response and S is the slope of the calibration curve.

The limit of quantification (LOQ) is also determined following the same rules further explained for the LOD and should be based on the LOD calculation. LOQ values are calculated by using equation 3.2. as follows.^{79,80}

$$LOQ: (10 \times \sigma) / S \quad (\text{Eq. 3.2.})$$

Where σ is the SD of the response and S is the slope of the calibration curve.

3.1.3.3. MALDI-TOF-MS/MS for peptide profile

Cell-penetrating peptides are the subject of numerous studies due to their potential in delivering drugs and nutrients across the cells. Peptides can be identified and characterized directly by using MALDI-TOF and quantified relative to a standard addition.^{81,82}

MALDI is an ionization method of MS, in which a matrix carrying the samples, is irradiated with a pulsed laser to cause the ablation and desorption of the material into the matrix, and the final ionization by protonation or deprotonation of the analyte. The ions are then accelerated to the MS detector through the mass analyzer, in this case, TOF. The basic principle of TOF is to accelerate the ions in a known space length, so the ions reach the detector according to their specific m/z relationship. The ion accelerator must speed the ions in the same initial position and velocity, and for this, an orthogonal accelerator is often used, guaranteeing an effective resolution. In addition, to increase the resolution and have a more reliable analysis, a reflector is often introduced into the TOF

system, named reflector. This reflector consists of high voltage electrodes that reflect the ions, creating a longer path to fly, and consequently a more time-resolved analysis.⁸³⁻⁸⁵

This technique is often applied to proteome studies including exact mass determination, peptide profile, and analysis of decomposition, among others.⁸³ For the purposes of this work, it was intended to analyze the peptides absorbed from a whey hydrolysate in two different transport experiments, the transwell®, and the loaC. Moreover, these peptides were compared to a previous identification made by previsoly in our Group using nano-LC (nLC)-MS and the software Proteome Discoverer® for the mass profile classification. The main goal of this peptide profile was to investigate possible calcium carriers in the hydrolysate Peptigen® boosted with calcium and compare it with the Peptigen itself.

3.2. OBJECTIVES

This part of the work aims to compare the samples from the transport of calcium and peptides through epithelial cells using different techniques. For this, Direct insertion ESI-MS and MALDI-TOF-MS/MS were used to identify and quantify the absorbed calcium ions and peptides from commercial samples of whey hydrolysate. A further evaluation of calcium transporters was also carried out on all platforms.

3.3. MATERIALS & METHODS

3.3.1. Transport experiment

For transwell®, the transport experiment was carried out by washing the monolayer of cells with HBSS for three times and placing the investigated solutions. Triplicate wells were used for each sample, and once the solutions were placed, 0 apical and 0 basal samples were collected. The plate was incubated at 37°C and mild agitation for 60 minutes. A final apical and basal aliquot was then collected for the analysis.

For the on-chip experiment, three final chips of each kind (acrylic and PDMS) were evaluated for performing the transport experiments. Once the monolayer assessment assured integrity, those devices were ready for the experiment. All devices were washed with HBSS previously, and then, a 10 µL/min flow of the investigated solution was established on the apical chamber. Simultaneously, a 10 µL/min flow of HBSS was established on the basal chamber. Both chamber's aliquots were collected at their specific

outlets for 60 minutes under 37 degrees Celsius. The same experiment was carried out for the three devices at a time. The same devices were used for the three samples (Pep, PepCa, and Ca(II), sequentially), and the devices were washed with HBSS in between each sample.

3.3.2. ESI-MS Analysis

All ESI-MS analyses were carried out by adding 50 μ L of sample (diluted in HBSS) and 50 μ L of a 30 mM EDTA aqueous $\text{NH}_3/\text{NH}_4\text{Cl}$ buffer solution, and for all analyses, a set of three independent calibration curves was prepared. The calibration curves were also prepared 1:1 (v/v) with a 30 mM EDTA aqueous $\text{NH}_3/\text{NH}_4\text{Cl}$ buffer solution. The analyses were made in a Thermo Scientific® LTQ Orbitrap Velos Mass Spectrometer with a direct insertion system, connecting the autosampler directly to the ESI source. Water with 10% methanol (v/v) was used as mobile phase and the samples were injected at 30 μ L/min in triplicate. Both calibration curves and samples were analyzed using the selective ion monitoring (SIM) mode. The specific conditions used were: ion trap, negative mode, scan (150-1000 m/z), SIM (291 m/z and 329 m/z), 2.5kV, 200°C capillary temperature, and 150°C for the heater. Data treatment was made according to the area of the extracted ion chromatogram (EIC) of the m/z 329 peak. These areas were then attributed to their respective concentrations. External calibration curves were constructed and the concentrations of calcium of the samples were determined based on these curves. The concentrations were then used for quantifying the respective Papp according to equation 2.3. The curves' LOQ, LOD and linear range were also determined. The final calculated values consider the dilution factor of two times for the mixture with EDTA and six times for the basal dilution plus the mixture with EDTA.

Materials: EDTA solution (30 mM) in $\text{NH}_3/\text{NH}_4\text{Cl}$ buffer 0.5 M (pH 10), Milli-Q water (10% methanol), CaCl_2 (Synth® cat no. 01C2013.01) solutions (0.025 to 20 mM), HBSS, Peptigen® IF3080 (Arla Foods Ingredients) (10 mg/mL), Peptigen+Ca (10 mg/mL + 15 mM CaCl_2 solution).

3.3.3. MALDI analysis

All the analyses were carried out on an AutoFlex Max (TOF/TOF) MS (Bruker Daltonics) using a solution of α -cyano-4-hydroxycinnamic acid in 50% acetonitrile/ 50% water, and 0.1% trifluoroacetic acid used as matrix. An internal standard (Angiotensin I) was used to quantify all the samples, by mixing them to sample aliquots to a final concentration of 0.5 μ M. For relative quantification, the intensity of the Angiotensin I signal (m/z 1296) was used to normalize all the peptide's intensities, and the mass spectra were acquired in positive ion reflector mode over the mass range 500-3500 m/z.

All data was treated considering ions present in at least 2 samples of the triplicate. HBSS was used as blank for excluding ions exclusive from the buffer solution. After this, an analysis was made with all the ions present on the basal chamber, compared to the apical chamber, searching for possible calcium ion carriers according to their masses. The Papp was calculated according to equation 2.3. and it was always relative to the concentration of the ion on the apical chamber.

Materials: CaCl₂.2H₂O (Synth® cat no. 01C2013.01) (15 mM), Peptigen® IF3080 (Arla Foods Ingredients) (10 mg/mL), Peptigen+Ca (10 mg/mL + 15 mM CaCl₂ solution), α -cyano-4-hydroxycinnamic acid (Bruker CAS 28166-41-8), acetonitrile 99.95% (Bio-Grade), Trifluoroacetic acid (Sigma Aldrich® CAS 76-05-1), Angiotensin I (Sigma Aldrich® CAS 70937-97-2).

3.4. RESULTS & DISCUSSION

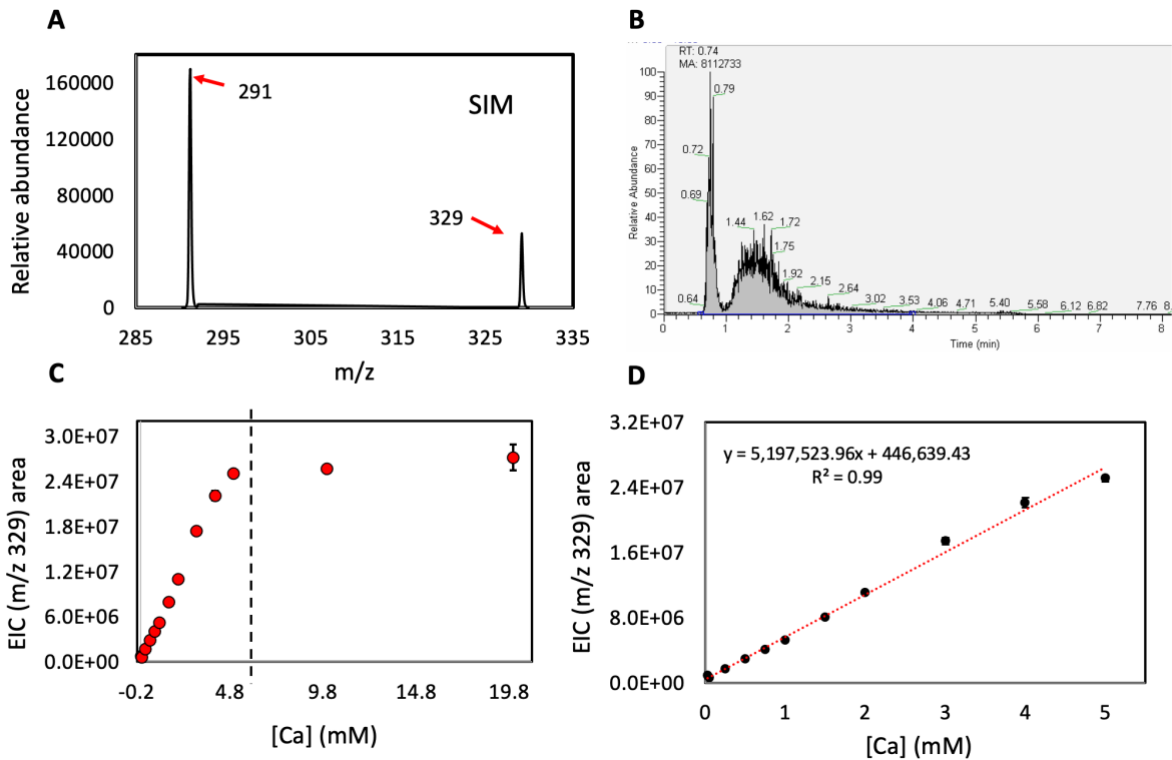
This section will be divided into the results and discussion from the MS, including the transwell® and the loaCs, and from the MALDI, including the transwell® and loaC peptide evaluation.

3.4.1. ESI-MS evaluation

For the detection of calcium ions in samples from the transport experiment, the approach used in this work, was to evaluate the complex formed between EDTA and Ca²⁺ by ESI-MS, observing the ion m/z 329 referred to this complex. As previously described by the literature⁷⁵, m/z 291 is attributed to EDTA, and m/z 329 to [EDTA+Ca²⁺-3H⁺]⁻. All samples were analyzed by direct insertion of a 1:1 solution of EDTA:sample and the

calcium concentration was determined by an external calibration curve. The calibration curve was constructed likewise, by adding 1:1 EDTA solution into each calcium concentration. Figure 3.4-1 is showing the Scan and SIM mass spectra for the samples, indicating the targeted masses, and the calibration curve for the standard calcium solutions. The mass spectra in Figure 3.4-1 A and B are illustrating parts of the methods used for constructing the calibration curve. SIM mode was used for the acquisition since it presented better results. Figure 3.4-1 B is showing a screenshot of the data treatment, using the EIC area of the m/z 329 as a parameter to define the concentration of calcium and determine the calibration curve. Figure 3.4-1 C shows the calibration curve in a broad range (until 20 mM of calcium ion concentration), evidencing that the linear range of this method is from 0 to 5 mM of calcium ion. Figure 3.4-1 D shows the final calibration curve used to quantify the calcium from the transport experiment. shows the final calibration curve used to quantify the calcium from the transport experiment. All the samples from the calibration curve were acquired in triplicate and the data is expressed as the mean \pm SD. The limits of detection (LOD) and quantification (LOQ) of the calibration curve were calculated by using equations 3.1. and 3.2., and were determined as LOD: 0.21 ± 0.06 (mM) and LOQ: 0.63 ± 0.17 (mM). For additional ESI-MS spectra, see Appendix A.

Figure 3.4-1. Mass spectrometry data A) SIM mode spectrum of a 1 mM Ca/EDTA sample, B) Example of a collected area of the EIC analysis, C) Broad concentration range calibration curve, showing the linear range limit, and D) Final calibration curve with equation and R^2

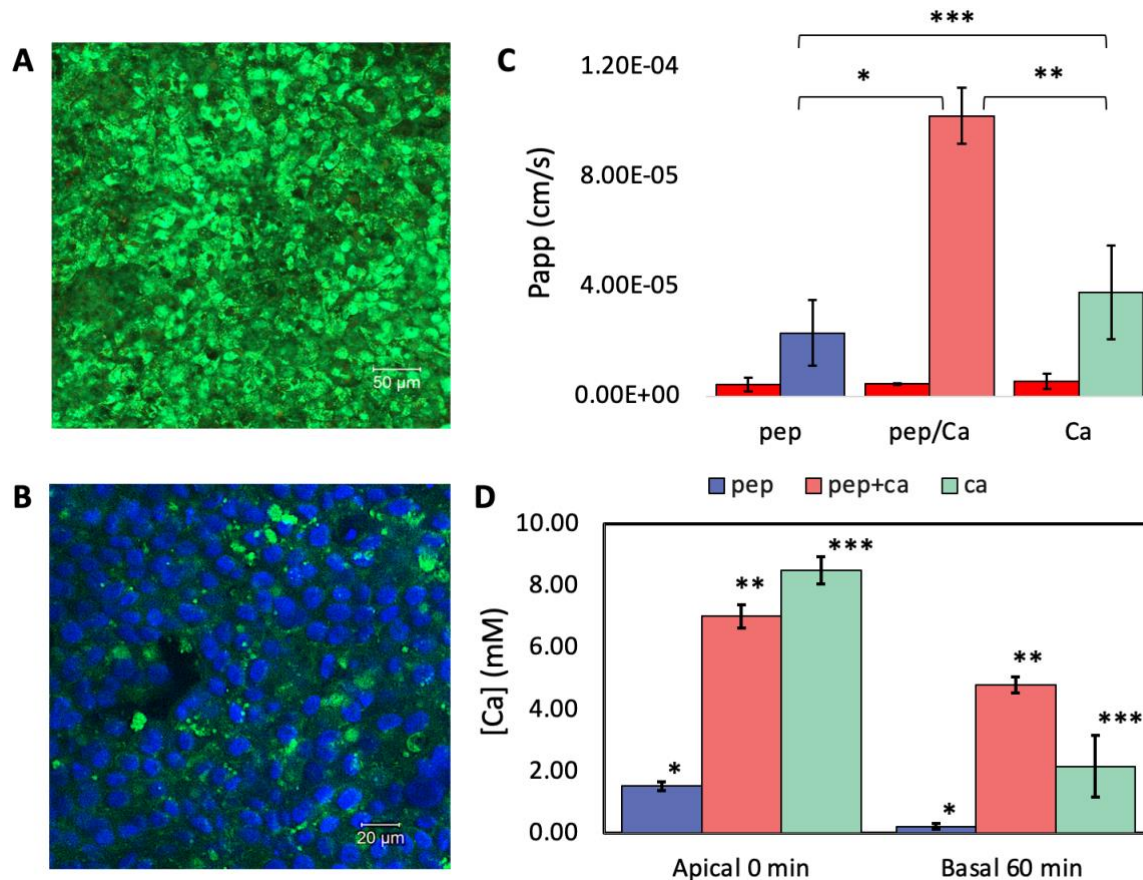


Source: Own authorship

*MA is the value of the collected area of the m/z 329 peak

For the transwell®, each solution was evaluated in triplicate wells and triplicate of ESI-MS acquisition for a more reliable result. Figure 3.4-2 shows mass results for the transport experiment using transwell®. All results are expressed as mean \pm SD and a Student's t-test was performed to evaluate the significance of the values ($p < 0.05$ significant). Figure 3.4-2 C shows the Papp for the phenol red paracellular marker in red, and the Papp for the investigated solutions (Pep, PepCa, and Ca) in colors.

Figure 3.4-2. Transwell® transport experiment of calcium ions: A) Cell monolayer viability, B) Cell monolayer assessment, with nuclei and TJ, C) Papp (cm/s) for PR in red as an average for the 3 wells used to each sample, and for the solutions (color bar) for the triplicate well of each investigated solution D) Comparative apical 0 min and basal 60 min calcium ion concentrations of the transport experiment.



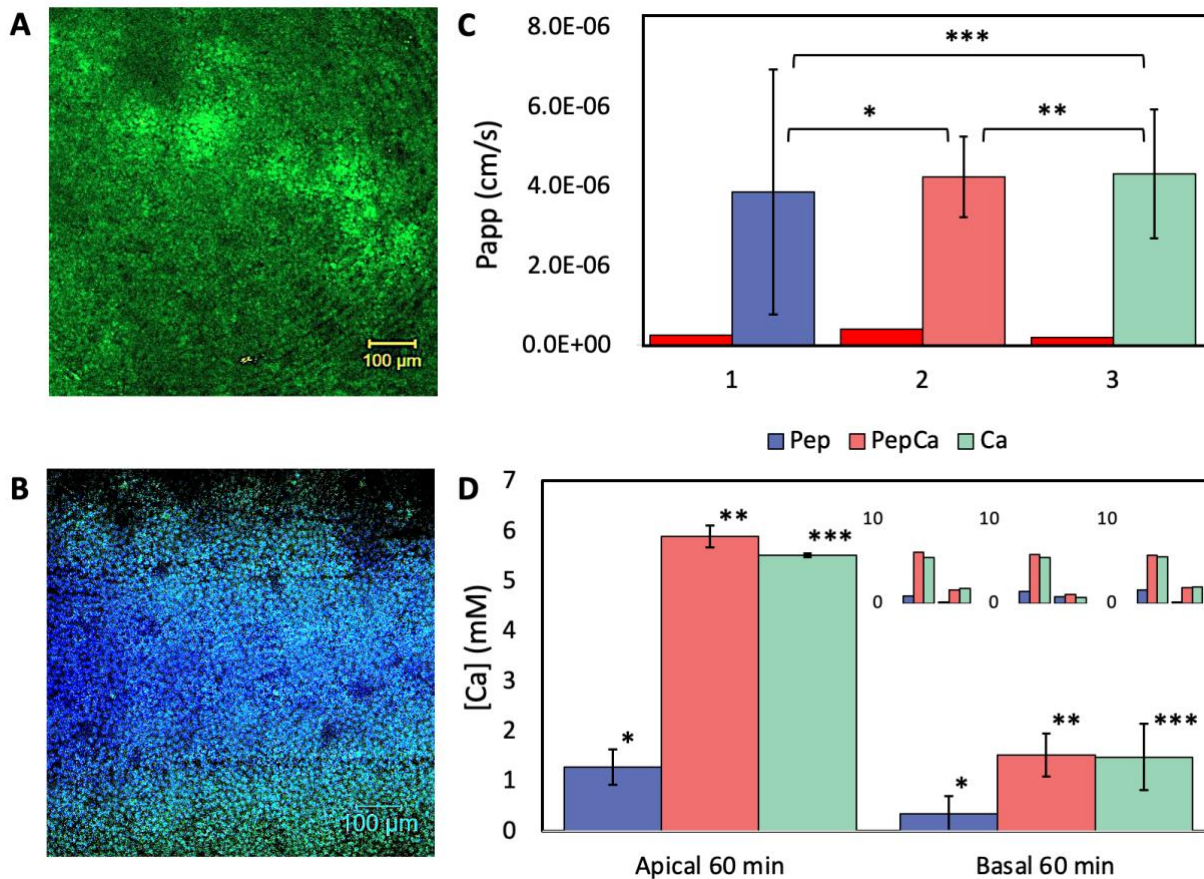
P values for C) * (p < 0.02), ** (p < 0.02), *** (ns); P values for D) * (p < 0.01), ** (p < 0.02), *** (p < 0.006).
 ns – non-significant
 Source: Own authorship

By analyzing the data displayed in Figure 3.4-2 A and B, it is possible to infer that the combination of methods for monolayer assessment guaranteed a reliable analysis, including the PR values of $P_{app} < 5 \cdot 10^{-6}$ cm/s in Figure 3.4-2 C. Furthermore, the ESI-MS data indicated a more efficient transport of calcium in the samples containing Pep+Ca in comparison with the other samples. PepCa presented absorbed calcium concentrations of 4.8 ± 0.3 mM, compared to 0.2 ± 0.09 mM for Pep, and 2.2 ± 0.1 mM for only Ca. The apparent permeability corroborated, indicating 2.3 ± 1.2 (10^{-5} cm/s) for Pep, 10.2 ± 1.0 (10^{-5} cm/s) for PepCa, and 3.8 ± 1.7 (10^{-5} cm/s) for Ca, with significant differences between Pep and PepCa, and PepCa and Ca.

In an effort to compare the validated commercial platform (transwell®) with the developed loaC devices, the same experiment of transport was executed in both models. Three different devices were used for running the experiments at the same time. The final samples of apical 60 min and basal 60 min were collected for analysis at the ESI-MS. All data collected for the three devices were analyzed and a one-way ANOVA test was applied to compare the results, proving the non-significant difference ($p < 0.05$) among them. Therefore, the results from calcium absorption were expressed as the mean \pm SD for the three devices. Figure 3.4-3 shows the monolayer assessment assays, as well as the results for calcium absorption and apparent permeability.

The monolayer assessment guaranteed the integrity of Caco-2 cells by the day of the experiment as exposed in Figure 3.4-3 A and B. The phenol red apparent permeability also corroborated this result, presenting $P_{app} < 10^{-6}$ cm/s. By Figure 3.4-3 C it is also possible to conclude that the apparent permeability of the three independent solutions is non-significantly different, indicating very similar values of 3.9 ± 3.0 (10^{-6} cm/s) for Pep, 4.2 ± 1.0 (10^{-6} cm/s) for PepCa, and 4.3 ± 1.6 (10^{-6} cm/s) for Ca. Although non-significant, PepCa still presented higher levels of calcium permeability compared to the Pep solution and equal numbers if compared to the Ca solution. Figure 3.4-3 D shows the comparative calcium ion concentrations for the final apical and basal samples, showing the absorptions of 0.3 ± 0.3 mM for Pep with a high SD, 1.5 ± 0.4 mM for PepCa, and 1.5 ± 0.6 mM for only Ca. The high SD value for Pep is explained by the fact that chip 2 presented a different reading compared to chips 1 and 3 for this sample. In general, chip 2 presented less consistent data compared to the others.

Figure 3.4-3. Acrylic loaC transport experiment of calcium ions. A) Cell monolayer viability, B) Cell monolayer assessment, with nuclei and TJ, C) Papp for PR in red, and for the solutions in the triplicate devices in colors, D) Comparative apical 60 min and basal 60 min calcium ion concentrations of the transport experiment, the small graphs are the triplicate.



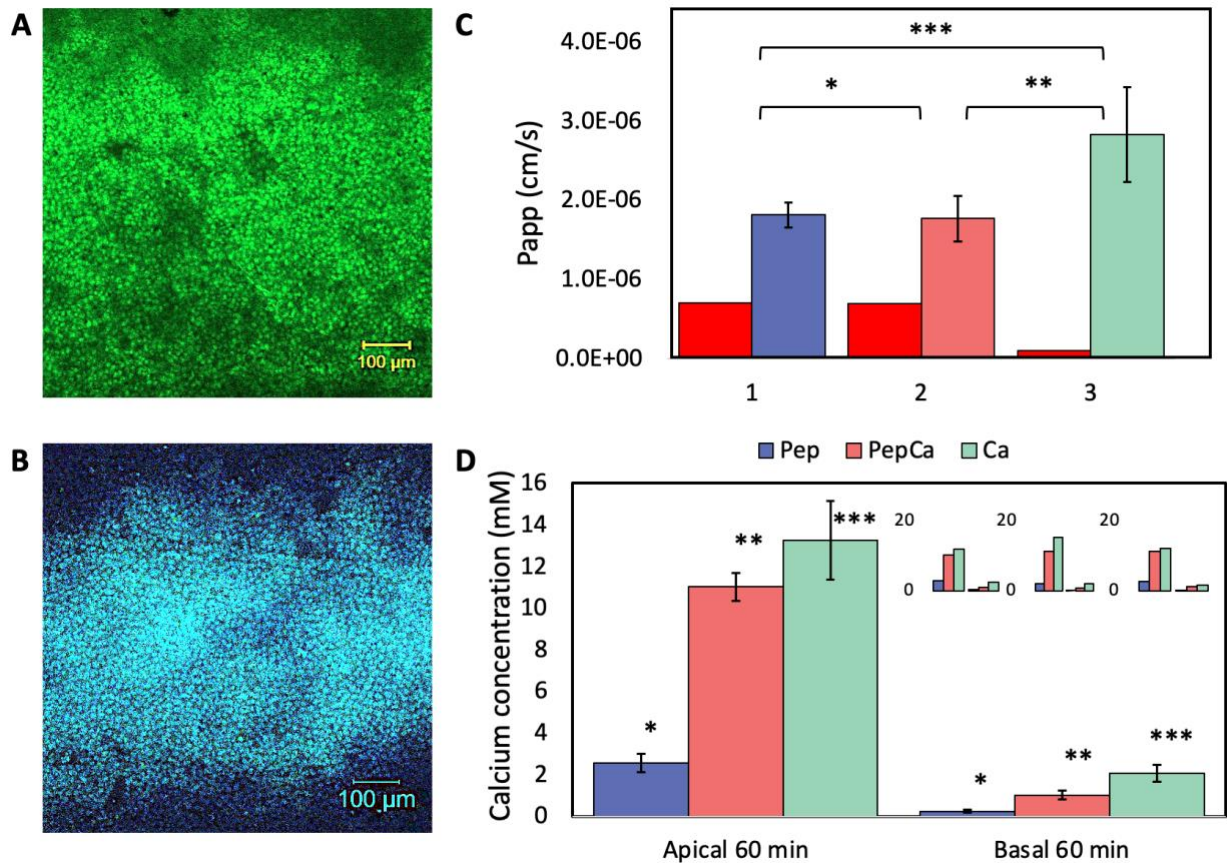
P values for C) * (ns), ** (ns), *** (ns); P values for D) * (ns), ** (p< 0.005), *** (p< 0.007).
 ns – non-significant

1, 2, and 3 are the device numbers, and all devices performed the transport experiment of all solutions.
 Source: Own authorship

Two different models of loaC were developed in this work, therefore both were evaluated to compare the results among each other and with the transwell® platform. As above mentioned, a triplicate of devices was used for the transport experiment of calcium and peptides in all the different samples. The final samples of apical 60 min and basal 60 min were collected for analysis at the ESI-MS. One-way ANOVA was performed to indicate whether there were significant differences among the general device's results. This was confirmed to be non-significant with a 95% confidence interval, as for the other model. Therefore, the results from calcium ion absorption were expressed as the mean ±

SD for the three chips. Figure 3.4-4 shows all the results for monolayer assessment and calcium ion absorption using ESI-MS for the PDMS loaC.

Figure 3.4-4. PDMS loaC transport experiment of calcium ions. A) Cell monolayer viability, B) Cell monolayer assessment, with nuclei and TJ, C) Papp for PR in red and for the solutions in the triplicate chips (colors), D) Comparative apical 60 min and basal 60 min calcium ion concentrations of the transport experiment, the small graphs are the triplicate.



P values for C) * (ns), ** (ns), *** (ns); P values for D) * ($p < 0.01$), ** ($p < 0.005$), *** ($p < 0.01$).

ns – non-significant

1, 2, and 3 are the device numbers, and all devices performed the transport experiment of all solutions.

Source: Own authorship

As for the previous experiments, the integrity of the cell monolayer was determined by the three independent assays, including the viability (A), counterstaining of DAPI/ZO-1 (B), and the phenol red diffusion (C), presenting $P_{app} < 10^{-6}$ cm/s. On Figure 3.4-4 C the colors in the bar chart indicates the apparent permeability of the investigated solutions using the PDMS chip, concluding that they are not significantly different. For this device, oppositely to the other experiments, the Ca ion solution presented the highest absorption of calcium. Although the differences among the solutions are not significant statistically,

the profile of absorption, in this case, changed. The hypothesis is that the compounds from the investigated solutions might also be adsorbed in the PDMS surface, causing the lower permeabilities for the peptides.^{86,87} This was later investigated by Raman spectroscopy, but with inconclusive results (see Appendix B). The values of Papp are 1.8 ± 0.2 (10^{-6} cm/s) for Pep, 1.8 ± 0.3 (10^{-6} cm/s) for PepCa, and 2.8 ± 0.6 (10^{-6} cm/s) for Ca did not present high SD values, indicating that the three devices shown an acceptable reproducibility for this study. Figure 3.4-4 D shows the comparative calcium concentrations for the final apical and basal samples, with the absorptions of 0.2 ± 0.06 mM for Pep, 1.0 ± 0.2 mM for PepCa, and 2.1 ± 0.4 mM for Ca. Student's t-test was performed to compare the apical and basal portions, concluding that all the investigated solutions are significantly different in means of concentration, from the beginning to the end.

Finally, to compare the three platforms, a one-way ANOVA and a paired t test were performed to identify if the Papp for the solutions were different for each method. A significant difference in both tests was indicated with $p < 0.00001$, concluding that either transwell® and the devices or the different devices did not present similar results for Papp. The only similar characteristic present in each one of the platforms was the higher concentration of absorbed calcium for PepCa if compared to Pep alone, but only in terms of calcium ion concentration. An important characteristic observed was that the Papp for the devices, was significantly lower than for the transwell®, explained by the lower residence time of the solutions with the cells in the loaC system. This was previously described by numerous works in the literature^{1,13,88,89}, that under continuous flow, the interaction between the solution and the cell is shorter, allowing a more realistic cell absorption pattern. Furthermore, it is important to highlight the manual aspect of these devices' production, and likewise, the different characteristics attributed to each one of them. The ideal loaC manufacturing would diminish manual steps, enhancing the repeatability of the production.

To support the idea that the delivery of calcium ion by hydrolyzed whey proteins might be enhanced by increasing calcium concentration, MALDI-TOF-MS/MS analysis was performed for the same transport experiment samples to evaluate the transported peptides and whether those are promoting the transport of calcium.

3.4.2. MALDI evaluation of peptides

The analysis of peptides from Peptigen® was made in an effort to identify possible calcium ion transporters and analyze if those were also present in the solutions fortified with calcium ions. For this, the samples from the transport experiment on the transwell®, and the two models of IoaC were analyzed. Besides the calcium carriers, a peptidome analysis of the most absorbed peptides was also carried out. Typical MALDI spectra are depicted in Appendix C.

For the transwell®, the results of the absorbed peptides are shown in Table 3.4-1 for the Pep solution, and in Table 3.4-2 for PepCa. The amino acid (AA) sequence, protein precursor, and apparent permeability of each m/z are collected in this table. All Papp values are expressed as the mean \pm SD. The bold lines were the peptides that were not present on the apical compartment, therefore, their Papp could not be calculated. It is important to emphasize that the peptide content of Pep was previously characterized by nLC-MS in our Group by using nLC-ESI-MS data and the Proteome Discoverer® software. Due to the low match attributed to most masses found in this work, the amino acid (AA) sequences with low probability were not used as a parameter to take conclusions, since a wide number of different sequences were attributed to each of those masses.

Table 3.4-1. Transport of peptides and Papp for the Peptigen® solution with the protonated masses, AA sequence attributed to the mass, possible protein origin, and the Papp. Uncalculated Papp is due to the absence of the ion on the apical compartment in time 0.

[M-H] ⁺ (Da)	AA Sequence	Protein	Papp (10 ⁻⁵ cm/s)	Sample
728.32	PPRPDF*	Sorting nexin 6 (Fragment) OS=Bos taurus GN=SNX6 PE=2 SV=1 - [A5D9F7_BOVIN]	0.41 \pm 0.07	Pep
792.34	LVYFPFG*	Beta-casein OS=Bos taurus GN=CSN2 PE=1 SV=2 - [CASB_BOVIN]	-----	Pep
808.32	EEDDAVM*	Diacylglycerol O- acyltransferase 1 OS=Bos taurus GN=DGAT1 PE=2 SV=2 - [DGAT1_BOVIN]	2.09 \pm 1.24	Pep
826.37	EAHDEEP*	-----	0.56 \pm 0.33	Pep
932.36	DTDYKKY**	Beta-lactoglobulin OS=Bos taurus	1.92 \pm 1.87	Pep

		GN=LGB PE=1 SV=3 - [LACB_BOVIN]		
1019.46	IVQNNDSTE*	Alpha-lactalbumin OS=Bos taurus GN=LALBA PE=1 SV=2 - [LALBA_BOVIN]	-----	Pep
1035.44	YQKDDNGVP*	Fructose-bisphosphate aldolase OS=Bos taurus GN=ALDOC PE=2 SV=2 - [Q3ZBY4_BOVIN]	2.69 ± 1.93	Pep
1059.43	VRTPEVDDE***	Kappa-casein OS=Bos taurus GN=CSN3 PE=1 SV=1 - [CASK_BOVIN]	0.35 ± 0.29	Pep
1106.47	YCFHLCLAH*	Toll-like receptor 9 OS=Bos taurus GN=tlr9 PE=4 SV=1 - [Q866B2_BOVIN]	0.81 ± 0.70	Pep
1122.52	TYAVSAAGVVNA*	Protein Wnt OS=Bos taurus GN=BT.88484 PE=3 SV=1 - [E1BDG5_BOVIN]	0.77 ± 0.48	Pep
1138.46	VYPFPGPIP(+Ca)***	Beta-casein OS=Bos taurus GN=CSN2 PE=1 SV=2 - [CASB_BOVIN]	0.81 ± 0.48	Pep
1140.48	SDEADCDVCL*	Uncharacterized protein (Fragment) OS=Bos taurus GN=Bt.68746 PE=4 SV=1 - [F1N1K8_BOVIN]	0.87 ± 0.51	Pep
1282.60	VCYNPMETHI(+2Ca)*	Carnitine acetyltransferase OS=Bos taurus GN=MGC142781 PE=2 SV=1 - [Q08DN5_BOVIN]	-----	Pep
1679.89	AIPPKKNQDKTEIPT***	Beta-lactoglobulin OS=Bos taurus GN=LGB PE=1 SV=3 - [LACB_BOVIN]	1.27 ± 0.78	Pep
1701.90	KCVRAKIQEYHILT*	-----	1.55 ± 0.96	Pep
1717.85	AIPPKKNQDKTEIPT(+Ca)***	Beta-lactoglobulin OS=Bos taurus GN=LGB PE=1 SV=3 - [LACB_BOVIN]	1.54 ± 0.90	Pep

The bold lines are the ions further characterized as calcium bound to peptides.

* low probability, ** medium probability, *** high probability.

Table 3.4-2. Transport of peptides and Papp for the Peptigen® + Ca solution (PepCa), with the protonated masses, AA sequence attributed to the mass, possible protein origin, and the Papp. Uncalculated Papp is due to the absence of the ion on the apical compartment.

[MH] ⁺ (Da)	AA Sequence	Protein	Papp (10 ⁻⁵ cm/s)	Sample
728.32	PPRPDF*	Sorting nexin 6 (Fragment) OS=Bos taurus GN=SNX6 PE=2 SV=1 - [A5D9F7_BOVIN]	0.34 ± 0.14	PepCa
892.92	QIFKGS LQPNASHTHDI*	-----	-----	PepCa
908.88	KVLPVPQK**	Beta-casein OS=Bos taurus GN=CSN2 PE=1 SV=2 - [CASB_BOVIN]	-----	PepCa
932.36	DTDYKKY**	Beta-lactoglobulin OS=Bos taurus GN=LGB PE=1 SV=3 - [LACB_BOVIN]	1.06 ± 0.37	PepCa
1059.43	VRTPEVDDE***	Kappa-casein OS=Bos taurus GN=CSN3 PE=1 SV=1 - [CASK_BOVIN]	0.23 ± 0.10	PepCa
1122.51	TYAVSAAGVVNA*	Protein Wnt OS=Bos taurus GN=BT.88484 PE=3 SV=1 - [E1BDG5_BOVIN]	0.66 ± 0.24	PepCa
1138.46	VYFPFGPIP(+Ca)***	Beta-casein OS=Bos taurus GN=CSN2 PE=1 SV=2 - [CASB_BOVIN]	0.67 ± 0.14	PepCa
1140.50	SDEADCAVCL*	Uncharacterized protein (Fragment) OS=Bos taurus GN=Bt.68746 PE=4 SV=1 - [F1N1K8_BOVIN]	0.55 ± 0.08	PepCa
1173.497	GANRLTLEDAN*	Uncharacterized protein (Fragment) OS=Bos taurus GN=Bt.68746 PE=4 SV=1 - [F1N1K8_BOVIN]	0.62 ± 0.21	PepCa
1250.55	VKDVDFFFEH*	Sorting nexin 6 (Fragment) OS=Bos taurus GN=SNX6 PE=2 SV=1 - [A5D9F7_BOVIN]	1.2 ± NA	PepCa
1282.80	VCYNPMETHI(+2Ca)*	Carnitine acetyltransferase OS=Bos taurus GN=MGC142781 PE=2 SV=1 - [Q08DN5_BOVIN]	-----	PepCa
1294.50	PFYACACPTGVQ(+Ca)*	Uncharacterized protein (Fragment) OS=Bos taurus GN=Bt.68746 PE=4 SV=1 - [F1N1K8_BOVIN]	-----	PepCa
1372.57	KRKWEAAGAAER*	-----	-----	PepCa
1466.67	SSRQPQSQNP KLP*	Glycosylation-dependent cell adhesion molecule 1 OS=Bos taurus	0.66 ± 0.27	PepCa

		GN=GLYCAM1 PE=1 SV=2 - [GLCM1_BOVIN]		
1679.84	AIPPKKNQDKTEIPT***	Beta-lactoglobulin OS=Bos taurus GN=LGB PE=1 SV=3 - [LACB_BOVIN]	0.88 ± 0.37	PepCa
1701.88	KCVRAKIQEYHILT*	-----	0.89 ± 0.33	PepCa
1717.82	AIPPKKNQDKTEIPT(+Ca)***	Beta-lactoglobulin OS=Bos taurus GN=LGB PE=1 SV=3 - [LACB_BOVIN]	1.13 ± 0.02	PepCa

The bold lines are the ions further characterized as calcium bound to peptides. * low probability, ** medium probability, *** high probability

NA – non applied for the 1250.55 Da mass, which only appeared in one apical sample

A further study was made in order to compare all the ions from the basal compartment (absorbed) with the masses from the apical compartment to verify if a mass difference would be attributed to calcium binding to peptides. The same comparison was made among the apical ions to verify if the carriers were also present in this compartment. Table 3.4-3 shows the attributions and conclusions about the masses. As previously reported by (Jobst *et al.*, 2008)⁹⁰ Ca ions binds to peptides through deprotonated acidic sites and oxygens from carbonyl groups, being the most common AAs carrying calcium the aspartic and glutamic acids, followed by leucine, histidine, asparagine, alanine, glycine, glutamine, cysteine, arginine, and lysine in order of binding affinity.⁹¹ It is possible to observe mass differences in the MALDI spectrum of 37.95 Da for [M-H+Ca]⁺ and 75.95 Da for [M-3H+2Ca]⁺, indicating one or two calcium bound to peptides.⁹⁰ Therefore, all masses from the apical and basal compartments were evaluated to find possible carriers. Table 3.4-3 shows the relation of the carriers found and their respective mass differences.

Table 3.4-3. Analysis of possible calcium transporters from transwell® with the masses from basal and apical compartments, and their subtractions. The designations were based on the literature.

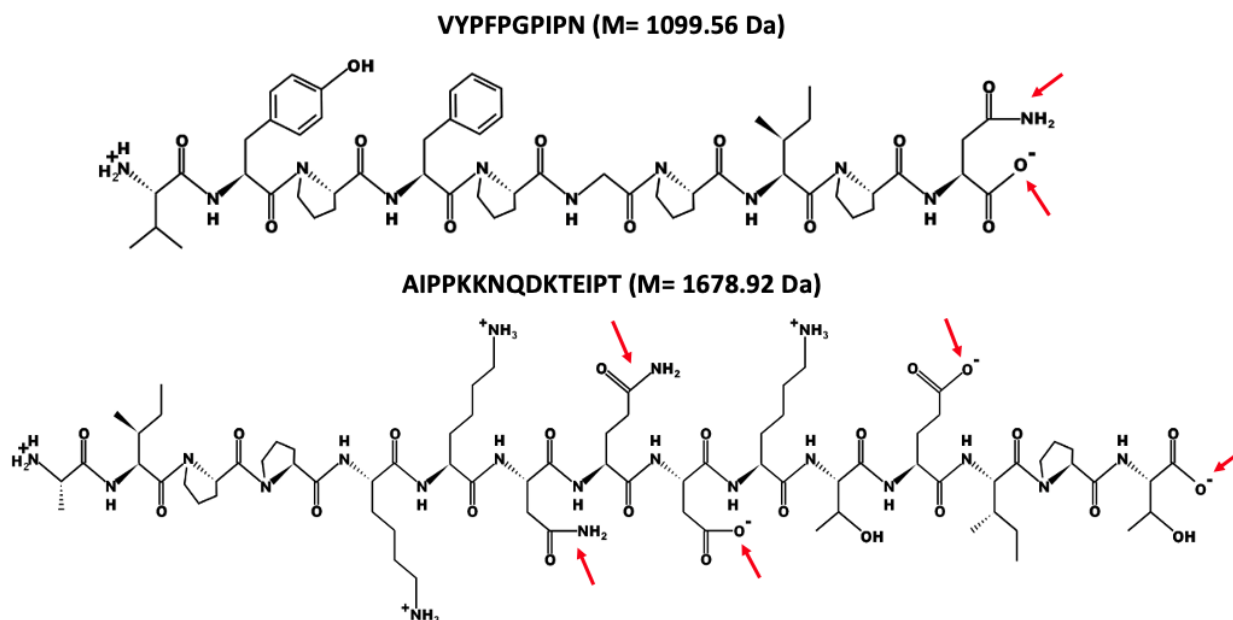
[M-H+Ca] ⁺ or [M-3H+2Ca] ⁺ (Da)	[MH] ⁺ (Da)	M1-M2 (Da)	AA Sequence	Designations	Sample
1138.46 (B)	1100.49 (A)	37.97	VYFPFGPIPN***	[M-H+Ca] ⁺	Pep
1717.85 (B)	1679.78 (A)	38.06	AIPPKKNQDKTEIPT***	[M-H+Ca] ⁺	Pep
988.36 (A)	912.37 (A)	75.99	RGDCMYAP*	[M-3H+2Ca] ⁺	Pep
1138.43 (A)	1100.49 (A)	37.94	VYFPFGPIPN***	[M-H+Ca] ⁺	Pep
1717.73 (A)	1679.78 (A)	37.95	AIPPKKNQDKTEIPT***	[M-H+Ca] ⁺	Pep

1138.50 (B)	1100.48 (A)	38.02	VYFPFGPIP ^N ***	[M-H+Ca] ⁺	PepCa
1282.80 (B)	1206.51 (A)	76.29	VCYNPMETHI [*]	[M-3H+2Ca] ⁺	PepCa
1294.50 (B)	1256.58 (A)	37.92	PFYACACPTGVQ [*]	[M-H+Ca] ⁺	PepCa
1717.82 (B)	1679.78 (A)	37.96	AIPPKKNQDKTEIPT ^{***}	[M-H+Ca] ⁺	PepCa
1138.46 (A)	1100.48 (A)	37.99	VYFPFGPIP ^N ***	[M-H+Ca] ⁺	PepCa
1178.49 (A)	1140.52 (A)	37.97	IHYGSGSLSGY [*]	[M-H+Ca] ⁺	PepCa
1717.78 (A)	1679.85 (A)	37.92	AIPPKKNQDKTEIPT ^{***}	[M-H+Ca] ⁺	PepCa

(A) is apical and (B) is basal, *low probability, ** medium probability, *** high probability
In bold, the masses for the peptides identified as calcium carriers.

On Table 3.4-3 it is possible to observe a few calcium carriers such as ions m/z 912.37, 1100.49, 1140.52, 1206.51, 1256.58, and 1679.78. Most of those ions were found only in the apical compartments for both solutions, with the exception for m/z 1140.52, and m/z 1679.78 that were also found in the basal. All the identified ions bound to calcium were found in both chambers (apical and basal). Ions with m/z 1100.49 and m/z 1679.78 presented high confidence AA sequences, being annotated to VYFPFGPIP^N, and AIPPKKNQDKTEIPT, respectively. According to their molecule structure, it was possible to observe a few sites in which calcium might be bound. Figure 3.4-5 shows the molecules for both peptides and the possible sites of calcium bonding in red. The theoretical mass of each peptide is also indicated in the figure, showing differences of approximately 1Da to the experimental mass, regarding the protonation of the analysis. Finally, evaluating the actual transport of the AAs carrying calcium across the cell monolayer, for Pep only two were observed (ions m/z 1138.46, and m/z 1717.73). An important observation is that the ion m/z 1282.80 was present in the basal side of this sample, although the precursor peptide (m/z 1206.51) was not found in any compartment. For PepCa, four different ions were transported (m/z 1138.46, 1282.80, 1294.50, and 1717.73). The reason for having more peptides transporting calcium in the PepCa solution might be related to the higher concentration of this ion, shifting the complexation equilibrium and leading to a more efficient transport, corroborating the ESI-MS results with higher P_{app} of calcium for the PepCa solution.

Figure 3.4-5. Chemical structures of peptides m/z 1100.49 and 1679.78, indicating the possible binding sites for calcium into the side chain of the amino acids.



Source: Own authorship

As for the transwell®, the transport of peptides was also evaluated on the loaC devices. Table 3.4-4 shows the resultant transported peptides and their Papp for the acrylic device.

Table 3.4-4. Transport of peptides for the acrylic loaC, with the protonated masses, AA sequence attributed to the mass, possible protein origin, and the Papp. Uncalculated Papp is due to the absence of the ion on the apical compartment.

[MH] ⁺ (Da)	AA Sequence	Protein	Papp (10 ⁻⁴ cm/s)	Sample
932,36	DTDYKKY**	Beta-lactoglobulin OS=Bos taurus GN=LGB PE=1 SV=3 - [LACB_BOVIN]	8.26 ± 13.7	Pep
1059,43	VRTPEVDDE***	Kappa-casein OS=Bos taurus GN=CSN3 PE=1 SV=1 - [CASK_BOVIN]	1.19 ± 1.29	Pep
1679,89	AIPPKKNQDKTEIPT***	Beta-lactoglobulin OS=Bos taurus GN=LGB PE=1 SV=3 - [LACB_BOVIN]	2.48 ± 3.48	Pep
1717,85	AIPPKKNQDKTEIPT(+Ca)***	Diacylglycerol O- acyltransferase 1 OS=Bos taurus GN=DGAT1 PE=2 SV=2 - [DGAT1_BOVIN]	3.65 ± 3.46	Pep
932,36	DTDYKKY**	Beta-lactoglobulin OS=Bos taurus GN=LGB	1.17 ± 0.55	PepCa

		PE=1 SV=3 – [LACB_BOVIN]		
1059,43	VRTPEVDDE***	Kappa-casein OS=Bos taurus GN=CSN3 PE=1 SV=1 - [CASK_BOVIN]	0.86 ± 1.01	PepCa
1122,51	TYAVSAAGVVNA*	Protein Wnt OS=Bos taurus GN=BT.88484 PE=3 SV=1 - [E1BDG5_BOVIN]	0.92 ± 0.76	PepCa
1679,84	AIPPKKNQDKTEIPT***	Beta-lactoglobulin OS=Bos taurus GN=LGB PE=1 SV=3 - [LACB_BOVIN]	3.29 ± 2.76	PepCa
1701,88	KCVRAKIQEYHILT*	-----	17.7 ± 26.3	PepCa
1717,95	AIPPKKNQDKTEIPT(Ca)***	Beta-lactoglobulin OS=Bos taurus GN=LGB PE=1 SV=3 - [LACB_BOVIN]	17.1 ± 31.9	PepCa
1723.95	-----	-----	-----	PepCa

The bold lines are the ions further characterized as calcium bound to peptides. * low probability, ** medium probability, *** high probability

On Table 3.4-4 it is possible to observe that all peptides found on the transport experiment for the acrylic loaC were also found on the transwell®, with the only exception being the ion 1723.94. This ion was also not annotated in the peptidome analysis of Pep by nLC-MS, indicating that this may be a result of cellular metabolism or remnants from the device components. Moreover, Papp values for peptide transport across de Caco-2 cell monolayer presented high SD due to the different measurements for the different devices. The SD for Papp values of transwell® were also high, but this method have shown a better reproducibility on the data if compared to the acrylic loaC in this scenario. For the acrylic loaC, the evaluation of possible calcium carriers was also carried out. Table 3.4-5 shows the results for this study.

Table 3.4-5. Analysis of possible calcium transporters from the acrylic loaC with the masses from basal and apical compartments, and their subtractions. The designations were based on the literature.

[M-H+Ca] ⁺ or [M-3H+2Ca] ⁺ (Da)	[MH] ⁺ (Da)	M1-M2 (Da)	AA Sequence	Designation	Sample
1717.97 (B)	1679.98 (A)	37.99	AIPPKKNQDKTEIPT***	[M-H+Ca] ⁺	Pep
1717.97 (A)	1679.98 (A)	37.99	AIPPKKNQDKTEIPT***	[M-H+Ca] ⁺	Pep
1717.94 (B)	1679.96 (A)	37.98	AIPPKKNQDKTEIPT***	[M-H+Ca] ⁺	PepCa

719.83 (A)	681.96 (A)	37.98	VFRLQNPVKARVPEQ*	[M-H+Ca] ⁺	PepCa
1144.53 (A)	1106.57(A)	37.96	LNVNEEYLI*	[M-H+Ca] ⁺	PepCa
1717.91 (A)	1679.96 (A)	37.95	AIPPKKNQDKTEIPT***	[M-H+Ca] ⁺	PepCa

(A) is apical and (B) is basal, *low probability, ** medium probability, *** high probability
In bold, the masses for the peptides identified as calcium carriers.

By observing Table 3.4-5 it is possible to identify the ions m/z 681.96, 1106.57, and 1679.78 as peptides bound to calcium ion. Those ions were attributed to the AA sequences and the only attribution with high probability was the ion with m/z 1679.98, also detected in the transwell® samples. The only possible peptide bound to calcium that was effectively absorbed in the acrylic loaC was the ion m/z 1717.97 in both solutions (Pep and PepCa). Moreover, for this method, three peptides bounding calcium were found in the PepCa solution, while only one in the Pep. As for the transwell®, PepCa tends to show more peptides bounding calcium, which might consequently lead to a more efficient absorption of this nutrient, also corroborant to the MS data.

For the PDMS loaC the same study was carried out to evaluate the same parameters as for the other two methodologies. Table 3.4-6 shows the results for the peptides found on the basal chamber of the PDMS loaC.

Table 3.4-6. Transport of peptides for the PDMS loaC, with the protonated masses, AA sequence attributed to the mass, possible protein origin, and the Papp. Uncalculated Papp is due to the absence of the ion on the apical compartment.

[MH] ⁺ (Da)	AA Sequence	Protein	Papp (10 ⁻⁴ cm/s)	Sample
761.06	GPEDSLHEQCSPWRKNACC SVNTSI*	-----	-----	Pep
799.01	-----	-----	-----	Pep
1283.09	ILEKKVEKVVV*	-----	-----	Pep
1291.32	DVYHSDGTPLTS*	Carnitine acetyltransferase OS=Bos taurus GN=MGC142781 PE=2 SV=1 - [Q08DN5_BOVIN]	-----	Pep
1679,89	AIPPKKNQDKTEIPT***	Beta-lactoglobulin OS=Bos taurus GN=LGB PE=1 SV=3 - [LACB_BOVIN]	0.96 ± 0.58	Pep
1702.02	SELLSGININKIDISS*	Toll-like receptor 9 OS=Bos taurus GN=tlr9 PE=4 SV=1 - [Q866B2_BOVIN]	-----	Pep

755.02	TGLIRPV*	Uncharacterized protein (Fragment) OS=Bos taurus GN=Bt.68746 PE=4 SV=1 - [F1N1K8_BOVIN]	-----	PepCa
798.98	Ca carrier (NI)	-----	-----	PepCa
1059.43	VRTPEVDDE***	Kappa-casein OS=Bos taurus GN=CSN3 PE=1 SV=1 - [CASK_BOVIN]	1.44 ± 2.15	PepCa
1291.06	GSAQGLGSFVHCE*	-----	-----	PepCa
1294.49	-----	-----	-----	PepCa
1305.10	PFDPKITCKQE*	-----	-----	PepCa
1679.84	AIPPKKNQDKTEIPT***	Beta-lactoglobulin OS=Bos taurus GN=LGB PE=1 SV=3 - [LACB_BOVIN]	6.08 ± 5.40	PepCa
1702.00	RMTIEPNTFLAVPTL*	-----	9.30 ± 8.00	PepCa
1717.99	AIPPKKNQDKTEIPT(+Ca)***	Beta-lactoglobulin OS=Bos taurus GN=LGB PE=1 SV=3 - [LACB_BOVIN]	3.07 ± 0.98	PepCa
1724.01	-----	-----	-----	PepCa

*low probability, ** medium probability, *** high probability, NI – Non identified.
In bold, the masses for the peptides identified as calcium carriers.

The results collected in Table 3.4-6 show that a few peptides found on the transport experiment carried out on the PDMS loaC, were not found neither on the transwell®, nor on the acrylic loaC. Those are ions m/z 761.06, 798.98, 799.01, and 1294.49. In addition, ion m/z 1724.01 was also not found on transwell®, although it appeared for the acrylic loaC experiment as well. Except for those ions, all the others were found for transwell® and are attributed to the whey hydrolysate, being the ones not found in any analysis, possibly attributed to Caco-2 cell metabolism. The Papp calculations for this device also presents high SD, assigned to the different measurements found in the three different devices, leading to the conclusion that this device is also not as reproducible as the transwell® for this analysis. The evaluation of calcium carriers for the PDMS loaC was also carried out. Table 3.4-7 shows the results for this study.

Table 3.4-7. Analysis of possible calcium transporters for the PDMS loaC with the masses from basal and apical compartments, and their subtractions.

[M-H+Ca]⁺ or [M-3H+2Ca]⁺ (Da)	[MH]⁺ (Da)	M1-M2 (Da)	AA Sequence	Designation	Sample
914.98 (A)	877.04 (A)	37.94	AKLAEAFK*	[M-H+Ca] ⁺	Pep
970.37 (A)	932.43 (A)	37.94	DTDYKKY**	[M-H+Ca] ⁺	Pep
1144.51 (A)	1106.56 (A)	37.95	PVMIWIYGGA*	[M-H+Ca] ⁺	Pep
1160.48 (A)	1122.54 (A)	37.95	LSEYFKHAK*	[M-H+Ca] ⁺	Pep
798.98 (B)	760.99 (A)	37.99	-----	[M-H+Ca] ⁺	PepCa
1717.99 (B)	1679.99 (A)	38.00	AIPPKKNQDKTEIPT***	[M-H+Ca] ⁺	PepCa
744.85 (A)	706.82 (A)	38.02	-----	[M-H+Ca] ⁺	PepCa
893.01 (A)	855.04 (A)	37.97	QVRVEPK*	[M-H+Ca] ⁺	PepCa
908.99 (A)	871.02 (A)	37.97	ILDKVGIN*	[M-H+Ca] ⁺	PepCa
1104.03 (A)	1066.06 (A)	37.97	-----	[M-H+Ca] ⁺	PepCa
1120.02 (A)	1082.04 (A)	37.98	HCATQGQLPQ*	[M-H+Ca] ⁺	PepCa
1717.97 (A)	1679.99 (A)	37.98	AIPPKKNQDKTEIPT***	[M-H+Ca] ⁺	PepCa

(A) is apical and (B) is basal, *low probability, ** medium probability, *** high probability
In bold, the masses for the peptides identified as calcium carriers.

The results collected in Table 3.4-7 show different possible carriers from the ones first noted, most of them only observed in the apical compartment of the PDMS device. The possible calcium carrier ions are m/z 706.82, 760.99, 855.04, 871.02, 877.04, 1066.06, 1082.04, 1106.56, and 1679.99. In this experiment, the only peptides bound to calcium actually transported to the basal compartment were ions m/z 798.98 and 1717.99 from the PepCa solution, none from Pep. This again indicates a more efficient transport of calcium for PepCa solution, although in this specific experiment, this was not observed in the ESI-MS results. For this experiment, fewer possible peptides carrying calcium was observed, which might corroborate to the hypothesis of the adsorption on the PDMS surface as previously pointed out. Moreover, the only ion with a high probability AA sequence attribution was m/z 1679.99, found in all other experiments. Ions with m/z 706.82, 760.99, and 1066.06 were not assigned in the peptidomic analysis of the whey hydrolysate, and might be generated from cell metabolism.

3.5. CONCLUSION

The ESI-MS analysis of calcium ion transport for biological samples has proven to provide reliable results. The transwell® results demonstrated a more efficient transport of calcium for the PepCa solutions ($P_{app}: 10.2 \pm 1.0 (10^{-5} \text{ cm/s})$), with a significant difference from the other investigated solutions. The transport experiment of calcium ions using the loaCs (acrylic and PDMS) first indicated no significant differences from the data set of the 3 independent devices, being able to use them as a triplicate for the experiment. All cell monolayer assessments of the 6 independent devices indicated that they were ready for the experiment. The acrylic loaC showed non-significant differences among the P_{app} values for the three sample solutions (Pep, PepCa, and Ca). However, PepCa solutions still presented higher P_{app} values ($4.2 \pm 1.0 (10^{-6} \text{ cm/s})$) if compared to Pep solutions alone. The PDMS loaC instead, demonstrated a different pattern for calcium absorption, with the highest P_{app} of calcium on the basal side being addressed to the Ca solution ($2.8 \pm 0.6 (10^{-6} \text{ cm/s})$), although non-significant differences among the solutions were observed. Similar to the acrylic loaC, the P_{app} results from the three different absorbed solutions for the PDMS loaC did not present significant differences. Those P_{app} were also lower compared to the transwell®, explained by the dynamic of the system with shorter residency time of the solutions in contact with the cells in the on-chip platforms. Finally, the three methods used for the transport experiment of calcium ions presented significant differences in the results, indicating that the platforms function in a different manner.

MALDI results for the transwell® annotated a list of different absorbed peptides and their P_{app} could be determined, although with a few high values of SD. For the loaC devices, it was also possible to observe the same and a few additional peptides absorbed. The additional peptides found for the devices were assigned to arise from cell metabolism. The P_{app} of the absorbed peptides from the loaC experiments was determined presenting high SD values, explained by the low intensity of those ions, and the handmade character attributed to the chips' manufacture. The loaC technique for quantifying the P_{app} of peptides using MALDI did not present repeatable results in terms of area and it is not the most indicated for these calculations. Furthermore, a study of possible calcium carrier peptides was carried out for all the platforms (transwell® and loaCs) and it was possible to point a few candidates. Two of those ions were sequenced with high probability, being

m/z 1100.49 (VYFPFGPIP_N) and m/z 1679.78 (AIPPKKNQDKTEIPT), and their possible calcium binding sites were indicated. For both the loaC devices, a few other possible calcium carriers were identified, but the only ion present in all samples and absorbed by all platforms was the m/z 1679.78 or m/z 1717.95 (paired with calcium). Finally, the MALDI results were mostly corroborant to the MS, indicating in all platforms, the presence of calcium transporters in the basal chamber in a higher amount for the PepCa solution if compared to Pep alone. This might indicate the more efficient calcium absorption of this commercial product if boosted with a higher concentration of this nutrient. A final remark for the PDMS device is that fewer possible peptides carrying calcium was observed if compared to the other platforms, which could also be addressed to the peptide adsorption on the PDMS surface as previously pointed out.

FINAL REMARKS

The main goal of this work was to use a new technology for the evaluation of calcium and peptides absorption from dairy products. Moreover, to compare the new method with the in-course commercial platform, the transwell®, proved costly and obsolete, according to the literature. Two models of functional loaC were developed during this research, with the possibility of cell growth and their use for a range of different analysis.

The calcium and peptide absorption experiments demonstrated different results for the transwell® in comparison to the loaC devices, and a further comparison with a real system may indicate which system is more realistic in this sense. The literature indicates OoaCs as a reliable attractive tool for pharmaceutical purposes, and now this technology is becoming tempting for the food industry as well.

More insights and experimentation are still needed to reliably ensure the high efficacy and mimic potential of OoaC devices for evaluation of intestinal absorption. In this research, the construction of the loaCs was very manual, leading to a range of different sources of error. Among the loaCs created, the acrylic device was more suitable for the purposes of this research, due to the possible adsorption associated with the PDMS material and the challenges encountered with the microfabrication using this material. However, it is valuable to study the replacement of old-fashioned methods and seek recyclable ideas, such as the PDMS device. The PDMS device might not be the best choice for this specific approach, but might be perfectly suitable to other purposes. Moreover, although the loaC platforms were not indicated for quantification of peptide's Papp on MALDI, they proved to be a great tool for a qualitative and semi-quantitative analysis in this sense, indicating the presence of important absorbed molecules.

REFERENCES

1. ZHUANG, Q. C.; NING, R. Z.; MA, Y.; LIN, J. M. Recent developments in microfluidic chip for in vitro cell-based research. **Chinese Journal of Analytical Chemistry**, Beijing, v. 44, n. 4, p. 522–532, 2016.
2. BEIN, A.; SHIN, W.; JALILI-FIROOZINEZHAD, S.; PARK, M. H.; SONTHEIMER-PHELPS, A.; TOVAGLIERI, A.; CHALKIADAKI, A.; KIM, H. J.; INGBER, D. E. Microfluidic organ-on-a-chip models of human intestine. **Cellular and Molecular Gastroenterology and Hepatology**, San Diego, v. 5, n. 4, p. 659, 2018.
3. ALAM, M. A.; AL-JENOobi, F. I.; AL-MOHIZEA, A. M. Everted gut sac model as a tool in pharmaceutical research: limitations and applications. **Journal of pharmacy and pharmacology**, Oxford, v. 64, n. 3, p. 326–336, 2012.
4. ROZEHNAL, V.; NAKAI, D.; HOEPNER, U.; FISCHER, T.; KAMIYAMA, E.; TAKAHASHI, M.; YASUDA, S.; MUELLER, J. Human small intestinal and colonic tissue mounted in the Ussing chamber as a tool for characterizing the intestinal absorption of drugs. **European journal of pharmaceutical sciences**, Amsterdam, v. 46, n. 5, p. 367–373, 2012.
5. SATO, T.; VAN ES, J. H.; SNIPPERT, H. J.; STANGE, D. E.; VRIES, R. G.; VAN DEN BORN, M.; BARKER, N.; SHROYER, N. F.; VAN DE WETERING, M.; CLEVERS, H. Paneth cells constitute the niche for Lgr5 stem cells in intestinal crypts. **Nature**, Berlin, v. 469, n. 7330, p. 415–418, 2011.
6. JUNG, P.; SATO, T.; MERLOS-SUÁREZ, A.; BARRIGA, F. M.; IGLESIAS, M.; ROSSELL, D.; AUER, H.; GALLARDO, M.; BLASCO, M. A.; SANCHO, E.; CLEVERS, H.; BATLLE, E. Isolation and in vitro expansion of human colonic stem cells. **Nature medicine**, Berlin, v. 17, n. 10, p. 1225–1227, 2011.
7. HUH, D.; HAMILTON, G. A.; INGBER, D. E. From 3D cell culture to organs-on-chips. **Trends in Cell Biology**, London, v. 21, n. 12, p. 745–754, 2011.
8. HAYCOCK, J. W. 3D cell culture: a review of current approaches and techniques. **Methods in molecular biology**, Clifton, v. 695, p. 1–15, 2011.
9. BHATIA, S. N.; INGBER, D. E. Microfluidic organs-on-chips. **Nature biotechnology**, Berlin, v. 32, n. 8, p. 760–772, 2014.
10. XIANG, Y.; WEN, H.; YU, Y.; LI, M.; FU, X.; HUANG, S. Gut-on-chip: Recreating human intestine in vitro. **Journal of Tissue Engineering**, Thousand Oaks, v. 18, p.11, 2020.

11. IMURA, Y.; ASANO, Y.; SATO, K.; YOSHIMURA, E. A microfluidic system to evaluate intestinal absorption. **Analytical sciences**, London, v. 25, n. 12, p. 1403–1407, 2009.
12. POCOCK, K.; DELON, L.; BALA, V.; RAO, S.; PRIEST, C.; PRESTIDGE, C.; THIERRY, B. Intestine-on-a-chip microfluidic model for efficient in vitro screening of oral chemotherapeutic uptake. **ACS Biomaterials Science and Engineering**, Washington, v. 3, n. 6, p. 951–959, 2017.
13. KASENDRA, M.; TOVAGLIERI, A.; SONTHEIMER-PHELPS, A.; JALILI-FIROOZINEZHAD, S.; BEIN, A.; CHALKIADAKI, A.; SCHOLL, W.; ZHANG, C.; RICKNER, H.; RICHMOND, C. A.; LI, H.; BREault, D. T.; INGBER, D. E. Development of a primary human small intestine-on-a-chip using biopsy-derived organoids. **Scientific Reports**, Berlin, v. 8, n. 1, p. 1–14, 2018.
14. HUANG, C.; RAMADAN, Q.; WACKER, J. B.; TEKIN, H. C.; RUFFERT, C.; VERGÈRES, G.; SILACCI, P.; GIJS, M. A. M. Microfluidic chip for monitoring Ca²⁺ transport through a confluent layer of intestinal cells. **RSC Advances**, Cambridge, v. 4, n. 95, p. 52887–52891, 2014.
15. HOSIC, S.; BINDAS, A. J.; PUZAN, M. L.; LAKE, W.; SOUCY, J. R.; ZHOU, F.; KOPPEs, R. A.; BREault, D. T.; MURTHY, S. K.; KOPPEs, A. N. Rapid prototyping of multilayer microphysiological systems. **ACS Biomaterials Science and Engineering**, Washington, v. 7, n. 7, p. 2949–2963, 2021.
16. TAJEDDIN, A.; MUSTAFAOGLU, N. Design and fabrication of organ-on-chips: promises and challenges. **Micromachines**, Basel, v. 12, n. 12, p. 1443, 2021.
17. LEHMANN, R.; LEE, C. M.; SHUGART, E. C.; BENEDETTI, M.; CHARO, R. A.; GARTNER, Z.; HOGAN, B.; KNOBLICH, J.; NELSON, C. M.; WILSON, K. M. Human organoids: A new dimension in cell biology. **Molecular Biology of the Cell**, Hong Kong, v. 30, p. 1129–1137, 2019.
18. **Dow sylgard 184 silicone elastomer clear 0.5kg (1.1lb)**. Disponível em: <https://krayden.com/buy/sylgard-184-0-5kg-1-1lb-kit-dc4019862.html>. Acessado em: 9 maio, 2022.
19. **Glass price calculator**. Disponível em: <https://www.crystalglassny.com/Store/Glass-Products-Info>. Acessado em: 9 maio, 2022.
20. HIRAMA, H.; SATOH, T.; SUGIURA, S.; SHIN, K.; ONUKI-NAGASAKI, R.; KANAMORI, T.; INOUE, T. Glass-based organ-on-a-chip device for restricting small molecular absorption. **Journal of Bioscience and Bioengineering**, Osaka, v. 127, n. 5, p. 641–646, 2019.
21. **How much do acrylic sheets cost? | howmuchisit.org**. Disponível em: <https://www.howmuchisit.org/acrylic-sheets-cost/>. Acessado em: 9 maio, 2022.

22. BABO, S.; FERREIRA, J. L.; RAMOS, A. M.; MICHELUZ, A.; PAMPLONA, M.; CASIMIRO, M. H.; FERREIRA, L. M.; MELO, M. J. Characterization and long-term stability of historical PMMA: Impact of additives and acrylic sheet industrial production processes. **Polymers**, Basel, v. 12, n. 10, 2020.
23. APEL, P. Track etching technique in membrane technology. **Radiation Measurements**, Oxford, v. 34, n. 1–6, p. 559–566, 2001.
24. WLODARCZYK, K. L.; CARTER, R. M.; JAHANBAKHSH, A.; LOPES, A. A.; MACKENZIE, M. D.; MAIER, R. R. J.; HAND, D. P.; MAROTO-VALER, M. M. Rapid laser manufacturing of microfluidic devices from glass substrates. **Micromachines**, Basel, v. 9, n. 8, p. 409, 2018.
25. WEIBEL, D. B.; DILUZIO, W. R.; WHITESIDES, G. M. Microfabrication meets microbiology. **Nature Reviews Microbiology**, Berlin, v. 5, n. 3, p. 209–218, 2007.
26. WANG, X.; PHAN, D. T. T.; ZHAO, D.; GEORGE, S. C.; HUGHES, C. C. W.; LEE, A. P. An on-chip microfluidic pressure regulator that facilitates reproducible loading of cells and hydrogels into microphysiological system platforms. **Lab on a Chip**, Cambridge, v. 16, n. 5, p. 868–876, 2016.
27. KAARJ, K.; YOON, J. Y. Methods of delivering mechanical stimuli to organ-on-a-chip. **Micromachines**, Basel, v. 10, n. 10, p. 700, 2019.
28. LEUNG, C. M.; DE HAAN, P.; RONALDSON-BOUCHARD, K.; KIM, G. A.; KO, J.; RHO, H. S.; CHEN, Z.; HABIBOVIC, P.; JEON, N. L.; TAKAYAMA, S.; SHULER, M. L.; VUNJAK-NOVAKOVIC, G.; FREY, O.; VERPOORTE, E.; TOH, Y. C. A guide to the organ-on-a-chip. **Nature Reviews Methods Primers**, Berlin, v. 2, n. 1, p. 1–29, 2022.
29. BERTHIER, E.; YOUNG, E. W. K.; BEEBE, D. Engineers are from PDMS-land, biologists are from polystyrenia. **Lab on a Chip**, Cambridge, v. 12, n. 7, p. 1224–1237, 2012.
30. MA, H. L.; URBACZEK, A. C.; ZEFERINO, F.; DE SOUZA, R.; GOMES, P. A.; LEÃO, G. C.; PERUSSI, J. R.; CARRILHO, E. Rapid fabrication of microfluidic devices for biological mimicking: A survey of materials and biocompatibility. **Micromachines**, Basel, v. 12, n. 3, p. 346, 2021.
31. SMETANOVÁ, L.; STĚTINOVÁ, V.; SVOBODA, Z.; KVETINA, J. Caco-2 cells, biopharmaceutics classification system (BCS) and biowaiver. **Acta medica**, Hradec Králové, v. 54, n. 1, p. 3–8, 2011.
32. ARTURSSON, P. Epithelial transport of drugs in cell culture. I: A model for studying the passive diffusion of drugs over intestinal absorptive (Caco-2) cells. **Journal of pharmaceutical sciences**, New York, v. 79, n. 6, p. 476–482, 1990.

33. HAYESHI, R.; HILGENDORF, C.; ARTURSSON, P.; AUGUSTIJNS, P.; BRODIN, B.; DEHERTOGH, P.; FISHER, K.; FOSSATI, L.; HOVENKAMP, E.; KORJAMO, T.; MASUNGI, C.; MAUBON, N.; MOLS, R.; MÜLLERTZ, A.; MÖNKKÖNEN, J.; O'DRISCOLL, C.; OPPERS-TIEMISSEN, H. M.; RAGNARSSON, E. G. E.; ROOSEBOOM, M.; UNGELL, A. L. Comparison of drug transporter gene expression and functionality in Caco-2 cells from 10 different laboratories. **European journal of pharmaceutical sciences**, Amsterdam, v. 35, n. 5, p. 383–396, 2008.
34. KAMIYAMA, E.; SUGIYAMA, D.; NAKAI, D.; MIURA, S. I.; OKAZAKI, O. Culture period-dependent change of function and expression of ATP-binding cassette transporters in Caco-2 cells. **Drug metabolism and disposition**, Bathesda, v. 37, n. 9, p. 1956–1962, 2009.
35. ARTURSSON, P.; TAVELIN, S. Caco-2 and emerging alternatives for prediction of intestinal drug transport: A general overview. *In*: **Drug Bioavailability**. Hoboken: Wiley, 2003. p. 72–89.
36. ARTURSSON, P.; KARLSSON, J. Correlation between oral drug absorption in humans and apparent drug permeability coefficients in human intestinal epithelial (Caco-2) cells. **Biochemical and biophysical research communications**, San Diego, v. 175, n. 3, p. 880–885, 1991.
37. HUBATSCH, I.; RAGNARSSON, E. G. E.; ARTURSSON, P. Determination of drug permeability and prediction of drug absorption in Caco-2 monolayers. **Nature protocols**, Berlin, v. 2, n. 9, p. 2111–2119, 2007.
38. CAPES-DAVIS, A.; FRESHNEY, R. I. **Freshney's culture of animal cells: A manual of basic technique and specialized applications**. Hoboken: Wiley, 2021. p. 1–832.
39. LU, Y.; HEYDEL, J. M.; LI, X.; BRATTON, S.; LINDBLOM, T.; RADOMINSKA-PANDYA, A. Lithocholic acid decreases expression of ugt2b7 in caco-2 cells: A potential role for a negative farnesoid x receptor response element. **Drug metabolism and disposition**, Bathesda, v. 33, n. 7, p. 937, 2005.
40. STROBER, W. Trypan blue exclusion test of cell viability. **Current protocols in immunology**, Iowa City, v. 111, n. 1, p. A3.B.1-A3.B.3, 2015.
41. **Counting cells in a hemocytometer | Thermo Fisher Scientific - BR**. Disponível em: <https://www.thermofisher.com/br/en/home/references/gibco-cell-culture-basics/cell-culture-protocols/counting-cells-in-a-hemacytometer.html>. Acessado em: 3 agosto, 2022.
42. **MP 03224 LIVE/DEAD® Viability/Cytotoxicity kit product information**. Disponível em: <https://tools.thermofisher.com/content/sfs/manuals/mp03224.pdf>. Acessado em: 21 Junho, 2022.

43. FRANKLIN, W. A.; LOCKER, J. D. Ethidium bromide: a nucleic acid stain for tissue section. **Journal of Histochemistry & Cytochemistry**. London, v. 29, n. 4, p. 572–576, 2017.
44. GARCÍA-CASAL, M. N.; LEETS, I.; LAYRISSE, M. Beta-carotene and inhibitors of iron absorption modify iron uptake by Caco-2 cells. **Journal of nutrition**, Oxford, v. 130, n. 1, p. 5–9, 2000.
45. CAMARGO, A. C. DE; SILVA, A. P. de S.; SOARES, J. C.; DE ALENCAR, S. M.; HANDA, C. L.; CORDEIRO, K. S.; FIGUEIRA, M. S.; SAMPAIO, G. R.; TORRES, E. A. F. S.; SHAHIDI, F.; SCHWEMBER, A. R. Do flavonoids from durum wheat contribute to its bioactive properties? A prospective study. **Molecules**, Basel, v. 26, n. 2, 2021.
46. YU, A. S. L. Paracellular transport as a strategy for energy conservation by multicellular organisms? **Tissue Barriers**, Philadelphia, v. 2, p. 5, 2017.
47. YUAN, S. Y.; RIGOR, R. R. Regulation of endothelial barrier function. colloquium series on integrated systems physiology. **Morgan and Claypool Life Sciences**, San Rafael, v. 3, n. 1, p. 1–146, 2010.
48. SRINIVASAN, B.; KOLLI, A. R.; ESCH, M. B.; ABACI, H. E.; SHULER, M. L.; HICKMAN, J. J. TEER measurement techniques for in vitro barrier model systems. **Journal of laboratory automation**, Singapore, v. 20, n. 2, p. 107–126, 2015.
49. BRISKE-ANDERSON, M. J.; FINLEY, J. W.; NEWMAN, S. M. The influence of culture time and passage number on the morphological and physiological development of Caco-2 cells. **Proceedings of the Society for Experimental Biology and Medicine**, New York, v. 214, n. 3, p. 248–257, 1997.
50. TARNOWSKI, B. I.; SPINALE, F. G.; NICHOLSON, J. H. DAPI as a useful stain for nuclear quantitation. **Biotechnic & Histochemistry**, Oxon, v. 66, n. 6, p. 296–302, 2009.
51. GUMBER, S.; NUSRAT, A.; VILLINGER, F. Immunohistological characterization of intercellular junction proteins in rhesus macaque intestine. **Experimental and Toxicologic Pathology**, Jena, v. 66, n. 0, p. 437–444, 2014.
52. ZHANG, X.; CHENG, X.; WU, Y.; FENG, D.; QIAN, Y.; CHEN, L.; YANG, B.; GU, M. In vitro and in situ characterization of the intestinal absorption of *capilliposide b* and *capilliposide c* from *lysimachia capillipes hemsl.* **Molecules**, Basel, v. 24, n. 7, p. 1227, 2019.
53. NICKLAS, T. A.; O'NEIL, C. E.; FULGONI, V. L. The role of dairy in meeting the recommendations for shortfall nutrients in the American diet. **Journal of the American College of Nutrition**, Oxon, v. 28 Suppl 1, p. 73S-81S, 2009.

54. BERMEJO, L. M.; LÓPEZ-PLAZA, B.; SANTURINO, C.; CAVERO-REDONDO, I.; GÓMEZ-CANDELA, C. Milk and dairy product consumption and bladder cancer risk: a systematic review and meta-analysis of observational studies. **Advances in nutrition**, Bathesda, v. 10, n. suppl_2, p. S224–S280, 2019.
55. THORNING, T. K.; RABEN, A.; THOLSTRUP, T.; SOEDAMAH-MUTHU, S. S.; GIVENS, I.; ASTRUP, A. Milk and dairy products: good or bad for human health? An assessment of the totality of scientific evidence. **Food & Nutrition Research**, Lund, v. 60, 2016.
56. GUÉGUEN, L.; POINTILLART, A. The bioavailability of dietary calcium. **Journal of the American College of Nutrition**, Oxon v. 19, p. 119S-136S, 2000.
57. ROSS, A. C; TAYLOR, C. L.; YAKTINE, A. L.; VALLE, H. B. D. **Dietary reference intakes for calcium and vitamin D**. Washington: National Academies Press, 2011. p. 1-522.
58. GUÉGUEN, L. Dietary calcium intake in France: contribution of milk and cheese. *In: Proceedings. (1st World Congress on Calcium and Vitamin D in Human Life, Rome, 1996).*
59. CHENG, S.; LYYTIKÄINEN, A.; KRÖGER, H.; LAMBERG-ALLARDT, C.; ALÉN, M.; KOISTINEN, A.; WANG, Q. J.; SUURINIEMI, M.; SUOMINEN, H.; MAHONEN, A.; NICHOLSON, P. H. F.; IVASKA, K. K.; KORPELA, R.; OHLSSON, C.; VÄÄNÄNEN, K. H.; TYLAVSKY, F. Effects of calcium, dairy product, and vitamin D supplementation on bone mass accrual and body composition in 10-12-y-old girls: a 2-y randomized trial. **The American journal of clinical nutrition**, Oxford, v. 82, n. 5, p. 1115–1126, 2005.
60. ALLEN, L. H. Calcium bioavailability and absorption: a review. **The American Journal of Clinical Nutrition**, Oxford, v. 35, n. 4, p. 783–808, 1982.
61. SKIBSTED, L. H. Mineral nutrient interaction: Improving bioavailability of calcium and iron. **Food Science and Biotechnology**, Seoul, v. 25, n. 5, p. 1233–1241, 2016.
62. ROSEN, C. J. **Primer on the metabolic bone diseases and disorders of mineral metabolism**: Eighth edition. Hoboken: Wiley. p. 1–1078, 2013.
63. FAVUS, M. J.; GOLTZMAN, D. Regulation of calcium and magnesium. *In: Primer on the metabolic bone diseases and disorders of mineral metabolism*: Eighth edition. Hoboken: Wiley, 2013. p. 171–179.
64. BRANDOLINI, M.; GUÉGUEN, L.; BOIRIE, Y.; ROUSSET, P.; BERTIÈRE, M.-C.; BEAUFRÈRE, B. Higher calcium urinary loss induced by a calcium sulphate-rich mineral water intake than by milk in young women. **British Journal of Nutrition**, Cambridge, v. 93, n. 2, p. 225–231, 2005.

65. PANSU, D.; BELLATON, C.; BRONNER, F. Effect of Ca intake on saturable and non-saturable components of duodenal Ca transport. **The American journal of physiology**, Bethesda, v. 240, n. 1, 1981.
66. BRONNER, F.; PANSU, D. Nutritional aspects of calcium absorption. **The Journal of nutrition**, Oxford, v. 129, n. 1, p. 9–12, 1999.
67. ZHANG, W.; LIU, Q. Y.; HAQQANI, A. S.; LECLERC, S.; LIU, Z.; FAUTEUX, F.; BAUMANN, E.; DELANEY, C. E.; LY, D.; STAR, A. T.; BRUNETTE, E.; SODJA, C.; HEWITT, M.; SANDHU, J. K.; STANIMIROVIC, D. B. Differential expression of receptors mediating receptor-mediated transcytosis (RMT) in brain microvessels, brain parenchyma and peripheral tissues of the mouse and the human. **Fluids Barriers CNS**, London, v. 17, p. 47, 2020.
68. BRONNER, F. Intestinal calcium absorption: mechanisms and applications. **The Journal of nutrition**, Oxford, v. 117, n. 8, p. 1347–1352, 1987.
69. SHKEMBI, B.; HUPPERTZ, T. Calcium absorption from food products: food matrix effects. **Nutrients**, Basel, v. 14, p. 180-211, 2022.
70. KIELA, P. R.; GHISHAN, F. K. Physiology of intestinal absorption and secretion. **Best Practice and Research in Clinical Gastroenterology**, Oxford, v. 30, n. 2, p. 145–159, 2016.
71. ZHU, C.; HUANG, M.; LAN, J.; CHUNG, L. W.; LI, X.; XIE, X. Colorimetric calcium probe with comparison to an ion-selective optode. **ACS Omega**, Washington, v. 10, n. 3, p. 12476-12481, 2018.
72. DEVINNEY, M. J.; REYNOLDS, I. J.; DINELEY, K. E. Simultaneous detection of intracellular free calcium and zinc using fura-2FF and FluoZin-3. **Cell calcium**, Oxford, v. 37, n. 3, p. 225–232, 2005.
73. PAREDES, R. M.; ETZLER, J. C.; WATTS, L. T.; ZHENG, W.; LECHLEITER, J. D. Chemical calcium indicators. **Methods**, San Diego, v. 46, n. 3, p. 143–151, 2008.
74. RAMADAN, Q.; JAFARPOORCHEKAB, H.; HUANG, C.; SILACCI, P.; CARRARA, S.; KOKLÜ, G.; GHAYE, J.; RAMSDEN, J.; RUFFERT, C.; VERGERES, G.; GIJS, M. A. M. NutriChip: nutrition analysis meets microfluidics. **Lab on a Chip**, Cambridge, v. 13, n. 2, p. 196–203, 2012.
75. WU, Y. T.; CHEN, Y. C. Determination of calcium in complex samples using functional magnetic beads combined with electrodeless/sheathless electrospray ionization mass spectrometry. **Rapid communications in mass spectrometry: RCM**, Hoboken, v. 20, n. 13, p. 1995–1999, 2006.
76. CAGLAR, P.; TUNCEL, S. A.; MALCIK, N.; LANDERS, J. P.; FERRANCE, J. P. A microchip sensor for calcium determination. **Analytical and bioanalytical chemistry**, Heildeberg, v. 386, n. 5, p. 1303–1312, 2006.

77. SMITH, R. W. Mass spectrometry. *In: Encyclopedia of forensic sciences: second edition*. Amsterdam: Elsevier, 2013. p. 603–608.
78. HOFFMAN, E. DE & STROOBANT, V. **Mass spectrometry, principles and applications, third edition**. Hoboken: Wiley, 2007. p. 1-476.
79. MILLER, J. N.; MILLER, J. C. **Statistics and chemometrics for analytical chemistry**. Hoboken: Pearson Prentice Hall, 2005. p. 1-268.
80. FOOD & DRUG ADMINISTRATION. **Q2(R1) validation of analytical procedures: text and methodology, guidance for industry**. Silver Spring, 2005. p. 1-10.
81. ARRANZ-GIBERT, P.; GUIXER, B.; PRADES, R.; CIUDAD, S.; GIRALT, E.; TEIXIDÓ, M. A MALDI-TOF-based method for studying the transport of bbb shuttles—enhancing sensitivity and versatility of cell-based in vitro transport models. **Scientific Reports**, Berlin, v. 9, n. 1, p. 1–11, 2019.
82. AUBRY, S.; AUSSÉDAT, B.; DELAROCHE, D.; JIAO, C. Y.; BOLBACH, G.; LAVIELLE, S.; CHASSAING, G.; SAGAN, S.; BURLINA, F. MALDI-TOF mass spectrometry: A powerful tool to study the internalization of cell-penetrating peptides. **Biochimica et Biophysica Acta (BBA) - Biomembranes**, Amsterdam, v. 1798, n. 12, p. 2182–2189, 2010.
83. DUNCAN, M. W.; RODER, H.; HUNSUCKER, S. W. Quantitative matrix-assisted laser desorption/ionization mass spectrometry. **Briefings in functional genomics & proteomics**, Oxford, v. 7, n. 5, p. 355–370, 2008.
84. XIAN, F.; HENDRICKSON, C. L.; MARSHALL, A. G. High resolution mass spectrometry. **Analytical Chemistry**, v. 84, n. 2, p. 708–719, 2012.
85. GROSS, J. H. **Mass spectrometry: A textbook: Second edition**. Hoboken: Wiley, 2011. p. 1–753.
86. VAN MEER, B. J.; DE VRIES, H.; FIRTH, K. S. A.; VAN WEERD, J.; TERTOOLEN, L. G. J.; KARPERIEN, H. B. J.; JONKHEIJM, P.; DENNING, C.; IJZERMAN, A. P.; MUMMERY, C. L. Small molecule absorption by PDMS in the context of drug response bioassays. **Biochemical and Biophysical Research Communications**, San Diego, v. 482, n. 2, p. 323–328, 2017.
87. NIANZHEN LI; SCHWARTZ, M.; IONESCU-ZANETTI, C. PDMS compound adsorption in context. **Journal of Biomolecular Screening**, Thousand Oaks, v. 14, n. 2, p. 194–202, 2009.
88. MASTRANGELI, M.; MILLET, S.; EIJNDEN-VAN RAAIJ, J. VAN DEN. Organ-on-chip in development: Towards a roadmap for organs-on-chip. **ALTEX - Alternatives to animal experimentation**, Heildeberg, v. 36, n. 4, p. 650–668, 2019.

89. MA, C.; PENG, Y.; LI, H.; CHEN, W. Organ-on-a-chip: A new paradigm for drug development. **Trends in pharmacological sciences**, London, v. 42, n. 2, p. 119–133, 2021.
90. JOBST, K. J.; TERLOUW, J. K.; LUIDER, T. M.; BURGERS, P. C. On the interaction of peptides with calcium ions as studied by matrix-assisted laser desorption/ionization Fourier transform mass spectrometry: Towards peptide fishing using metal ion baits. **Analytica Chimica Acta**, Amsterdam, v. 627, n. 1, p. 136–147, 2008.
91. TANG, N.; SKIBSTED, L. H. Calcium binding to amino acids and small glycine peptides in aqueous solution: Toward peptide design for better calcium bioavailability. **Journal of Agricultural and Food Chemistry**, Washington, v. 64, n. 21, p. 4376–4389, 2016.

APPENDIX A

Mass spectra:

Figure A-1. Mass spectrum of 0 mM Calcium/ 30 mM EDTA

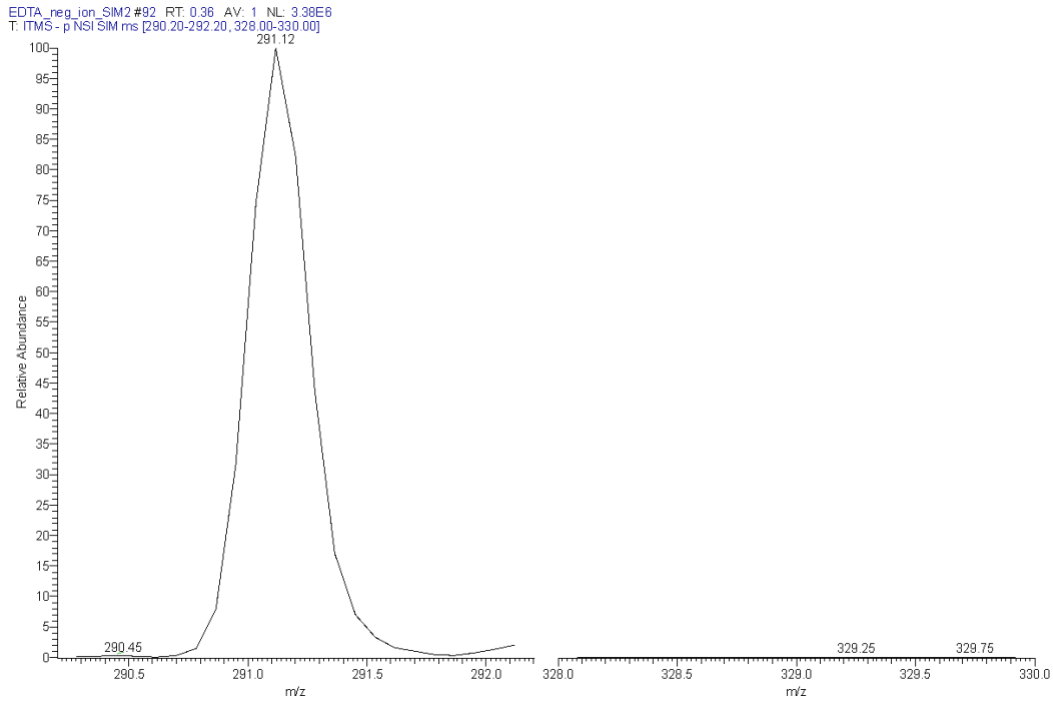
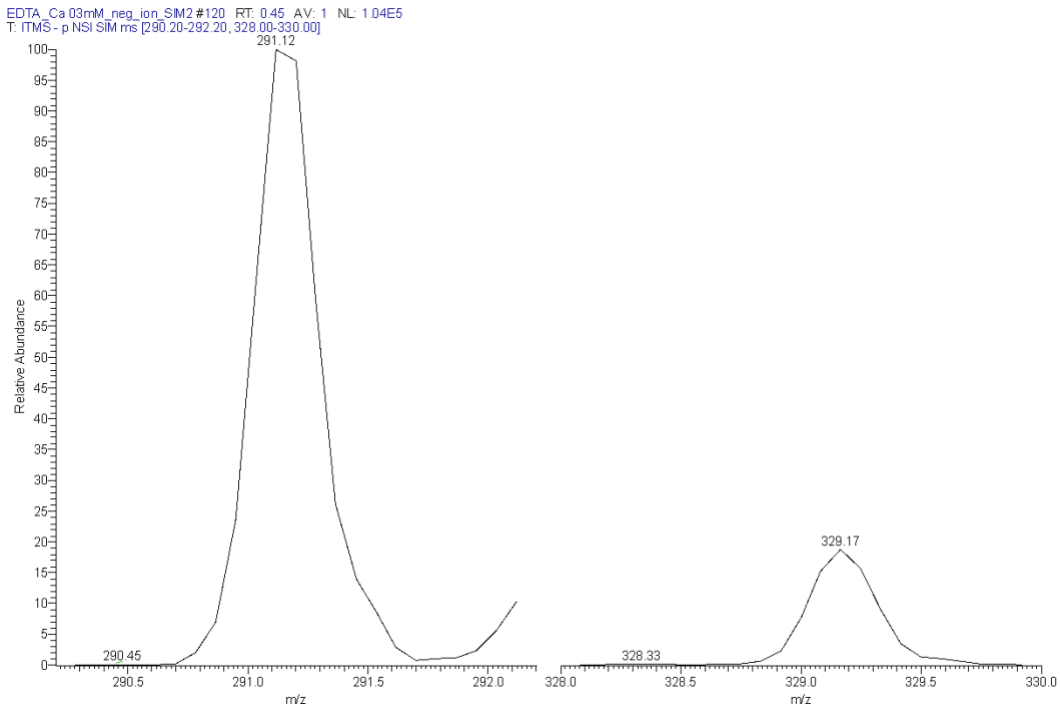
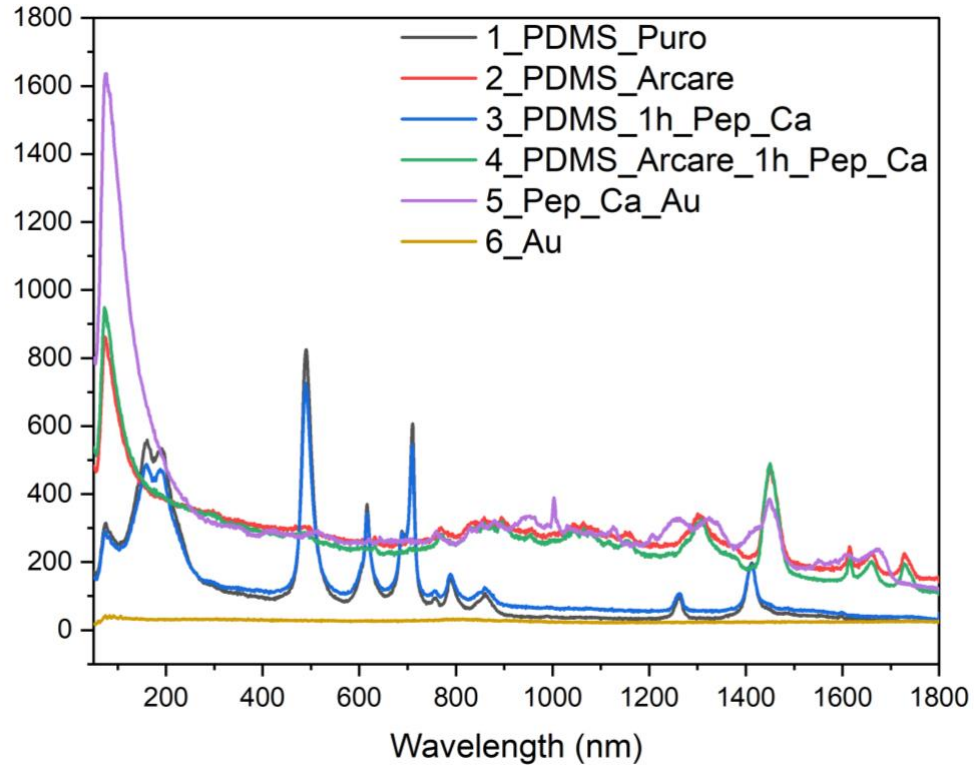


Figure A-2. Mass spectrum of 0.3 mM Calcium/ 30 mM EDTA



APPENDIX B

Figure B-1. RAMAN spectroscopy for identifying PDMS adsorption



APPENDIX C

MALDI spectra

Figure C-1. MALDI spectra for the transwell® samples

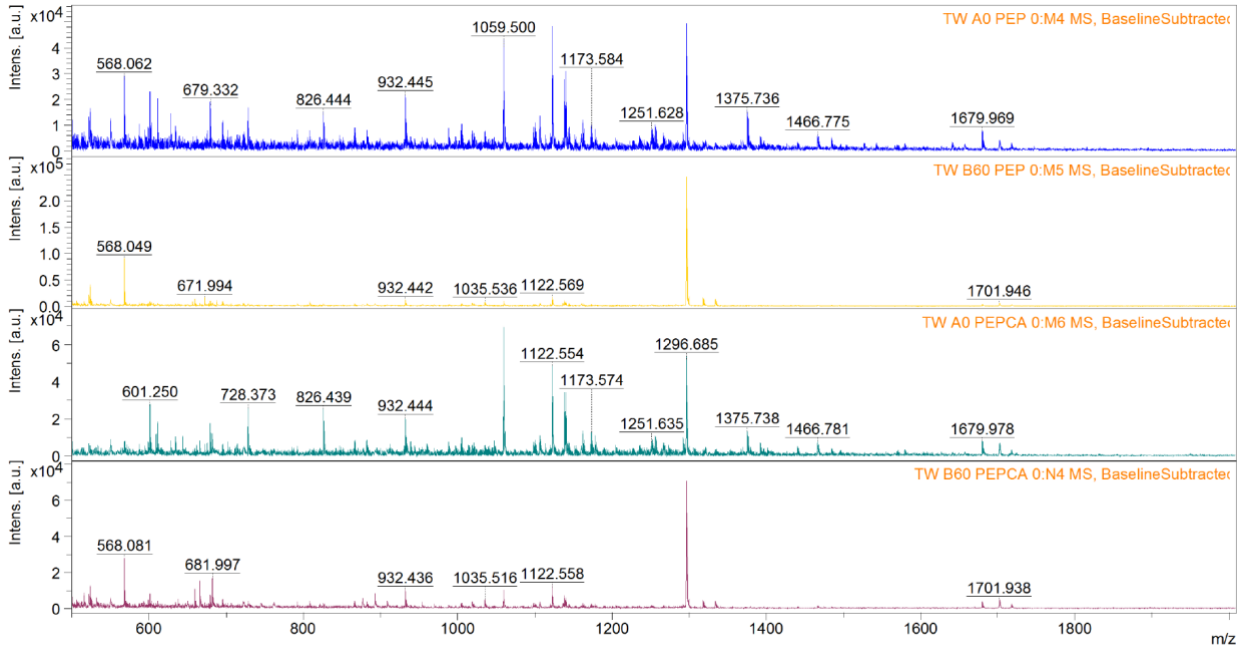


Figure C-2. MALDI spectra for the Acrylic loAC

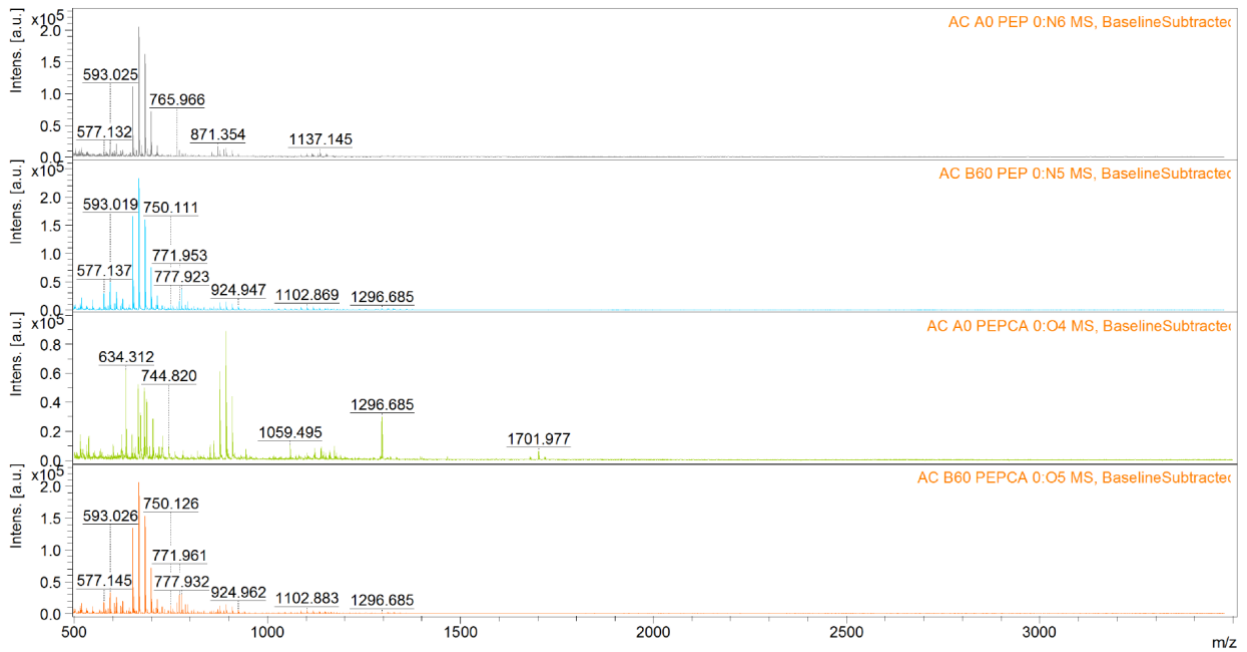


Figure C-3. MALDI spectra for the PDMS loaC

